

THE ROLES OF LIM KINASE (LIMK) INHIBITORS IN THE REGULATION OF ACTIN
DYNAMICS DURING HIV-1 INFECTION

by

Fei Yi

A Dissertation

Submitted to the

Graduate Faculty

of

George Mason University

in Partial Fulfillment of

The Requirements for the Degree

of

Doctor of Philosophy

Biosciences

Committee:

_____	Dr. Yuntao Wu, Dissertation Director
_____	Dr. Tshaka Cunningham, Committee Member
_____	Dr. Jia Guo, Committee Member
_____	Dr. Ramin M. Hakami, Committee Member
_____	Dr. Kylene Kehn-Hall, Committee Member
_____	Dr. Iosif Vaisman, Acting Director, School of Systems Biology
_____	Dr. Donna M. Fox, Associate Dean, Office of Student Affairs & Special Programs, College of Science
_____	Dr. Peggy Agouris, Dean, College of Science
Date: _____	Spring Semester 2016 George Mason University Fairfax, VA

The Roles of LIM Kinase (LIMK) Inhibitors in the Regulation of Actin Dynamics
During HIV-1 Infection

A dissertation submitted in partial fulfillment of the requirements for the degree of
Doctor of Philosophy at George Mason University

By

Fei Yi

Doctor of Medicine

Tongji Medical College, Huazhong University of Science and Technology, 2010

Director: Yuntao Wu, Professor
Department of Molecular and Microbiology

Spring Semester 2016
George Mason University
Fairfax, VA

Copyright 2016
All Rights Reserved

Dedication

This work is dedicated to my dear grandfather, Prof. Daogen Yi (1931-2015), who raised me up and encouraged me to pursue the “way” of science. No matter you were on the other side of the Earth or above in the Heaven, you will live in my memory forever.

Acknowledgements

I would like to thank all my committee members for sharing their experiences and advices altruistically. I also would like to say thank you to all my lab members and Diane St.Germain, you gave me great help and support. Lastly, I must thank all my family members, who always put their trust on me and encouraged me.

Table of Contents

	Page
List of Tables	vi
List of Figures.....	vii
Abstract.....	ix
Chapter 1: An introduction to Human Immunodeficiency Virus and its entanglement with actin signal transduction	1
Chapter 2: LIMK inhibitors screening and candidate drug selection	11
Chapter 3: Medicinal chemistry of R10015 and its in vitro assay	20
Chapter 4: Molecular and cellular characterization of R10015.....	32
Chapter 5: Mechanism of R10015's inhibition of HIV replication	48
Chapter 6: Exploration of broad spectrum antiviral activity of R10015	80
Chapter 7: Summary of R10015 project and the future of LIMK inhibitor design	92
Supplementary Figures	95
References	111

List of Tables

Table	Page
Chapter 1	
Table 1.1	10
Chapter 3	
Table 3.1	29

List of Figures

Figure	Page
Chapter 1	
Figure 1.1	5
Figure 1.2	9
Chapter 2	
Figure 2.1	15
Figure 2.2	16
Figure 2.3	17
Figure 2.4	18
Chapter 3	
Figure 3.1	26
Figure 3.2	27
Figure 3.3	28
Chapter 4	
Figure 4.1	39
Figure 4.2	40
Figure 4.3	41
Figure 4.4	42
Figure 4.5	43
Figure 4.6	44
Figure 4.7	45
Chapter 5	
Figure 5.1	64
Figure 5.2	65

Figure 5.3	66
Figure 5.4	67
Figure 5.5	68
Figure 5.6	69
Figure 5.7	70
Figure 5.8	71
Figure 5.9	72
Figure 5.10	73
Figure 5.11	74
Figure 5.12	75
Figure 5.13	76
Figure 5.14	77
Chapter 6		
Figure 6.1	86
Figure 6.2	87
Figure 6.3	88
Figure 6.4	89
Figure 6.5	90

Abstract

THE ROLES OF LIM KINASE (LIMK) INHIBITORS IN THE REGULATION OF ACTIN DYNAMICS DURING HIV-1 INFECTION

Fei Yi, Ph.D.

George Mason University, 2016

Dissertation Director: Dr. Yuntao Wu

A dynamic actin cytoskeleton is necessary for viral entry, intracellular migration, and virion release. For HIV-1 infection, during viral entry, the virus triggers early actin activity through hijacking chemokine coreceptor signaling which activates a viral dependency host factor cofilin and its kinase, the LIM domain kinase (LIMK). Although knockdown of human LIMK1 with siRNA inhibits HIV infection, no specific small molecule inhibitor of LIMK is available. Here we describe the design and discovery of novel classes of small molecule inhibitors of LIMK for inhibiting HIV infection. We identified R10015 as a lead compound that blocks LIMK kinase activity by binding to the ATP-binding pocket. R10015 specifically blocks viral DNA synthesis, nuclear migration, and virion release. In addition, R10015 inhibits multiple viruses including EBOV, RVFV, VEEV, and HSV-1, suggesting that LIMK inhibitors could be developed as a new class of broad-spectrum anti-viral drugs.

Chapter 1: An introduction to Human Immunodeficiency Virus and its entanglement with actin signal transduction

The HIV and AIDS pandemic

HIV was unknown to humanity until the first case reported on June 5th 1981 regarding *Pneumocystis pneumonia* (PCP) [1]. The CDC confirmed 5 cases of this disease on homosexual drug abusers from San Francisco which is highly related to severe immune deficiency. Shortly after the first discovery, similar cases were reported in US with other opportunistic infections such as Kaposi's sarcoma, an aggressive and rapidly developing cancer [2, 3]. Later in 1982, these new clinical findings are summarized by the CDC in the report entitled "Current Trends Update on Acquired Immune Deficiency Syndrome (AIDS) --United States" and that was the first time the word AIDS is used for describing this new disease. Researchers found a lymphatic virus, HTLV-III, to be the cause of AIDS [4-6], but this pathogen was found not belonging to the HTLV category and was renamed as the human immunodeficiency virus (HIV) in 1986. The global concern of HIV infection has began since then and this virus still remains a significant issue for both scientists and physicians today. According to "GAP report 2014" from UNAIDS, there are 34 million people living with HIV today and it's estimated that 19 million HIV carriers

are unaware of their infection.

HIV biology

It's believed that HIV derived from a simian immunodeficiency virus (SIV) carried by chimpanzee and transmitted to human in Africa [7]. Then it adapted into human host and leads to AIDS symptoms. But interestingly, SIV infection of some primates does not cause similar symptoms as HIV although high level of viral load was detected in blood [8, 9].

HIV is a lentivirus of the Retroviridae family. The HIV virion particle contains positive sense single strand RNA. This 9.7kb RNA consists of 9 genes (gag, pol, env, tat, rev, nef, vpr, vif and vpu) and can encode 19 viral proteins from spliced or unspliced mRNA [10]. By their functions, these proteins are categorized into 3 classes: viral structural protein, essential regulatory protein and accessory regulatory proteins. HIV infection of CD4⁺ T cells initiates with the viral protein gp120 binding to host cell receptor CD4 [11-13] and predominant coreceptor (either CXCR4 [14] or CCR5 [15, 16]). Following this interaction, gp120 changes its conformation, brings virion closer to cell membrane and expose a previously hidden spike-shaped viral protein gp41. The gp41 causes the fusion of virion and cell membrane and assists the viral entry [17]. In the meanwhile, gp120 binding to one of the coreceptors also triggers signal transduction to break the cortical actin barrier and allows the virion moving further into the cell [18].

After viral entry, the RNA packaged in virion reverse transcribes a double strand

DNA in cytoplasm catalyzed by viral protein reverse transcriptase (RT). This linear viral DNA will further rearrange itself and binds with viral proteins such as integrase (IN) and vpr as well as cellular protein and form an enclosed construction named pre-integration complex (PIC) [18-20]. PIC enters nucleus through nuclear pore complex and viral DNA integrates into host genome mediated by integrase [21]. Following integration, viral DNA regions consisting of U3, R and U5 which is named the Long Terminal Repeat (LTR) regulates the gene expression of all HIV genes in a similar pattern to other lentivirus [22, 23]. Additionally, HIV gene expression is also promoted by Tat [24, 25] and Rev protein [26]. Rev protein is a required factor for partial spliced and non-spliced mRNA nuclear export. In the absence of Rev, only spliced mRNAs which encode Tat, Nef and Rev are exported for early translation. The translation of other proteins is only possible when Rev binds to their mRNAs Rev Response Element (RRE) and facilitates their export [26-28]. Once the essential regulatory proteins (Tat and Rev) occur, the full-length HIV genome can be expressed, both viral structural proteins and accessory regulatory proteins then will be translated and assemble into new viral particles together on cell membrane [29].

HIV clinical manifestation and the current clinical solution to AIDS

As HIV specifically infecting CD4⁺ T cell, researchers traced the viral titer in peripheral blood and compared it with CD4⁺ T cell counts. As presented in **Figure 1.1** [29], the HIV infection is usually considered a three-step process. During the first step of primary infection, there is a reduction in total lymphocyte count as the

response of the acute infection [30]. Due to the peak of plasma viral load (pVL), CD4⁺ T cells deplete and CD8⁺ T cells proliferate, causing an inversion of CD4/CD8 ratio. Then the asymptomatic phase of the infection follows, featuring a long term of low level viral titer and comparatively stable CD4⁺ counts in peripheral blood. Lastly, after several years of latent infection, pVL surges again and leads to progressive immune dysregulation indicated by the decreasing counts of CD4 and CD8⁺ cells.

At first, AIDS patients are treated with anti-HIV drugs such as protease and reverse transcriptase inhibitors, but individually rather than combined. These treatments showed limited benefits [31]. In 1996, a remarkable treatment, Highly Active Anti Retroviral Therapy (HAART) was introduced and was proved to be much more effective than the traditional therapies. The HAART combines 3 drugs of protease and RT inhibitors in order to target different stages of HIV replication cycle. This design provides a sustainable control of the viral replication as well as abates the change of viral mutation and causing drug resistance [32]. However, HAART is not the final solution to AIDS as its major function is to reduce viremia to undetectable level but fails to annihilate all latent infected virus in the reservoir. As a result, the asymptomatic phase of infection is extended but the AIDS phase is still inevitable. Currently, more types of drugs have been used in ART, such as integrase inhibitors [33], CCR5 antagonists and viral envelop protein blockers [34]. Despite the tremendous efforts already made in finding new target of inhibiting HIV replication, there is still no drug or treatment that can guarantee the cure of AIDS.

The intertwined HIV and actin

In addition to the anti-HIV targets mentioned above, the discovery of HIV envelop protein gp120 regulating cortical actin activity provides another path for the drug design [18]. The viral protein gp120 binding to host cell receptor CD4 actually not only leads to the fusion of viral and cellular membranes [11-13], but also induces

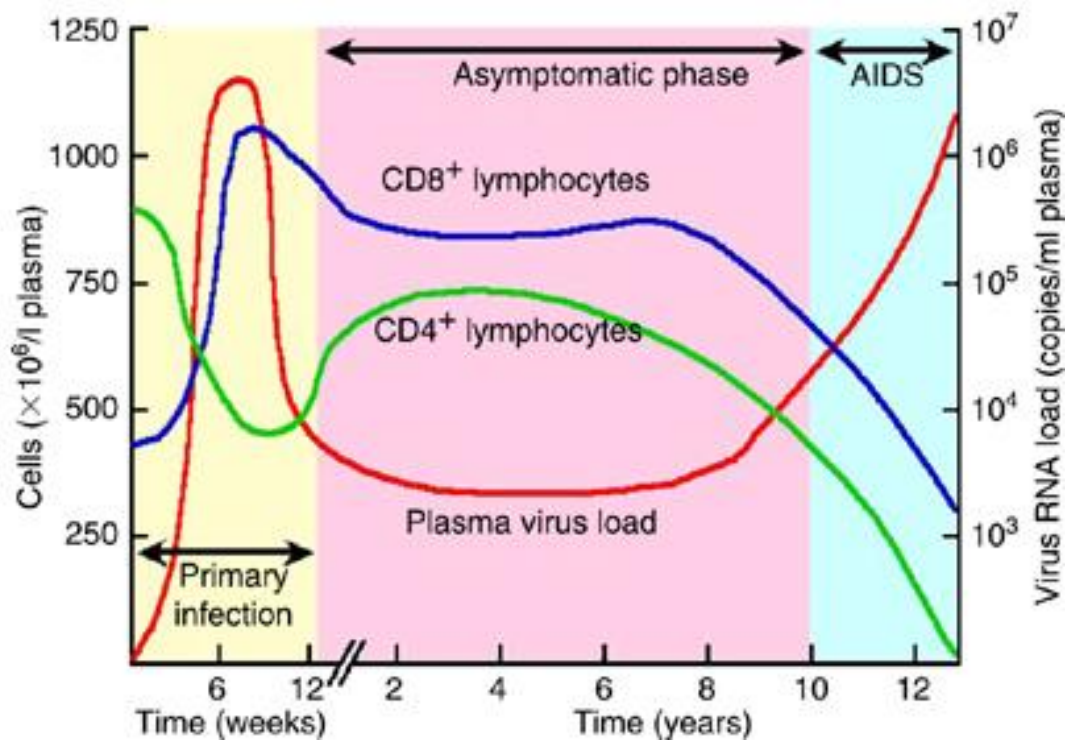


Figure 1.1 Schematic of typical course of HIV-1 infection showing changes in CD4 and CD8 T-cell counts in peripheral blood and plasma viral load (pVL).

signal transduction via the binding of co-receptor CXCR4 (X4) or CCR5 (R5). The end point of this signal is a key regulator of actin assembly and disassembly called cofilin, an actin-depolymerizing factor (ADF) family protein [35]. Before this discovery, it's believed the major function of gp120's interaction with co-receptor is to induce membrane fusion, and F-actin is necessary for the formation of reverse transcription complex and reverse transcription [36]. Now people have a more profound understanding about the HIV and actin interaction. When dephosphorylated, cofilin is activated and binds to F-actin promoting the depolymerization of actin filaments from the pointed (-) end [37]. Cofilin activation causes the treadmilling of actin skeleton which can be utilized by HIV to migrate further into the cell. One upstream regulator of cofilin, LIM domain Kinase (LIMK), once activated will cause cofilin phosphorylation at serine 3, preventing its binding with F-actin [38]. A possible signal pathway is the RhoA-ROCK-LIMK-cofilin cascade [39]. Another two cofilin upstream phosphatases, PP1 and PP2A, dephosphorylate cofilin and stimulate its association with F-actin inducing actin depolymerization [40].

Research showed another actin binding protein complex Arp2/3 is also important for HIV infection [41]. Triggered by another actin dynamic pathway ERK2-WAVE2-Arp2/3 [42], Arp2/3 is activated and improves actin branching [43, 44], benefits HIV nuclear migration. However, in Arp2/3 knockdown cell lines, HIV infection is inhibited indicating that HIV requires robust actin activity to complete its replication cycle.

LIMK and LIMK inhibitors

LIMK is a serine-threonine and tyrosine protein kinase with two isoforms identified as LIMK1 and LIMK2 [45-48]. Highly homologous in their composition, LIMK1 and LIMK2 share about 50% of identities whereas their distribution in tissue and organs slightly differs from each other. They both have two amino-terminal LIM domains, adjacent PDZ and proline/serine-rich regions as well as carboxyl terminal protein kinase domain [49]. Research showed that LIMK2's distribution is more general than LIMK1, almost widely expressed in all tissues [50]. LIMK1 was found to be highly expressed particularly in kidney and testis where the expression of LIMK2 is comparatively lower. Since LIMK directly regulates cofilin activity and actin dynamics (**Figure 1.2**), it's associated with a variety of diseases related to synaptic function and smooth muscle contraction, including Williams Syndrome [51], Alzheimer's disease [52, 53], primary pulmonary hypertension [54, 55] and ocular hypertension [56]. LIMK is also believed to associate with HIV infections [57-59]. Vorster et al studied the HIV infection of a LIMK knocking down cell line and this study indicated that cortical actin level was decreased in this cell line as well as much lower HIV replication was measured [60]. This discovery is a direct proof that abated LIMK activity can lead to inhibition of HIV replication and based on this conclusion it's rationale that small molecule LIMK inhibitor is capable of inhibiting HIV replication in T cells and cell lines.

Several research groups are working on the development of novel LIMK inhibitors: T56-LIMKi decreases phosphorylated cofilin (p-cofilin) levels in multiple cancerous cell lines [61]; Damnacanthal, invented by a Japanese group, also inhibits LIMK activity at a low IC₅₀ around 800nM [62]. However, currently there is no report showing LIMK inhibitors' activity against HIV or other viral infection. Dr. Yangbo Feng's group from the Scripps Research Institute designed a series of novel LIMK inhibitors with high biochemical potency (IC₅₀ < 50 nM) and good in vitro pharmacokinetic properties as shown in **Table 1.1** [63]. Our group established cooperation with Dr. Feng's group and focused on the study of these inhibitors impact on viral replication, especially focusing on HIV-1 infection. Our major goal of this project is to screen 25 LIMK inhibitors for antiviral activity and to select the best candidate drug for further mechanism elucidation.

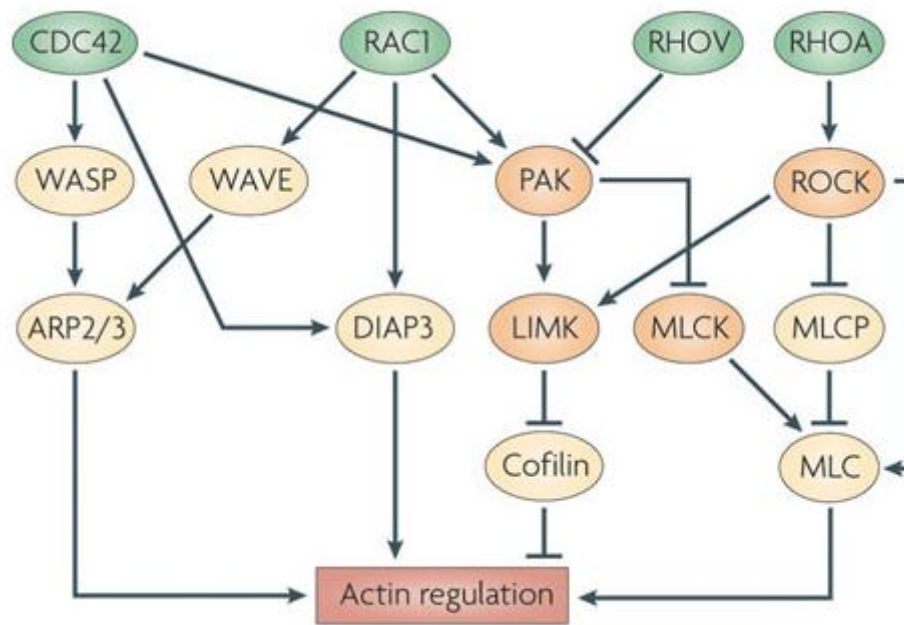
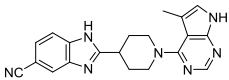
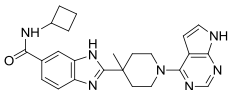
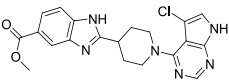
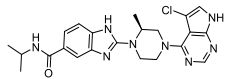
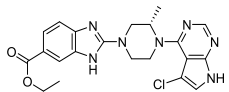
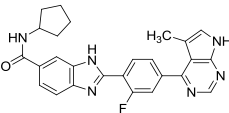
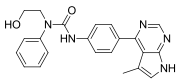


Figure 1.2 LIMK's role in the actin dynamics pathway, adapted from "*Rho family GTPases and their regulators in lymphocytes*" by Tybulewicz et al [64].

Table 1.1 Lead LIMK inhibitors with $IC_{50} \leq 50$ nM.

Compound	Scaffold	Structure	LIMK1 Biochemical Inhibition IC_{50} (nM)*
R8212	A		44 ± 6
R8482	A		41 ± 4
R10015	A		38 ± 5
R10543	A		5 ± 2
R10659	A		45 ± 6
R8584	B		50 ± 7
R7826	C		43 ± 4

* IC_{50} values are from ≥ 2 in vitro kinase assays using purified LIMK1.

Chapter 2: LIMK inhibitors screening and candidate drug selection

Introduction

As mentioned in the previous section, The 25 inhibitors screened in this project are provided by Dr. Yangbo Feng. These leading LIMK inhibitors are based on three chemotypes: scaffold A is based on the 4-yl-piperidine- or piperazine-benzimidazole derivatives; scaffold B is derived from phenyl benzimidazole analogs, and scaffold C is based on the bis-aryl urea moiety (**Table 1**) [63]. All compounds from these three scaffolds are Type-I ATP-competitive kinase inhibitors.

Our screening of these small molecule inhibitors is performed on an HIV Rev-dependent indicator cell line Rev-CEM-GFP-Luc [65, 66]. As indicated in **Figure 2.1**, the gene expression of GFP and Luciferase on this cell line is controlled by a RRE region on the genome. As we mentioned in “HIV biology” in previous Chapter, RRE is an element on mRNA only activated if HIV Rev protein binds to it [27, 28] otherwise the mRNA with RRE cannot export from nucleus preventing its protein to be translated. Rev specifically assists the export of mRNA with RRE, so for this cell line there will be no GFP expression unless HIV infects the cell and starts expression of Rev [67-73]. Another reporter cell line is designed base on HIV Tat restrictions [74-76]. The Tat-dependent reporter expression can be non-specifically up or down modulated by cellular inhibitors, cytokines, mitogens, or free viral proteins

such as gp120 [74, 77-81]. The high stringency of the Rev-dependent cell permitted effective screening of anti-HIV compounds that target HIV dependency cellular proteins such as LIMK. Treating this cell line with an RT inhibitor, for instance Etravirine, can demonstrate the fidelity of the reporter cell line during HIV infection as Etravirine inhibits viral DNA conversion, thus no cell should express Rev protein as well as GFP [82].

Since these small compounds may drastically inhibit cofilin phosphorylation and cause actin depolymerization, the drug treatment could be highly toxic. We used propidium iodide (PI) to stain cells and cell survival rate was measured by flow cytometry.

Materials and Methods

Cells: Rev-CEM-GFP-Luc cells are a CEM CD4 T lymphoblast derivative and were maintained at less than 1 million cells per milliliter in RPMI 1640 (Life Technologies) supplemented with 10% FBS and penicillin/streptomycin (Life Technologies). Unless otherwise indicated, cells were cultured at 37 °C and 5% CO₂.

Wild type HIV-1 virus: Virus stocks of HIV-1(NL4-3) were prepared by transfection of HeLa or HEK293T cells with cloned proviral DNA as described [18, 83]. Levels of p24 in the viral supernatant were measured in triplicate with ELISA using an in-house ELISA Kit. Viral titer (TCID₅₀) was determined on the Rev-dependent GFP and Luciferase indicator cell Rev-CEM-GFP-Luc.

LIMK inhibitors treatment: All drugs are dissolved in DMSO. For HIV infection of Rev-CEM-GFP-Luc, 2×10^5 cells were treated with 100 μ M, 10 μ M or 1 μ M of LIMK inhibitors for 1 hour, and then infected with 10^3 to $10^{4.5}$ TCID₅₀ units of HIV-1 for 3 hours with the addition of LIMK inhibitors to maintain the same drug concentration. Infected cells were washed twice and then resuspended into 1ml fresh medium without the addition of inhibitors. Cells were incubated for 2 days, and viral infection was measured by flow cytometry (FACSCalibur, BD Biosciences) for GFP positive cells. To exclude drug cytotoxicity, propidium iodide (PI) (2 μ g/ml, Fluka) was added into the cell suspension prior to flow cytometry, and only viable cells (PI-negative) were used for measuring GFP expression.

Etravirine treatment: Similar to the LIMK inhibitor treatment mentioned above, Rev-CEM-GFP-Luc cells were pretreated with 100nM Etravirine for 2h then infected with HIV-1 for 3 hours with the addition of Etravirine to maintain the drug concentration during infection. GFP expression was measured 2 days post infection.

Results

Rev-CEM-GFP-Luc cells showed low false-positive rate for measuring HIV infection

As presented in **Figure 2.2**, Rev-CEM-GFP-Luc cells' expression of reporter protein GFP is highly dependent on the existence of viral protein Rev. In the absence of Rev (Etravirine treated cells), the cell lines showed only 0.01% GFP positive cells whereas the HIV infection rate is 3.87% in cells without Etravirine treatment. This

data indicates that Rev-CEM-GFP-Luc is highly reliable in large scales of drug screening.

6 compounds showed good potential of anti-HIV activity in cell line

As shown in **Figure 2.3**, using HIV-1 infection of Rev-CEM-GFP-Luc, we screened 25 of these newly designed small molecules of LIMK inhibitors, and identified seven lead compounds (R10015, R8584, R8482, R8212, R7826, R10543, and R10659) that blocked the X4 HIV infection at non-toxic dosages in T cells. All these drugs showed around 50% or higher inhibition of HIV-1 replication at 100 μ M which is a safe dosage that the cells could tolerate (**Figure 2.4**). Among the candidate drugs, R10015 showed outstanding anti-HIV activity at lower dosages (higher than 50% HIV inhibition at 10 μ M and 1 μ M) while other drugs' effect prominently reduced when a lower concentration is applied.

All original flow cytometry data are attached in the supplementary figures section right before the reference part.

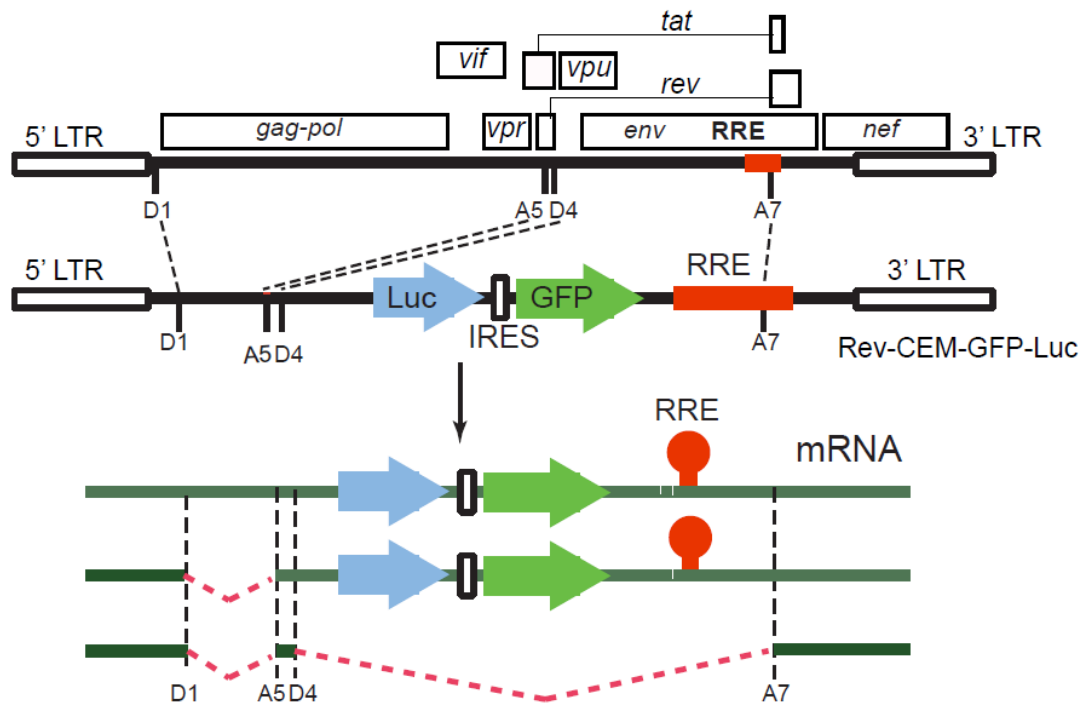


Figure 2.1 Schematics of the Rev-dependent reporter construct and its transcripts in the HIV Rev-dependent indicator cell, Rev-CEM-GFP-Luc. The presence of RRE in unspliced and singly-spliced transcripts renders GFP/Luc expression Rev-dependent.

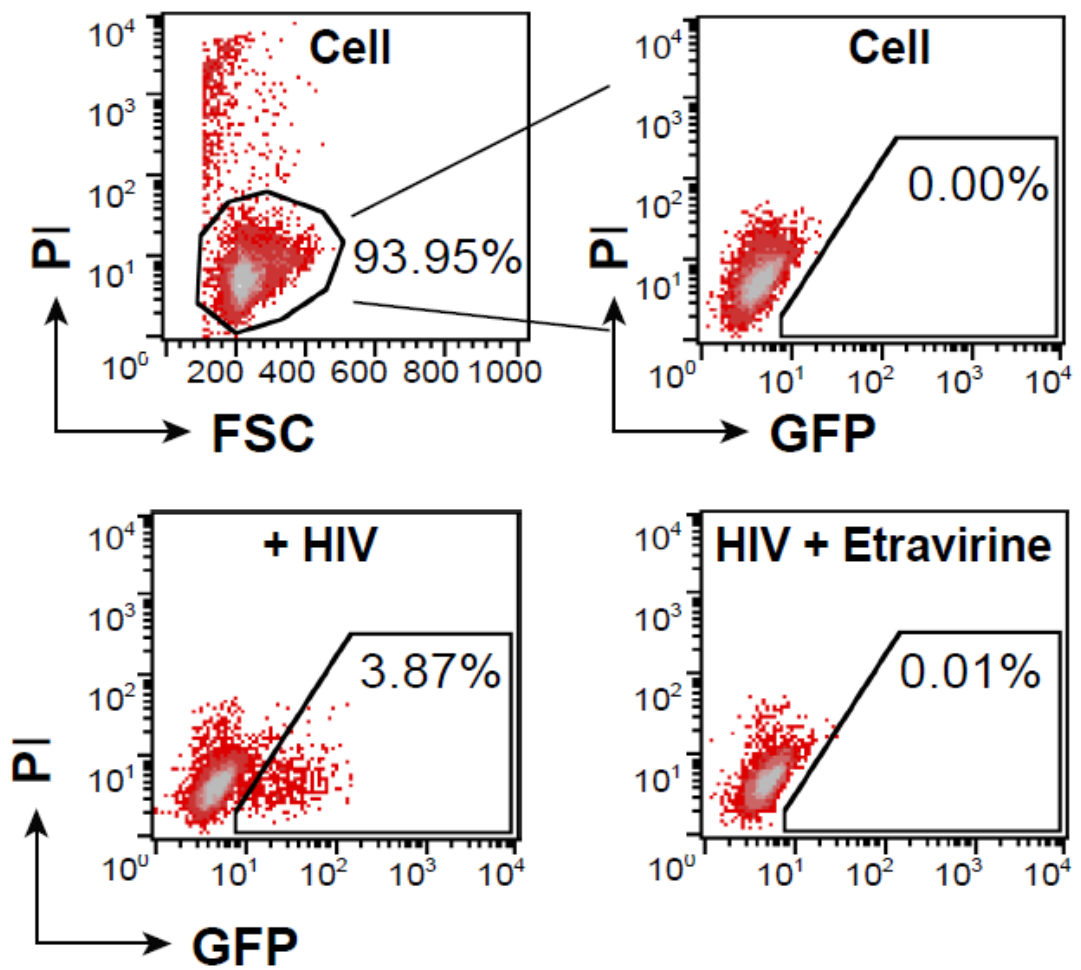


Figure 2.2 Examples of HIV-dependent expression of GFP in Rev-CEM-GFP-Luc.

Cells were not infected, or infected with HIV(NL4-3), or infected with HIV(NL4-3) and treated with the reverse transcriptase inhibitor Etravirine (100 nM). Cells were washed to remove the virus and the inhibitors, and incubated for 48 hours.

HIV-dependent GFP expression was measured by flow cytometry. Propidium iodide (PI) was added during flow cytometry to simultaneously measure cell viability. To exclude non-specific cytotoxicity, only viable cells were used for GFP quantification.

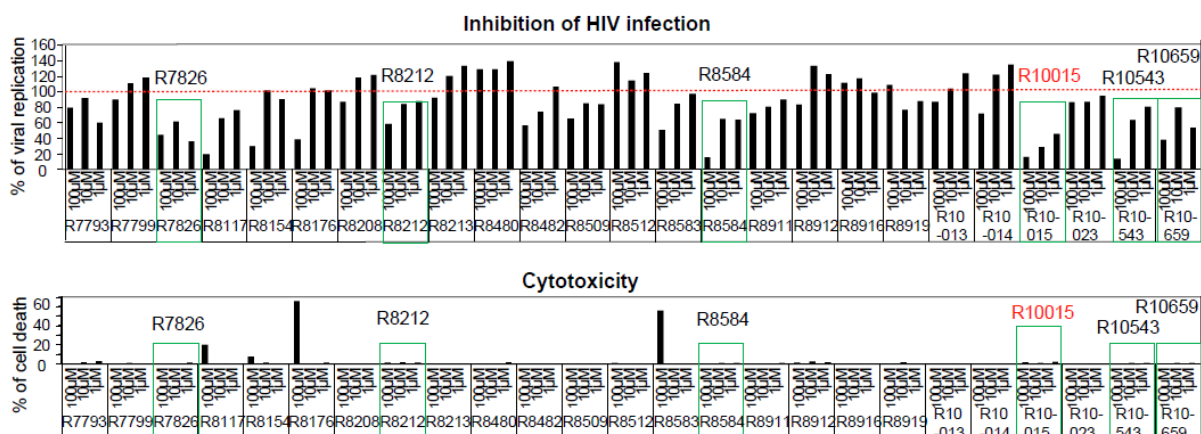


Figure 2.3 Screening LIMK inhibitors with Rev-CEM-GFP-Luc. The relative infection rates in drug-treated versus DMSO-treated cells (100%) were plotted using the relative percent of GFP⁺ cells. The drugs highlighted with green boxes are the best candidates for inhibiting HIV replication. Red labeled drug R10015 is selected for anti viral mechanism study.

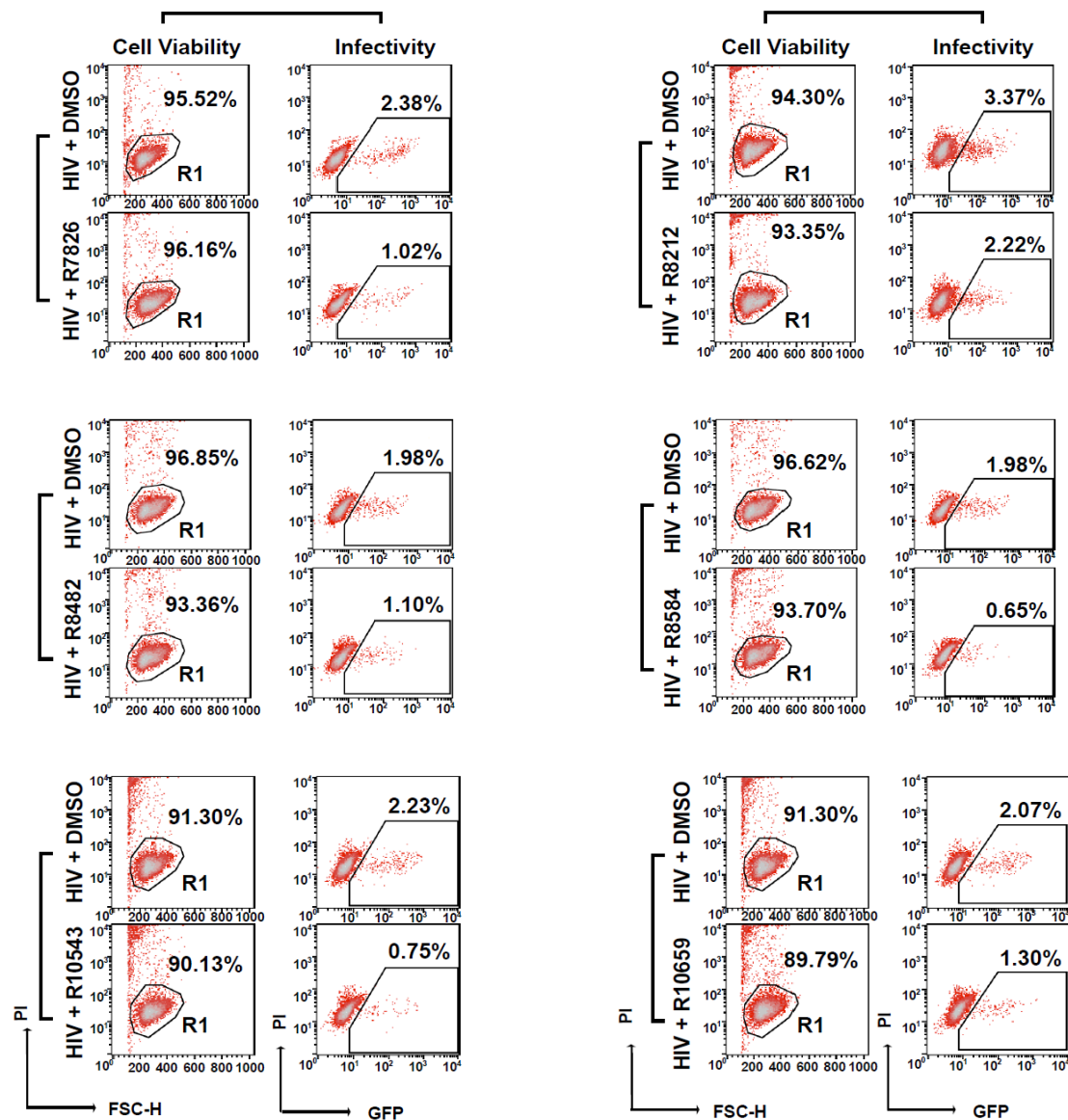


Figure 2.4 Potent LIMK inhibitors from anti-HIV activity screening. All LIMK inhibitors treated cells were compared with DMSO treated groups which served as cytotoxicity control.

Discussion

The 6 potent drugs are coming from all 3 scaffolds of inhibitor designs (scaffold A based on the 4-yl-piperidine- or piperazine-benzimidazole derivatives; scaffold B derived from phenyl benzimidazole analogs, and scaffold C based on the bis-aryl urea moiety), but according to **Table 1.1** most of the ideal structures belong to the Scaffold A, including 2 compounds with the lowest IC₅₀, R10015 at 38nM and R10543 at 5nM. The scaffold A seems to be a better prototype than scaffold B and C for further structure modification.

Noticeably, all compounds showed IC₅₀ in nano molar ranges in in vitro assay but the in vivo anti-HIV activity requires much high dosage at around 100μM. There are several possible reasons for this huge difference. These compounds are hydrophobic molecules and well dissolved in DMSO, their solubility in RPMI cell culture medium might be much lower than the calculated value; therefore the actual concentration of drug in cell culture is lower than 100μM. Another possibility is that once the drugs are delivery into cells they are degraded or converted, losing their original bioactivity. Since all previous data are performed in vitro and the pharmacokinetic properties of these compounds in T cells or T cell lines are unknown, there is no guarantee that these drugs can retain their structure long enough and block LIMK's phosphatase activity in vivo.

Chapter 3: Medicinal chemistry of R10015 and its in vitro assay

Introduction

During our preliminary medicinal chemistry efforts, we have designed and developed a series of LIMK inhibitors from 3 scaffolds as mentioned in previous episodes. R10015 was chosen from the 25 compounds as the most ideal drug for mechanism study.

The synthesis of Methyl 2-(1-(5-chloro-7H-pyrrolo[2,3-d]pyrimidin-4-yl)piperidin-4-yl)-1H-benzo[d]imidazole-5-carboxylate (R10015) flowchart is provided by Dr. Yangbo Feng as shown in **Figure 3.1**. The general synthesis of all other compounds procedures are concisely described in methods part of this Chapter as well.

R10015 is designed to function as an ATP-site hinge binding group bound to the backbone of hinge residue Ile416 on LIMK crystal structure with H-bonding interactions, acting as Type-I ATP-competitive kinase inhibitors. The hinge interaction between LIMK and R10015 will be tested by docking studies. The specificity of R10015 targeting LIMK will be tested by biochemical assay against 62 kinases compared to the control (DMSO, 100%).

Materials and Methods

Synthesis of R10015: Commercially available reagents and anhydrous solvents were used without further purification unless otherwise specified. Thin layer

chromatography (TLC) analyses were performed with precoated silica gel 60 F254 plates. Mass spectra were recorded by LC/MS with a Finnigan LCQ Advantage MAX spectrometer from Thermo Electron®. Flash chromatography was performed on prepacked silica gel columns (230-400 mesh, 40-63 μm) by CombiFlash® with EtOAc/hexane or MeOH/DCM as eluent. Preparatory HPLC was performed on a SunFire C18 OBD column, 10 μm (30 x 250 mm), with CH₃CN + 50% MeOH/H₂O + 0.1% TFA as eluent to purify the targeted compounds. Analytic HPLC was performed on an Agilent Technologies 1200 Series HPLC with CH₃CN (Solvent B)/H₂O + 0.9% CH₃CN + 0.1% TFA (Solvent A) as eluent; the targeted products were detected by UV in the detection range of 215-310 nm. NMR spectra were recorded with a Bruker® 400 MHz spectrometer at ambient temperature with the residual solvent peaks as internal standards. The line positions of multiplets were given in ppm (δ) and the coupling constants (J) were given in Hertz. The high-resolution mass spectra (HRMS, electrospray ionization) experiments were performed with a Thermo Finnigan Orbitrap mass analyzer. Data were acquired in the positive ion mode at a resolving power of 100,000 at m/z 400. Calibration was performed with an external calibration mixture immediately prior to analysis.

General synthetic procedures: The scheme and synthetic procedures described below are for inhibitor R10015. The syntheses of other LIMK inhibitors listed on Extended Data Table 1 followed a similar protocol. As shown in Extended Data Fig. 2, EDC (1-Ethyl-3-(3-dimethylaminopropyl) carbodiimide hydrochloride) (1.2

equivalent) was added to stirring mixture of 1 (1 equiv), 2 (1.05 equivalent), HOBt (1-hydroxybenzotriazole) (1 equivalent), and DIEA (diisopropylethylamine) (3 equivalent) in DMF (dimethylformamide). The stirring was continued at room temperature overnight, after which LC-MS indicated a complete reaction. The solvent was removed in vacuo to residue which was suspended in EtOAc (ethyl acetate). The suspension was washed with brine and saturated NaHCO₃, dried over anhydrous Na₂SO₄, and evaporated under reduced pressure to give a mixture of crude amide products 3 and 4. Without further purification, this mixture was suspended in acetic acid, and heated at 70 °C for 4 hours for ring closure to give the Boc protected 4-yl-piperidinobenzimidazole, which was purified by flash chromatography. The Boc protection was then removed by 30% TFA in DCM to yield 5 as an oil staff. Finally, a mixture of 5 and 4,5-dichloro-7H-pyrrolo[2,3-d]pyrimidine in a small amount of isopropanol was heated at 130 °C under microwave condition for 3 hours to furnish the LIMK inhibitor R10015, which was purified by reverse-phase HPLC to give a purity of > 95% based on analytical HPLC analysis (UV detection at 254 nm).

R10015 docking studies: Inhibitor R10015 was prepared for glide docking using LigPrep (Schrodinger, New York, NY). Chain A of PDB ID 3S95 was prepared using the protein preparation wizard in Maestro V 9.8 (Schrodinger, New York, NY) by removing water molecules and bound ligand, and adding hydrogen atoms. The docking grid was generated around the original ligand with a box size of 18×18×18 Å³. Docking was conducted without any constraint. The top scored docking pose was

merged to the protein for energy minimization using Prime (Schrodinger, New York, NY).

LIMK1 biochemical assay: Biochemical LIMK1 assays for all inhibitors were carried out by Reaction Biology Corporation, Malvern, PA (<http://www.reactionbiology.com>) and followed the protocols described on its website. Compounds were tested in a 10-dose IC₅₀ mode with 3-fold serial dilution starting at 10 μ M. The control compound staurosporine was tested in 10-dose IC₅₀ mode with 3-fold serial dilution starting at 10 μ M. Reactions were carried out at 10 μ M ATP, 1 μ M substrate cofilin, and 50 nM LIMK1 (final concentrations).

LIMK1 kinase specific information: Genbank Accession # NP_002305; Recombinant catalytic domain (amino acids 285-638, His tagged, purified from insect cells), activated by co-expression of ROCK1. Reagents: Base Reaction buffer; 20 mM Hepes (pH 7.5), 10 mM MgCl₂, 1 mM EGTA, 0.02% Brij35, 0.02 mg/ml BSA, 0.1 mM Na₃VO₄, 2 mM DTT, 1% DMSO. No additional cofactors were added to the reaction mixture. Reaction Procedures: (a) Prepare indicated substrate in freshly prepared Base Reaction buffer; (b) Deliver any required cofactors to the substrate solution above; (c) Deliver indicated kinase into the substrate solution and gently mix; (d) Deliver compounds in DMSO into the kinase reaction mixture; (e) Deliver ³³P-ATP (specific activity 0.01 μ Ci/ μ l final) into the reaction mixture to initiate the reaction; (f) Incubate kinase reaction for 120 min. at room temperature; (g) Spot

reactions onto P81 ion exchange paper (Whatman # 3698-915) (GE Healthcare Bio-Sciences, Pittsburgh, PA); (h) Wash filters extensively in 0.1% phosphoric acid.

Results

R10015 inhibits LIMK phosphatase activity

Docking studies of R10015 indicates that the hinge interactions with crystal structure of LIMK1 (PDB ID 3S95) can block LIMK kinase activity. In addition to the hinge interactions, the terminal aromatic moiety of these LIMK inhibitors is bound to a pocket under the P-loop with strong hydrophobic interactions (**Figure 3.2**). Additional H-bonding interaction(s), which could contribute to the high affinity of these LIMK inhibitors, might also present in this binding motif depending on the functional substitution.

R10015 is high effective in targeting LIMK1 at an IC₅₀ around 38nM

We performed a cell-free assay to measure R1005 inhibition of the LIM domain kinase using purified human LIMK1 and its substrate cofilin. The biochemical IC₅₀ value of R10015 against purified LIMK1 was determined to be approximately 38 nM (**Figure 3.3**). We also performed a profiling of R10015 against a panel of 62 kinases (**Table 3.1**). The result demonstrated that R10015 has a high selectivity, with off-target inhibition of only LRRK2 and p70S6K ($\geq 90\%$ inhibition at 1 μ M of R10015), and moderate inhibition of PKA (~76%), ROCK2 (~70%), and FLT3

(~68%).

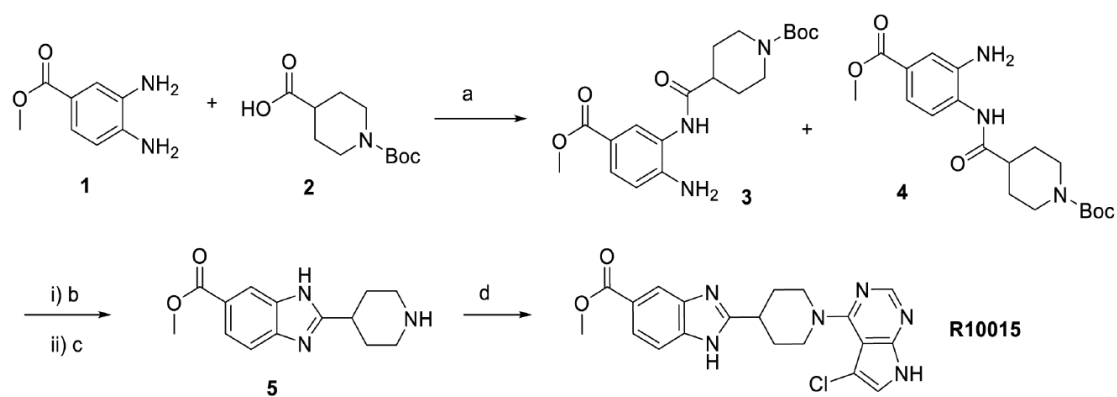


Figure 3.1 R10015 synthesis reagents and conditions. **a**, EDC/HOBt/DIEA, DMF, room temperature, 16 h. **b**, Acetic acid, 70 °C, 4 h. **c**, 30% TFA in DCM, room temperature, 1 h. **d**, 4,5-dichloro-7H-pyrrolo[2,3-d]pyrimidine, DIEA, isopropanol, 130 °C, microwave, 3 h.

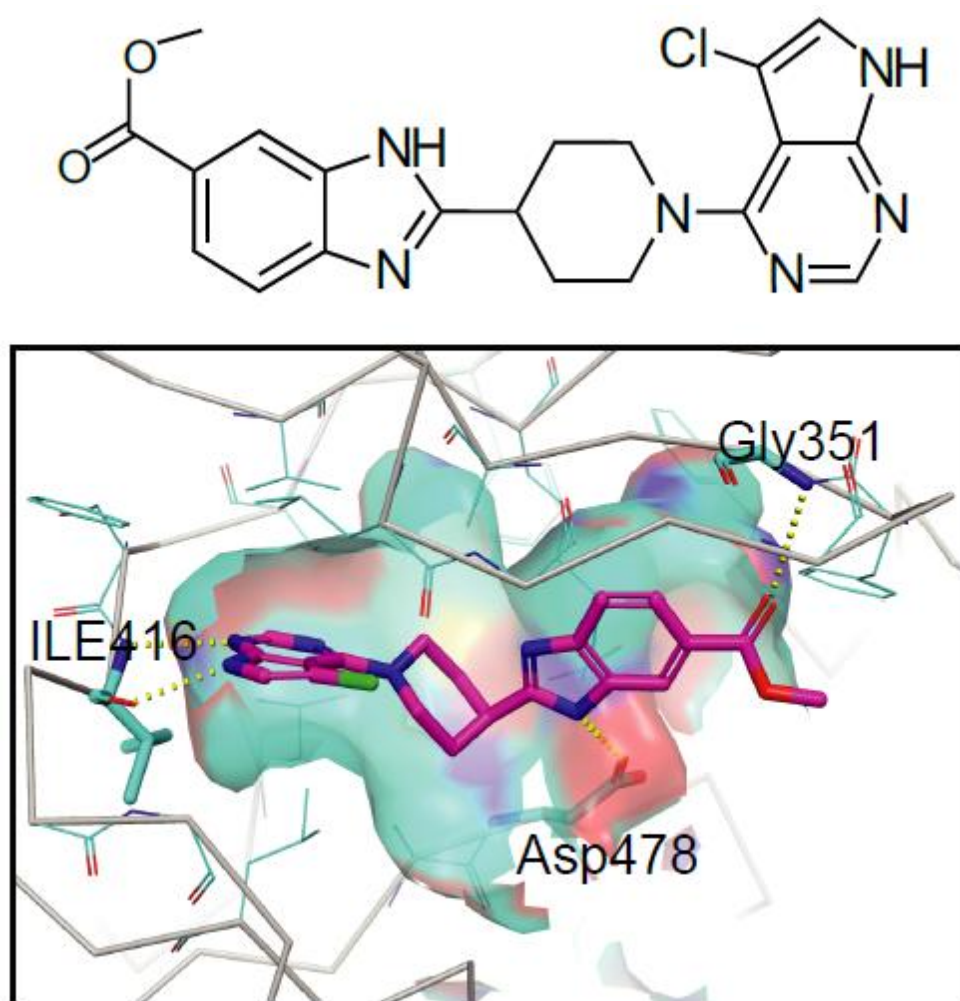


Figure 3.2 Chemical structure of R10015 and its docking into crystal structure of LIMK1 (PDB ID 3S95, Chain A). The binding motif of R10015 shows it is a typical Type-I ATP-competitive kinase inhibitor.

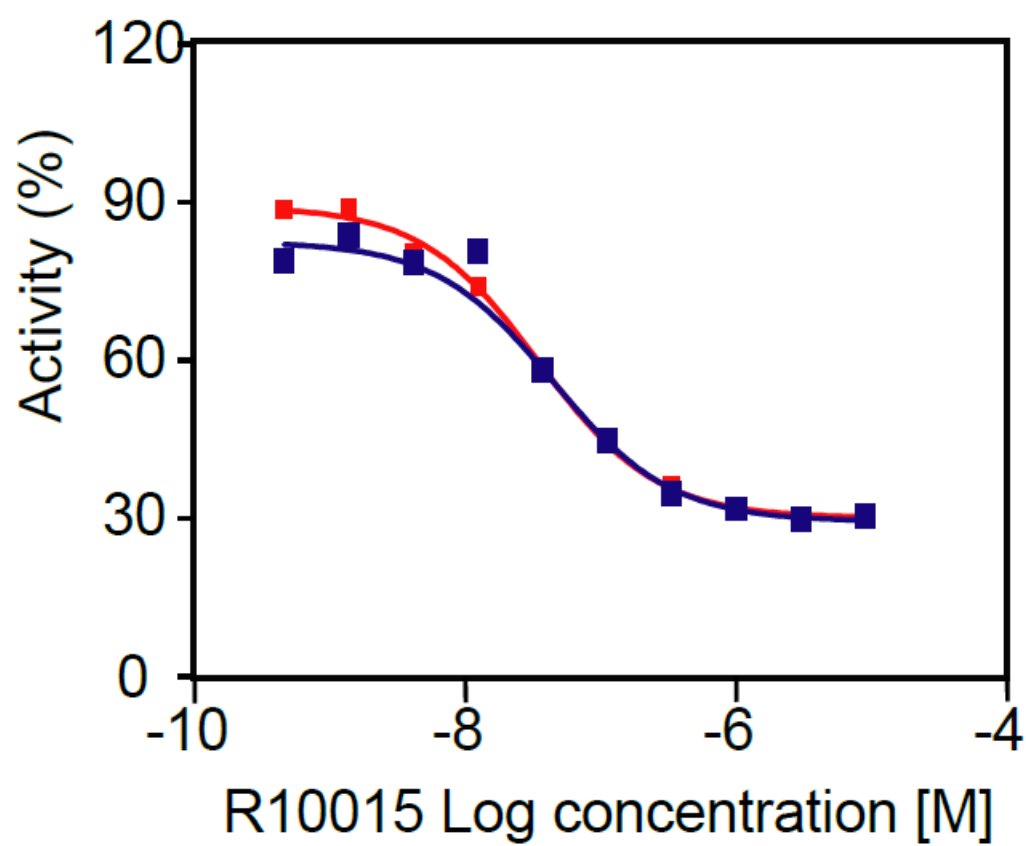


Figure 3.3 The 10-dose inhibition curve of R10015 against purified recombinant LIMK1 enzyme ($IC_{50} = 38 \pm 5$ nM).

Table 3.1 Profiling R10015 (1 μ M) against 62 kinases (DMSO control, 100% activity)

Kinase	% activity	Kinase	% activity
ABL1	89.2	LIMK1	6.4
AKT2	73.1	LRRK2 (G2019S)	6.7
ALK	95.5	MEK1	75.6
AMPK(A1/B1/G1)	76.6	MLCK/MYLK	83.3
Aurora A	60.3	MRCKa/CDC42BPA	96.5
BRAF	91.9	mTOR/FRAP1	100.0
BTK	90.2	NEK1	67.2
CAMK2b	90.8	P38a/MAPK14	98.6
CDK2/cyclin A	82.7	p70S6K/RPS6KB1	10.0
CDK5/p35	85.5	PAK2	98.2
CK1d	85.	PDGFRb	78.6
CK2a	94.2	PIM2	97.6
c-Kit	81.3	PKA	24.0
c-MET	82.1	PKCa	47.5
c-Src	92.4	PKN1/PRK1	58.6
DAPK1	87.8	PLK2	103.2
EGFR	93.2	RET	46.5

EPHA3	91.1	ROCK1	42.3
ERK2/MAPK1	87.2	ROCK2	29.5
FAK/PTK2	81.5	RSK1	47.2
FGFR1	86.5	SGK1	61.0
FLT3	32.2	SLK/STK2	108.0
GSK3b	67.8	STK16	48.6
IGF1R	90.0	STK33	56.5
IKKa/CHUK	90.5	TAK1	82.4
IKKb/IKBKB	85.1	TAOK1	54.0
IKKe/IKBKE	84.1	TBK1	82.0
JAK3	61.1	TESK1	90.2
JNK1	95.2	TLK1	98.5
JNK3	85.7	WEE1	97.2
KDR/VEGFR2	87.2	ZIPK/DAPK3	98.5

* Profiling was carried out at Reaction Biology Corporation following a protocol described at its website: <http://www.reactionbiology.com/webapps/site/>. The % data were the average of two determinations. The ATP concentration used was 10 μ M; staurosporine was used as the control for assay validation.

Discussion

The docking studies and kinase activity assay confirmed that R10015 targets LIMK and blocks its kinase activity towards cofilin. According to the kinase activity assay, R10015 is also highly effective in inhibiting Leucine-rich repeat kinase 2's (LRRK2) activity. LRRK2, believed to related to Parkinson's disease and also Crohn's disease, has protein-protein interactions with MSN, MBP and CDC37 etc which are not reported to associate with the major actin signaling pathways [84, 85]. However, R10015 partially blocks PKA and ROCK1/2 activity as well. These proteins have multiple functions on actin dynamics. Activation of PKA leads to filopodia formation while activated ROCK1/2 trigger lamellipodia formation [86-88]. Although they do not directly interact with LIMK, these two kinases both play an important role in actin activity regulation. This could be a possible explanation for the huge difference between the in vitro and in vivo IC₅₀ of R10015.

Chapter 4: Molecular and cellular characterization of R10015

Introduction

As mentioned afore in the last Chapter, R10015 inhibits the kinase activity of LIMK in vitro, its effects on T cell and T cell lines are our next concern. LIMK is known for regulation cytoskeleton, not only actin but also microtubule [89]. The two isoforms of LIMK both act as dual specific protein kinases that cause the phosphorylation of serine/threonine and tyrosine residues on cofilin [45-48]. Its own activation is dependent on the phosphorylation catalyzed by the kinase PAK1/2. Once activated, LIMK inactivates cofilin by phosphorylation. This signal leads to multiple cellular changes following actin deregulations such as cell migration, stress fiber formation, cell differentiation, extracellular matrix remodeling and metastasis [90]. Except the major downstream effector cofilin, LIMK is also believed to regulate microtubule activities by its PDZ domain. Reports showed that LIMK and tubulin colocalize in endothelial cells and overexpressed LIMK1 induces microtubule depolymerization [89]. LIMK also interact with tubulin-polymerization-promoting protein (TPPP/p25) which is a microtubule binding protein [91-93]. These studies suggest that LIMK serves as a signaling center of several cytoskeleton regulations. If the LIMK inhibitor R10015 is not highly specific to the LIMK-cofilin interaction, for instance, nonspecifically binding to the PDZ domain of LIMK, it may influence the

microtubule stability as well. Therefore, it's necessary to study the in vivo specificity of R10015. Previous studies reported by our research group showed knockdown of LIMK through siRNA decreases filamentous actin and promotes CXCR4 trafficking due to the dephosphorylation of cofilin [60]. These results suggest the inhibition of LIMK activity by R10015 may show an actin response similar to the LIMK knocking down cells. In the Chapter, we will look also look for the mechanism how the R10015 regulates actin dynamics by actin staining, chemotaxis assay etc.

Materials and Methods

Isolation of primary CD4⁺ T cell: CD4⁺ T cells were isolated by 2 rounds of negative selection using magnetic beads. The detailed procedure is described along with the methods for CD45RO memory T cells isolation in Chapter 5.

Western blotting for LIMK, cofilin and PAK2: One million resting CD4⁺ T cells were lysed in NuPAGE LDS Sample Buffer (Invitrogen, Carlsbad, CA), separated by SDS-PAGE, and then transferred onto nitrocellulose membranes (Invitrogen, Carlsbad, CA). The membranes were washed in TBST for 3 min and then blocked for 30 min at room temperature with Starting Block blocking buffer (Thermo Fisher Scientific, Grand Island, NY). For probing with different antibodies, blots were incubated with rabbit anti-p-LIMK1/2 antibodies (Cell Signaling, Danvers, MA, #3841), with rabbit anti -LIMK1 antibodies (Cell Signaling, Danvers, MA, #3842), with rabbit anti-p-cofilin antibodies (Cell Signaling, Danvers, MA, #3313), with rabbit anti- cofilin antibodies (Cell Signaling, Danvers, MA, #3318) or with rabbit anti-PAK2 antibody

(Cell Signaling, Danvers, MA, #2607). These antibodies were diluted in 2.5% milk/TBST and rocked overnight at 4 °C. The blots were washed three times for 15 min, incubated with anti-rabbit horseradish peroxidase-conjugated secondary antibodies (KPL, Gaithersburg, MD, 072-07-13-06) (1:5000) for 1 hour, and then developed with SuperSignal West Femto Maximum Sensitivity Substrate (Thermo Fisher Scientific, Grand Island, NY). For loading control, the same blots were also stripped and reprobed with antibodies against GAPDH (Abcam, ab9483) (1:1000). Images were captured with a CCD camera (Protein Simple, San Jose, CA).

Intracellular p-cofilin staining and flow cytometry: One million resting CD4⁺ T cells were fixed by adding (V/V=1/24) 4% paraformaldehyde directly into the culture medium to obtain a final concentration of 1.5% formaldehyde. Cells were incubated in fixative for 10 min at room temperature and pelleted, then permeabilized with 500 µl/ million cells ice cold methanol, washed twice in 2ml of PBS containing 4% BSA. Cells were pelleted and supernatant was decanted, leaving about 100 µl left in tube. Cells were stained with 2 µl/sample of rabbit anti-human p-cofilin antibodies (Cell Signaling, Danvers, MA) for 60 min at room temperature. Cells were washed twice with PBS plus 4% BSA and stained with 10 g/ml Alexa Fluor 647 (Abcam, Cambridge, MA)-labeled chicken anti-rabbit antibodies (Invitrogen, Carlsbad, CA) and incubated at room temperature for 30 min, avoid light. Cells were washed using the same wash medium twice, and then analyzed on a FACSCalibur (BD Biosciences, San Jose, CA).

Chemotaxis assay: Prior to chemotaxis assay, the polycarbonate membrane of a 24-well transwell plate (Corning, Corning, NY) was equilibrated in RPMI medium (The lower chamber was filled with 600 μ l of medium premixed with SDF-1 at 40 ng/ml and 100 μ l RPMI medium was filled in the upper chamber) at 37 $^{\circ}$ C for 2 hour before the assay. The upper chamber medium was then replaced with half million of Jurkat T cells in 100 μ l. Cells were allowed to undergo chemotaxis for 1 hour at 37 $^{\circ}$ C and 5% CO₂. Cells were then collected from the upper and lower chambers and counted. Where indicated, different concentrations of R10015 were added to the culture supernatant prior to the assay along with a DMSO control group

FITC-Phalloidin staining of F-actin and flow cytometry: F-actin staining using FITC-phalloidin (Sigma-Aldrich, St. Louis, MO) was carried out using 1×10^6 cells. Cells were pelleted, fixed, and permeabilized with CytoPerm/Cytofix buffer (BD Biosciences, San Jose, CA) for 20 min at room temperature and washed with cold Perm/Wash buffer (BD Biosciences, San Jose, CA) twice, followed by staining with 5 μ l of 0.3mM FITC-labeled phalloidin (Sigma-Aldrich, St. Louis, MO) for 30 min on ice in the dark. Cells were washed twice with cold Perm/Wash buffer, resuspended in 1% paraformaldehyde, and analyzed on a FACSCalibur (BD Biosciences, San Jose, CA).

Results

R10015 inhibits the phosphorylation of cofilin

To further confirm that the inhibition of cofilin phosphorylation is directly through blocking LIM kinase, we examine upstream signaling molecules that regulate LIMK kinase activity. As shown in **Figure 4.1**, we found that R10015 did not inhibit the threonine 508/505 phosphorylation of LIMK1/2 itself by the upstream kinase PAK2, whose activity is regulated by upstream Rho family GTPases such as Rac, cdc42, and Rho [60, 94]. Less than 5% of p-cofilin was left since 30 minute marker of the drug treatment, while the t-cofilin level slightly decreased during the drug treatment as presented in **Figure 4.2**. p-LIMK1/2 levels increased at 30 min but decreased at 2 hour which did not follow the trend of its kinase p-PAK2 levels **Figure 4.2**, indicating these changes are not significant in the PAK-LIMK pathway. These results strongly suggest that the inhibition of cofilin serine 3 phosphorylation by R10015 came from the direct inhibition of the kinase activity of LIMK; the LIMK upstream kinases and GTPases are not the targets of R10015. These cell-based studies confirmed the high selectivity of R10015 in blocking the LIM kinase activity in human CD4 T cells.

The western blot quantification of R10015 on cofilin phosphorylation represents the drug effect on cells as a whole population. We further quantified cofilin phosphorylation in individual T cells by intracellular staining and flow cytometry. Cells were treated with R10015 for a time course, permeabilized, and stained with a rabbit anti-human p-cofilin antibody, followed by staining with Alexa Fluor 647-labeled chicken anti-rabbit antibodies. Stained cells were analyzed with flow cytometry. As shown in **Figure 4.3**, in cells not treated with R10015 (0 h),

approximately 80% of cells stained relatively high on p-cofilin. Following R10015 treatment for 1 hour, 80% of cells stained low on p-cofilin. These results coincide with the western blot data, confirming that R10015 inhibits cofilin phosphorylation in a major population of T cells.

R10015 inhibits chemotaxis in response to SDF-1

We further tested R10015 for inhibiting SDF-1-mediated chemotaxis and actin dynamics, which are known to be regulated by LIMK [95]. We observed an R10015 dosage dependent inhibition of SDF-1 mediated chemotaxis. Less than 4×10^4 cells migrated if cells were treated with 100 μ M of R10015 while 4.6×10^5 cells migrated in the sample treated with DMSO. Lower dosages of R10015 (10 μ M, 1 μ M and 100nM) inhibits approximately 40% to 50% of cell migration and 10nM of R10015 appears to be insignificant for alternating chemotaxis **Figure 4.4**.

R10015 inhibits F-actin polymerization

To further confirm that the inhibition of SDF-1-mediated chemotaxis is directly related to R10015-mediated inhibition of actin dynamics, we measured actin polymerization following SDF-1 and R10015 treatment. For measuring actin polymerization, human blood resting CD4 T cells were treated with R10015 and SDF-1 for a time course. Cells were permeabilized, stained with FITC-phalloidin and analyzed by flow cytometry. (Phalloidin is a toxin found in the death cap mushroom. It binds to F-actin irreversibly and prevents it from depolymerization [96, 97].

FITC-phalloidin binds to F-actin and stabilizes it, also visualizes F-actin for flow cytometry measurement.) Consistently, pre-treatment of resting CD4 T cells with R10015 markedly depressed SDF-1-mediated actin polymerization (**Figure 4.5** and **Figure 4.6**).

We also tested the effect of R10015 on actin polymerization/depolymerization in CEM-SS T cell line in the absence of chemokine stimulation. As shown in **Figure 4.7**, throughout the 4 hours of drug treatment, we observed a progressive actin depolymerization pattern. This result further confirmed actin skeleton is destabilized due to the increasing activity of cofilin, as the LIMK kinase activity is inhibited.

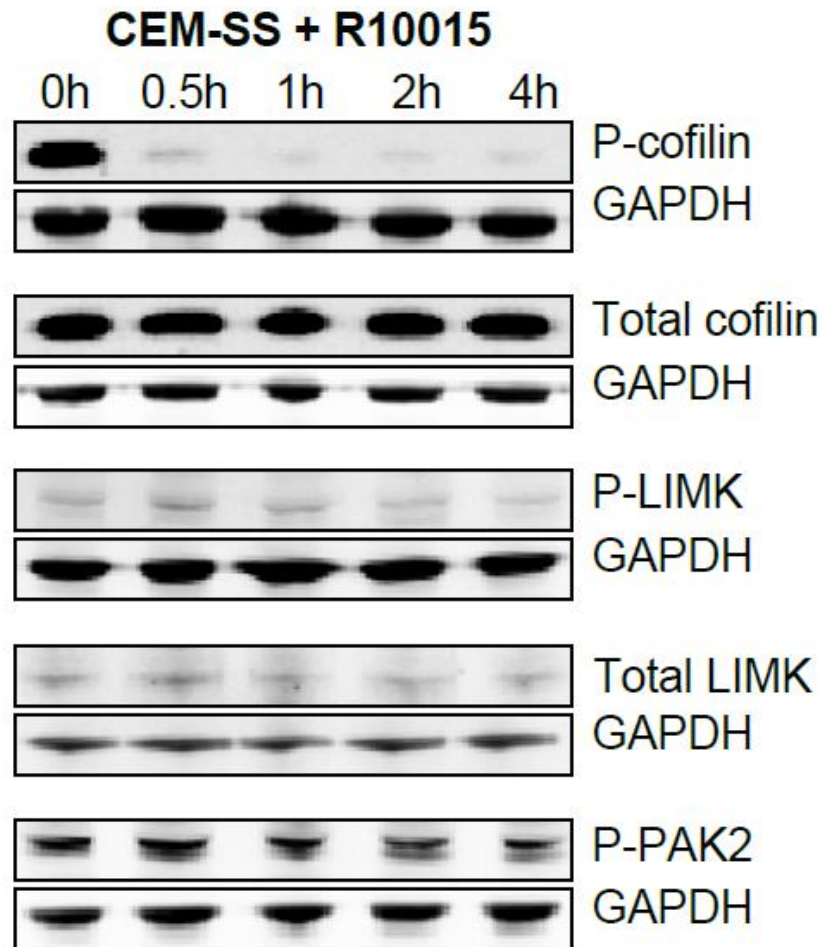


Figure 4.1 R10015 blocks cofilin serine 3 phosphorylation in human T cells.

CEM-SS T cells were treated with R10015 (100 μ M) for a time course, and the phosphorylation of cofilin, LIMK, and PAK1/2 was measured by Western blot as well as GAPDH.

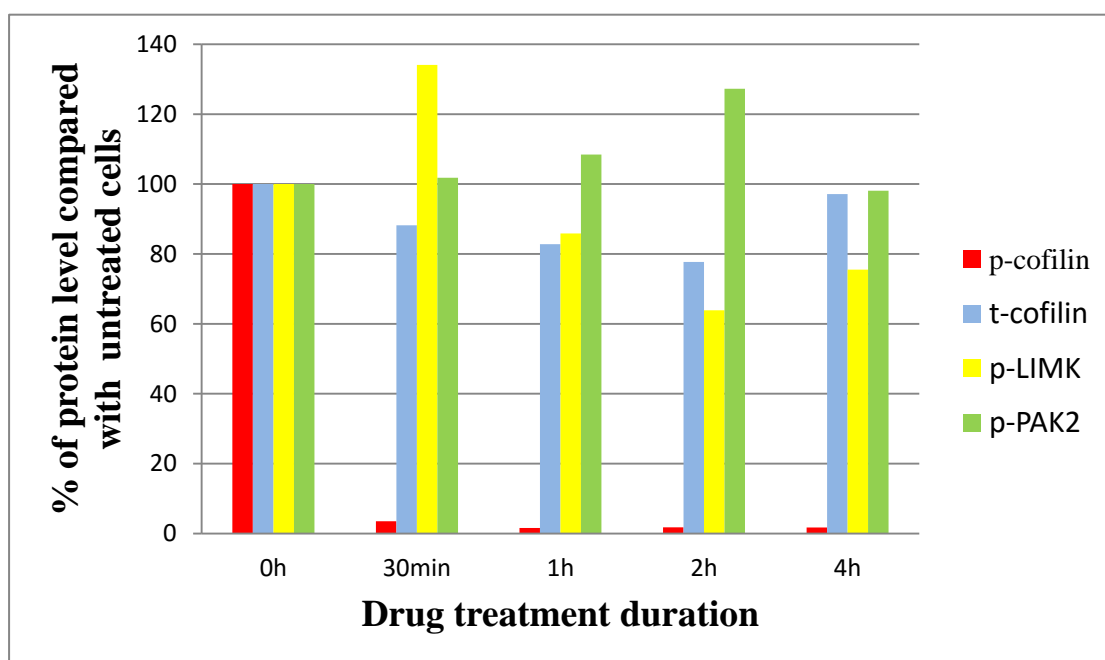


Figure 4.2 Western blot results of p-cofilin, t-cofilin, p-LIMK and p-PAK2

Normalized by GAPDH. All samples for each protein are compared with the “0h” cells which are not treated with R10015.

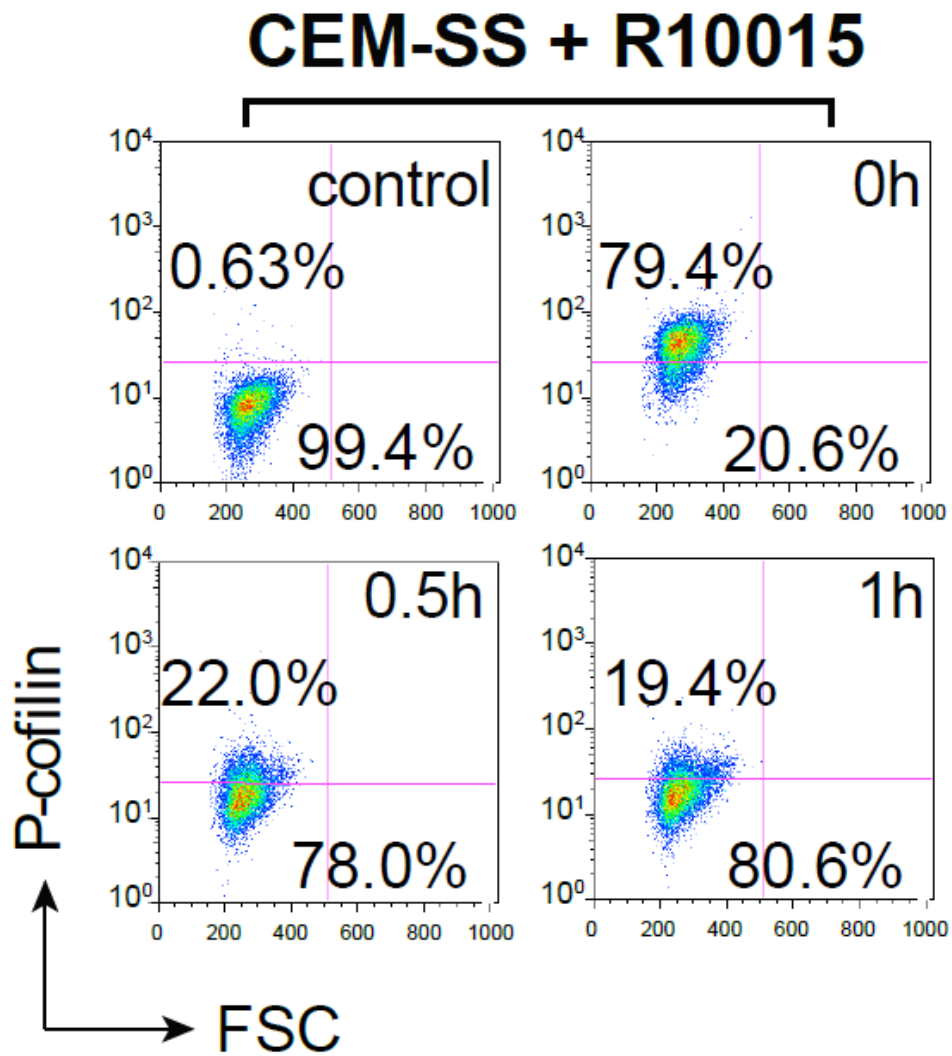


Figure 4.3 Cofilin phosphorylation in R10015 treated CEM-SS T cells was measured by intracellular staining.

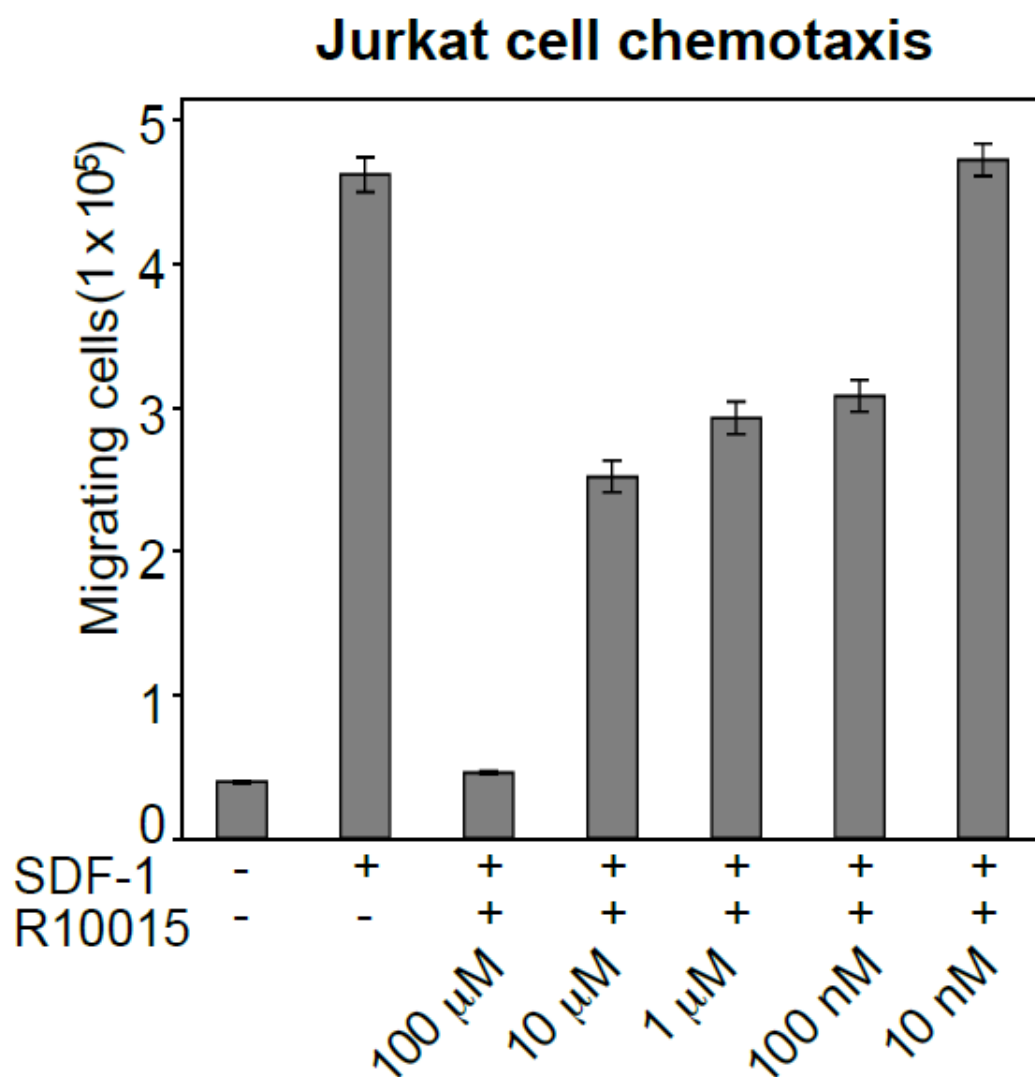


Figure 4.4 R10015 inhibits Jurkat T cell chemotaxis in responding to SDF-1. Cells were treated with of R10015 and added to the upper chamber of a 24-well transwell plate. The lower chamber was filled with SDF-1 (40 ng/ml). The plate was incubated at 37 °C for 2 hours, and cells migrated to the lower chamber were counted.

Actin polymerization (+ SDF-1)

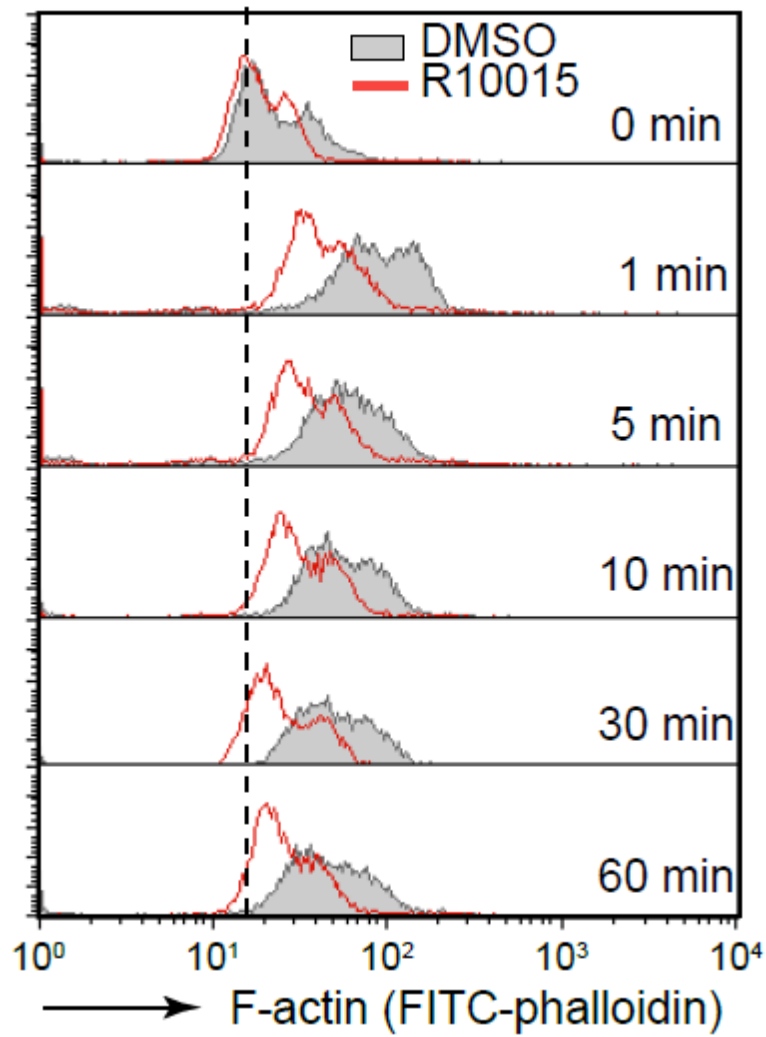


Figure 4.5 R10015 inhibits chemotactic actin activity. R10015-treated resting CD4 T cells were exposed to SDF-1. Actin polymerization was measured by FITC-phalloidin staining.

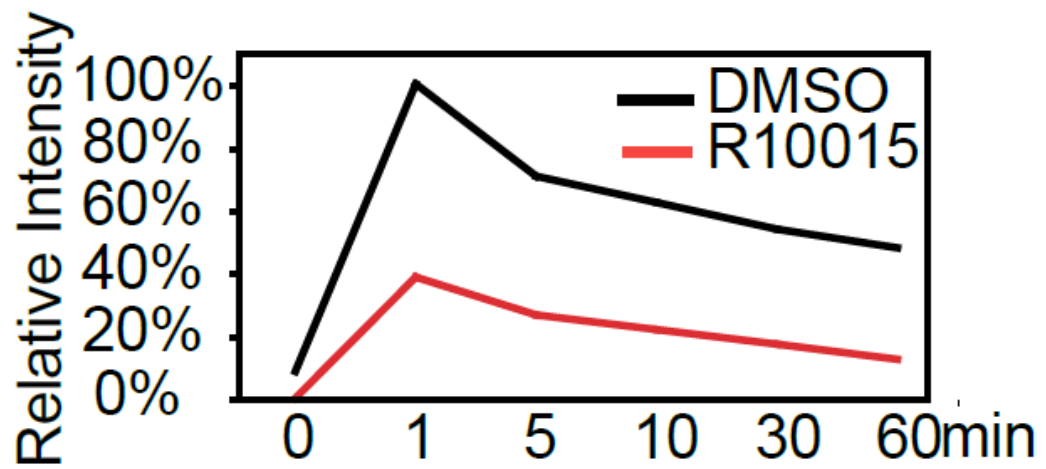


Figure 4.6 The relative intensity of F-actin staining indicates the cells treated with R10015 (red) have much weaker response to SDF-1 stimulation when compared with DMSO treated cells (black).

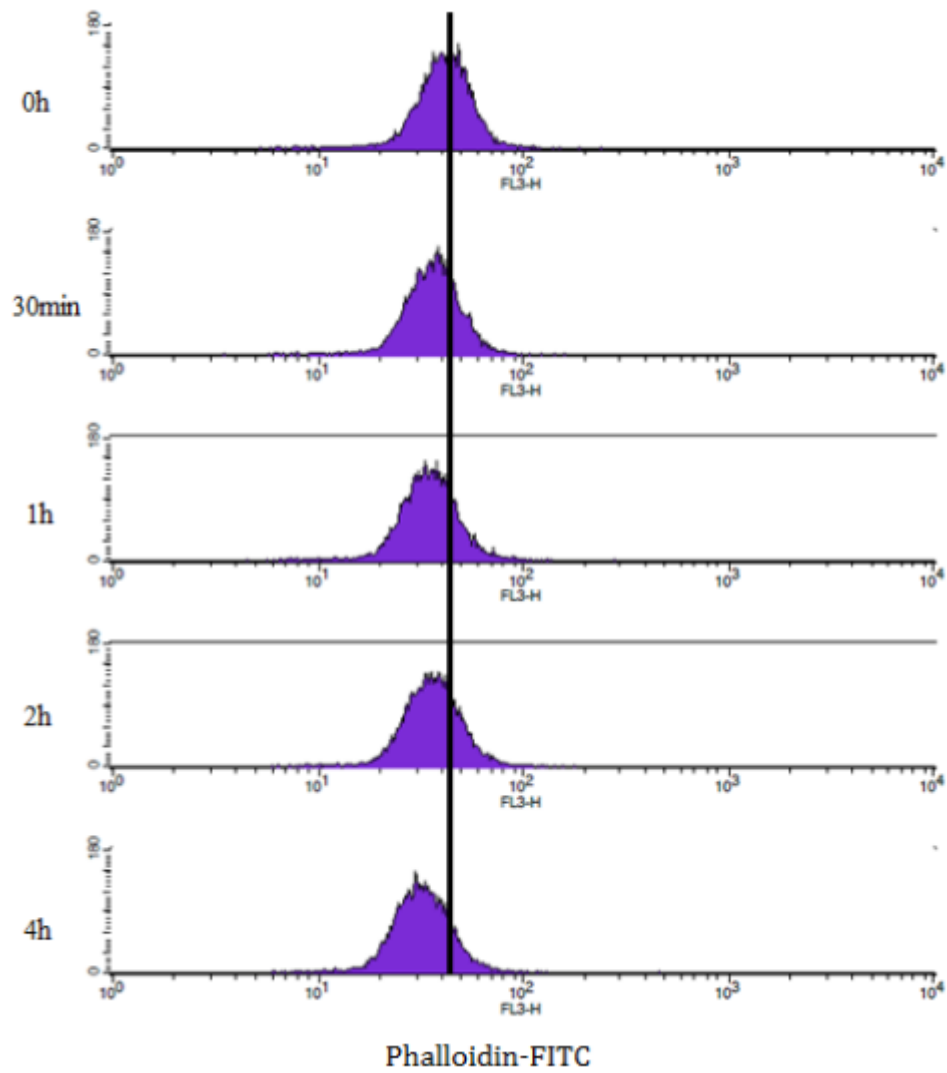


Figure 4.7 The relative intensity of F-actin without chemokine stimulation demonstrates that R10015 causes F-actin depolymerization in CEM-SS T cells. The black vertical bar indicates the location of F-actin peak of cells in the absence of R10015.

Discussion

The western blot of PAK, LIMK and cofilin indicates R10015 is highly effective in inhibiting the conversion from cofilin to p-cofilin which is catalyzed by p-LIMK. Although the t-cofilin, p-LIMK and p-PAK2 levels slightly changed during the drug treatment, p-cofilin diminished much more drastically when compare with the others (**Figure 4.2**). As previously mentioned in the in vitro kinase assay (**Table 3.1**), R10015 has only nuance effects on PAK (98% activity), but is able to partially inhibit ROCK1/2 proteins. ROCK is involved in the actin signal transduction as the downstream molecule of the Rho family proteins which is similar to PAK; it's also considered the upstream factor of LIMK for controlling microtubule dynamics and spindle orientation [87, 88, 92]. Due to the complexity of actin signal pathways, we cannot exclude the possibility that R10015 may nonspecifically bind to other molecules and alter actin activities. In addition, mentioned in the synthesis methods of R10015, the product purity is >95% meaning there are around 5% of byproduct left in the stock of R10015, we also cannot completely exclude the possibility that the byproduct has certain nonspecific inhibitor activity.

In the chemotaxis assay, we observed a dosage-dependent inhibition of Jurkat T cell chemotaxis, and the IC₅₀ was around 10 μ M, which is higher than the IC₅₀ (38 nM) observed in the in vitro LIMK kinase assay (**Table 3.1**). This difference in R10015 potency between the in vitro assay and in live cells likely resulted from

non-optimal properties of R10015 for intracellular delivery, which may require further medicinal chemistry optimization.

The results from chemotaxis assay and F-actin staining on resting CD4⁺ T cells both showed the R10015 treated cells' response to SDF-1 is prominently weakened. Additionally, F-actin staining in CEM-SS T cells showed direct evidence that the cells treated with R10015 underwent actin depolymerization. These data confirmed R10015 inhibits LIMK kinase activity of inactivating cofilin by phosphorylation, resulting in actin depolymerization and weaker cell migration.

Chapter 5: Mechanism of R10015's inhibition of HIV replication

Introduction

HIV infection of T cells relies on the regulation of actin activities at multiple stages of its replication process, such as receptor clustering, fusion, reverse transcription, nuclear migration, nuclear export, virion assembly and release.

The clustering of receptors CD4, CXCR4 and CCR5 are closely related to HIV viral entry process [18]. Previous research indicates these receptors' clustering is associated with an actin-crosslinking protein Filamin-A [39]. This study showed Filamin-A can link HIV-1 receptors to the actin cytoskeleton remodeling system by a RhoA-ROCK-LIMK dependent mechanism and facilitates the viral infection at early stage.

HIV reverse transcription is also believed to depend on actin modulation [36]. Following the interaction with cell surface receptors, HIV forms a structure, whose formation mechanism is yet unknown, called reverse transcription complex (RTC) in cytoplasm. Studies showed that RTC associates rapidly with the host cell cytoskeleton during HIV-1 infection and that reverse transcription occurs almost entirely in the cytoskeletal compartment. Additionally, the RTC functions are actin filaments dependent specifically (not related to the regulations of microtubule or intermediate

filaments).

After the RTC formation, the partially double-stranded DNA reverse transcription product is transported through the cytoplasm and into the nucleus as a component of a nucleoprotein preintegration complex (PIC) containing a subset of the Gag and Pol proteins. This poorly understood process, nuclear migration, very likely depends on host factors that actively transport the PICs from the plasma membrane to the nuclear pore. These early steps in the retrovirus replication cycle undoubtedly require the participation of multiple cellular factors for their successful completion. Naturally, people hypothesized the nuclear migration can relate to the cytoskeleton dynamics, such as microtubule and actin.

As suggested by several publications from colleagues in my lab [18, 60, 98] HIV nuclear migration is highly dependent on cortical actin, rather than microtubule. Researchers used multiple microtubule regulatory compounds such as taxol, vinblastine, colchicines and nocodazole to test the possible interaction between microtubule and HIV in CD4⁺ T cell. Despite these drugs are known for disturbing microtubule integrity, there was no impact observed on HIV replication, indicating that microtubule is not essential for HIV nuclear migration [71]. On the other hand, it's found that HIV infectivity in resting CD4⁺ T cells is hindered due to the static cortical actin layer that blocks nuclear migration. HIV mediates cofilin activity via binding to CXCR4 with viral protein gp120 and triggering signal transduction that

promotes actin treadmilling [18]. Furthermore, knocking down of cofilin's upstream factor LIMK by siRNA inhibits viral DNA synthesis. In resting CD4 T cells, actin polymerization can be triggered through transient treatment with okadaic acid which causes the activation of LIMK and promotes HIV latent infection of resting CD4 T cells [60]. Last but not least, inhibition of Arp2/3, an actin binding protein complex leading to actin nucleation and branching, drastically inhibited HIV-1 nuclear migration and infection of CD4 T cells. It's believed that Arp2/3 and its upstream regulator, WAVE2, are essential co-factors hijacked by HIV for intracellular migration [41].

Budding, considered as the final step in HIV-1 replication cycle, is the release of nascent viral particles from the host cell. As an enveloped virus, HIV-1 acquires its bilayer envelop by budding through the cellular membrane of CD4⁺ T cells. Studies showed that inhibiting small GTP binding proteins involved in cortical actin dynamics disrupts virus release. It's also suggested the actin polymerisation process is involved in viral budding, via Cdc42 [99].

For virus cell-cell transmission, actin-dependent filopodium is related to the formation of Env–receptor interactions; and for virion assembly and budding, the recruit of viral proteins is associated with actin rearrangements as well [100].

In this Chapter, we tested the LIMK inhibitor R10015's effects at different stages of HIV infection, including receptor clustering, fusion, nuclear migration, and virion

release. We also tested its inhibition of HIV in resting CD4⁺ T cells and memory T cell. Lastly, we applied several potent LIMK inhibitors, including R10015 and other newly designed compounds, onto mice models to evaluate their toxicity and the feasibility of future experiments on animal models.

Materials and Methods

Viruses and viral infection: The VSV-G pseudotyped HIV-1 was made from 293T cells by transfecting pNL4-3 $\Delta\Psi$ (gp160env), pCMV Δ R8.2 and pHCMV-G constructs together at the ratio of 1:3:4. Supernatant was harvested at 48 hours post cotransfection. VSV-G pseudotyped HIV-1 infection follows a similar procedure as described in Chapter 2.

The BalM-Vpr viruses were produced by cotransfection of HeLa cells with three plasmids: pHIV-1_{NL4-3}, pAdvantage (Promega) and pCMV4-3Blam-Vpr (from Dr. Warner C Greene) at the ratio of 6:1:2. Supernatant was harvested at 48 hours post cotransfection, concentrated with size exclusion Vivaspin 20 concentrator (Sartorius Stedim Biotech) at 6000g for 15 min 4 °C.

HIV-1(AD8) viruses were produced similarly to the procedure for wt HIV-1 production as mentioned in Chapter 2.

For viral infection of resting CD4⁺ T cells, unless otherwise specified, 10⁶ cells were treated by LIMK inhibitors for 1 hour. 10^{3.5} to 10^{4.5} TCID₅₀ units of HIV-1 were

used to infect 10^6 cells. During infection, LIMK inhibitors were added to maintain the drug concentration. Cells were washed once and then resuspended into fresh medium (10^6 cells per ml) and incubated for 5 days without stimulation. Cells were activated with anti-CD3/CD28 magnetic beads at 4 beads per cell. Culture supernant (100 μ l) was taken every two days or daily after stimulation. Cells were removed by centrifugation and the supernatant was saved for p24 ELISA.

Luciferase assay: To detect Luciferase enzyme activity in Rev-CEM-GFP-Luc cells, equal volume of cell mixture was collected and spun down at 12000rpm for 1 min, and the pellet resuspended in 1 ml PBS buffer. The cells were again spun down at 12000rpm for 1 min and supernatant was removed without disturbing the pellet. The cells were resuspended in 100 μ L of either $1\times$ reporter lysis buffer (Promega) or $1\times$ cell culture lysis reagent (Promega). The Luciferase substrate used in this protocol was the Luciferase Assay Substrate (Promega). To hydrate the lyophilized substrate, 10 ml of Luciferase Assay Buffer was added. The hydrated substrate was either used right away or stored in aliquots of 1 ml at -80°C . The substrate is light sensitive and therefore the product was covered at all times in aluminum foil. Before the samples were run on the Promega Glomax Multi Detection System, the PMT was activated and the machine was primed no longer than 10 min before the reading. The priming needs around 900 μ L of Luciferase Assay Buffer with substrate added. For each reading, a sample of cells only and a sample of lysis buffer only were run for the background reading control. Then the samples were pipette on a 96-well plate.

According to the selected protocol “Luciferase Assay Protocol”, 100µL of the Luciferase Assay Buffer with substrate was added to each sample. The data was transferred to Microsoft Excel for analysis.

Surface staining of CD4 and CXCR4: Cells were stained with PE-labeled monoclonal antibody against human CD4 (clone RPA-T4) or CXCR4 (clone 12G5): anti-CD4-PE, (BD Bioscience, Cat No. 555347), isotype: Mouse IgG1κ, anti-CXCR4-PE, (Biolegend, Cat No. 306506), isotype: Mouse IgG2α,κ. Cells were coated with ChromPure Mouse IgG (Jackson ImmunoResearch Lab, Cat No 015-000-003), stained on ice in PBS + 0.1% BSA for 30 minutes avoid light, washed twice with cold PBS-0.5% BSA, and then analyzed on a FACSCalibur (BD Biosciences, San Jose, CA).

Blam-Vpr Assay: Viral fusion assays were performed as described in detail in “*A sensitive and specific enzyme-based assay detecting HIV-1 virion fusion in primary T lymphocytes*” [101]. Briefly, the viron-based fusion assay was conducted in three sequential steps: (i) incubation of CD4+ T cells with virions, (ii) loading of cells with the CCF2/AM dye, and (iii) development and detection of the Blam reaction. For infection of resting CD4+ T cells, 1750ng p24 of HIV-1(Blam-Vpr) were incubated with 1 million cells at 37 °C for 2 hours, washed in CO₂-independent medium (Gibco), and then loaded with CCF2/AM dye (Invitrogen). To prepare the loading solution, 2 µl of CCF2/AM (1mM) was mixed with 81 ml of 0.1% acetic acid containing 100

mg/ml Pluoronic-F127R, and 1 ml of CO₂-independent medium was added to constitute the loading solution. Cells were incubated in 100 µl of the loading solution for 1 hour at room temperature. After two washes with CO₂-independent medium, the Blam reaction was allowed to develop for 16 hours at room temperature in 200 µl of CO₂-independent medium supplemented with 10% FBS and 2.5 mM probenecid, a nonspecific inhibitor of anion transport (Sigma Pharmaceuticals). No antibiotics were added to the culture medium. Finally, the cells were washed once in PBS and fixed in a 1.2% solution of paraformaldehyde. Flow cytometry was performed using a Becton Dickinson LSR II system (Becton Dickinson). B-lactamase and CFF2 measurements were performed using a 407 nm violet laser with emission filters of 525/50 nm (green fluorescence) and 440/40 nm (blue fluorescence), respectively. Green and blue emission spectra were separated using a 505LP dichroic mirror. The UV laser was turned off during the analysis. A fusion inhibitor, T20, was used in the assay as a control group [102].

HIV DNA synthesis by Quantitative real-time PCR: One million/sample of CEM-SS T cells were infected with a total of 135ng p24 of HIV-1 virion. At designed time points, cells were washed twice in RPMI medium and spun down at 13000rpm for 5min. After vacuuming the supernatant, cell pellet was resuspended in 175 µl of lysis buffer (SV Total RNA Isolation Kit, Promega). Genomic DNA was extracted using the SV Total RNA Isolation Kit as recommended by manufacturer. DNA extracted from different samples were normalized at the same concentration and equal

amount of cellular DNA (10ng/μl) was used for quantitative real-time PCR analyses of total, full-length DNA carried out by using the Bio-Rad iQ5 real-time PCR detection system. The TaqMan Gene Expression Master Mix (Applied Biosystems, Life Technology) was utilized in the quantitative real-time PCR with the forward primer: 5'LTR-U5: 5'-AGA TCC CTC AGA CCC TTT TAG TCA-3'; and the reverse primer: 3'gag: 5'-TTC GCT TTC AAG TCC CTG TTC-3'; and the probe, FAM-U5/gag: 5'-(FAM)-TGT GGA AAA TCT CTA GCA GTG GGG CC-(BHQ)-3' (Integrated DNA Technologies) at the final concentration of 300nM each. The DNA standard used for late viral DNA quantification was constructed by using plasmid pNL4-3. DNA was extracted and linearized by XhoI digestion. For the standard DNA copy, 10¹ to 10⁶ copies of pNL4-3 mixed with DNA (10ng/μl) from uninfected CEM-SS T cells were applied [18].

2-LTR-circles by Quantitative real-time PCR: The measurement of 2-LTR-circles follows a similar procedure as the HIV DNA synthesis mentioned above by using a different set of primer and probes (MH536, MH535 and MH603) [102, 103]. 2-LTR circle forward, MH535: 5'-AAC TAG GGA ACC CAC TGC TTA AG-3'; 2-LTR reverse, MH536: 5'-TCC ACA GAT CAA GGA TAT CTT GTC-3'; and 2-LTR probe, MH603: 5'-(FAM)-ACA CTA CTT GAA GCA CTC AAG GCA AGC TTT-(TAMRA)-3'.

In-house ELISA for p24 antigen: Wells were primed with 100μl of priming buffer containing HIV-1 p24 monoclonal antibody (NIH AIDS Reagent Program) over

night. (This affinity purified antibody had as stock concentration of 5 mg/ml and 8µl was diluted into 10 ml sterile PBS buffer). The next day, the plate was washed 3 times with PBS in a plate washer (Bio-tek EL50) then the plate was dried. Next, 250 µl blocking buffer (PBS+ 5%FBS) was added to each well and the plate was covered with an ELISA plate cover and incubated for 1 hour at 37 °C. The samples were thawed and dilution in a 1:10 serial pattern as needed. A standard was prepared from a p24 positive control with a stock concentration at 200 ng/ml. The standard was diluted in a 1:2 ratio from 1000 pg/ml to 7.8 pg/ml. After the incubation, the plate was washed 3 times in plate washer with PBS+ 0.05% Tween and dried. Afterwards, 100 µl of standard samples were transferred to allotted wells as well as other samples. Then the plate was incubated at the same condition for 2 hours. Following the same washing and drying protocol, 100 µl of diluted HIV-IG was added to each well. HIV-IG consists of 10ml dilution buffer (PBS+ 10% FBS+ 0.5% TritonX100) and added with 0.0067% stock biotin-antibodies. The plate was incubated for 1 hour, washed and dried again. 100 µl of Streptavidin-Horseradish peroxidase (HRP) antibodies consisting of PBS+ 0.1% BSA+ 0.67% stock antibodies was added to each well and the plate was incubated for another hour. Lastly, after washing and drying, 100 µl of peroxidase substrate (10 ml 0.1M sodium acetate+ 3% of 4mg/ml tetramethylbenzidine in DMSO+ 0.05% of 30% H₂O₂) was added to each well. Plate was immediately placed into Bio-tek ELx808iu ultra microplate reader and plate kinetics were read at 630nm.

Isolation of resting CD4 T cells and CD45RO memory cells from peripheral

blood: All protocols involving human subjects were reviewed and approved by the George Mason University institutional review board. Resting CD4 T cells were purified from peripheral blood of HIV-negative donors by two rounds of negative selection as previously described. Briefly, for the first-round depletion, we used monoclonal antibodies against human CD14, CD56 and HLA-DR, DP, and DQ (BD Biosciences). For the second-round depletion, we used monoclonal antibodies against human CD8, CD11b, and CD19 (BD Biosciences, San Jose, CA). Antibody-bound cells were depleted using Dynabeads Pan Mouse IgG (Invitrogen, Carlsbad, CA). For further negative selection of the memory CD4 T cell subsets, monoclonal antibody against CD45RO (0.1 μ l per million cells) (BD Biosciences) was added during the second round of depletion. Purified cells were cultured in RPMI-1640 medium supplemented with 10% heat-inactivated fetal bovine serum (Invitrogen, Carlsbad, CA), penicillin (50 U/ml) (Invitrogen, Carlsbad, CA), and streptomycin (50 μ g/ml) (Invitrogen, Carlsbad, CA). Cells were rested overnight before infection or treatment [83].

CD25 and CD69 surface staining: A half million resting CD4 T cells were cultured for 5 days and stimulated with anti-CD3/ CD28 beads (4 beads per cell) for 24hours. Before staining, beads were washed and detached from cells by pipetting repeatedly and rapidly then isolated by a magnetic particle concentrator. Cells were stained with PE-labeled monoclonal antibody against human CD25 (clone M-A251) or CD69 (clone FN50) (BD Biosciences, San Jose, CA).

Cells were stained on ice in PBS + 0.1% BSA for 30 minutes, washed with cold PBS-0.5% BSA, and then analyzed on a FACSCalibur (BD Biosciences, San Jose, CA). PE mouse IgG 1 κ was used as the isotype control group.

Animal Experiments: Six to eight week old female C3H/HeN mice were obtained from Harlan Laboratories. Groups of 3 mice were treated once a day with compounds as follows: R10904, R10906, R10907, or R7826 delivered via oral gavages at 20 mg/kg, PBS by oral gavage as a control, R10015 (dissolved in DMSO) by i.p. injection at 10 mg/kg, or DMSO by i.p. injection as a control. Mice were weighted daily and monitored for morbidity and mortality, including lethargy and ruffled fur for 7 days. Experiments were carried out in animal bio-safety level 2 (BSL-2) facilities in accordance with the National Research Council's Guide for the Care and Use of Laboratory Animals and under GMU IACUC protocol number 0211.

Results

R10015 inhibits HIV-1 replication on CEM-SS T cells

We first quantified R10015 inhibition of the early steps of HIV infection of CD4 T cells, in which R10015 was removed from the cell culture following infection. As shown in **Figure 5.1**, Rev-CEM-GFP-Luc cells were pre-treated with different dosages of R10015 for 1 hour, infected with HIV for 3 hours, washed to remove the input virus and R10015, and then cultured for 48 hours. HIV-dependent luciferase

expression was quantified. For inhibiting HIV, R10015 showed a half maximal inhibition concentration (IC₅₀) of 14.9 μ M (**Figure 5.1**), which is close to the IC₅₀ (10 μ M) for inhibiting SDF-1-mediated chemotaxis (**Figure 4.4**). The inhibition curve is steep in the 10⁴ to 10⁵ nM range while much flatter in lower dosages, indicating that only high concentration of drug is efficient for inhibiting HIV replication.

Fortunately, high dosages of R10015 did not imply high toxicity to CEM-SS T cell line. As shown in **Figure 5.2** measured by PI staining on flow cytometer, the drug had no detectable cytotoxicity for this short period of treatment (4 hours) at all the concentrations tested (up to 200 μ M).

Figure 5.1 and Figure 5.3 showed that R10015 minimally inhibited the early steps of VSV-G pseudotyped HIV even at 100 μ M when compared with wild type HIV-1 infection. While wild type HIV infection requires interaction between viral envelop protein gp120 and specific cellular co-receptors CXCR4 and CCR5, the Vesicular Stomatitis Virus envelop glycoprotein G (VSV-G) mediated viral entry is endocytosis conducted rather than specific receptor dependent [104, 105]. Thus the VSV-G pseudotyped HIV accomplishes entry through endocytosis, bypassing the engagement with surface receptors which involves cortical actin participation. These data demonstrate that the inhibition of HIV did not result from non-specific cytotoxicity, and is indeed specific to viral processes related to HIV gp120-mediated fusion and entry. HIV gp120-mediated infection of human CD4 T cells has been known to require cortical actin dynamics [18, 106, 107]. On the other hand, the

VSV-G-mediated endocytosis bypasses the cortical actin, and thus is less susceptible to R10015. This differential susceptibility of gp120- versus VSV-G-pseudotyped virus to R10015 is in agreement with the hypothesis that R10015 inhibits HIV through direct blockage of the LIMK-regulated actin dynamics.

R10015 caused slight down regulation of CD4 and CXCR4

To further elucidate the anti-HIV mechanism, we pre-treated human CEM-SS T cells with R10015 for 1 hour, and the effect of R10015 on the surface expression of the HIV receptors, both CD4 and CXCR4, was examined [60]. This brief treatment did not alter the surface expression of CD4 or CXCR4; prolonged treatment (4 hours), however, slightly decreased the surface density of CD4 (**Figure 5.4**) and minimally decreased the CXCR4 density (**Figure 5.5**).

The effect of R10015 on viral entry is insignificant for both VSV-G and wild type HIV virion

We further examined the effect of R10015 on viral entry using an HIV entry assays, the Vpr- β -lactamase (Blam-Vpr) assay. The β -lactamase fused Vpr virion is widely used as a sensitive and specific enzyme-based assay capable of detecting HIV virion fusion into T lymphocytes [101]. As indicated by the results from **Figure 5.6**, R10015 did not significantly inhibit viral entry, as measured by the infection with Blam-Vpr HIV-1. These data confirmed our previous experiment (**Figure 5.4** and **Figure 5.5**) that CD4 and CXCR4 surface distributions are not significantly regulated by R10015.

R10015 inhibits HIV-1 DNA synthesis

Since no prominent inhibition of HIV infection was observed from early stage, we looked into the post entry stage of viral infection such as viral DNA synthesis and nuclear migration etc. For these stepwise mappings, we used a single-cycle virus, HIV-1(Env), which is pseudotyped with HIV-1 gp160. CEM-SS T cells were pretreated with R10015 for 1 hour, and then infected with HIV-1(Env) for 2 hours in the presence of R10015. Following infection, cells were washed to remove HIV-1 and R10015, and cultured for 24 to 48 hours. The late products of HIV reverse transcription were quantified by real-time PCR. As shown in **Figure 5.7**, R10015 inhibited viral late DNA synthesis at all time points.

R10015 inhibits HIV-1 2-LTR circle formation

When HIV-1 infects host cell, its single-stranded RNA is converted into cDNA and then to double-stranded DNA that is integrated into the host chromosome. However, after the DNA fails to integrate, it transforms into a closed ring structure with two copies of the long-terminal repeat (LTR) and is referred to as 2-LTR circle [108]. Since the 2-LTR circle is a distinguishable viral DNA only exists in nucleus, it's an ideal symbol for viral nuclear migration [109, 110]. Following the HIV DNA synthesis, we also measured HIV nuclear migration using the synthesis of HIV 2-LTR circles as a surrogate. As shown in **Figure 5.8**, R10015 also inhibited viral nuclear migration, as measured by viral 2-LTR circles.

R10015 also inhibits HIV-1 replication at late stage of infection

Recently, LIMK has been suggested to be involved in retroviral budding and release; siRNA knockdown of LIMK1 prevents mature virions from leaving the plasma membrane [60]. We further tested efforts of R10015 on late stage of HIV infection. CEM-SS T cells were infected with HIV-1(Env) for 2 hours, washed, incubated for 12 hours, and then treated with R10015. Virion release from 12 to 72 hours post infection was quantified by measuring p24 release in the supernatant. As shown in **Figure 5.9**, R10015 also inhibited p24 release when applied at later stage of HIV infection. These results demonstrate that R10015 inhibited viral DNA synthesis, nuclear migration, and virion release, phenotypes consistent with those observed in shRNA/siRNA LIMK1 knockdown cells [60].

R10015 inhibits HIV-1 replication in resting CD4⁺ T cells and CD45RO memory CD4⁺ T

During HIV transmission, early viruses utilize CCR5, and mainly infect memory CD4 T cells and macrophages, whereas late viruses also utilize CXCR4 [111-113]. We tested the ability of R10015 to inhibit R5 and X4 latent infection of blood memory and resting CD4 T cells [18, 83]. In our viral latent infection system, total resting CD4 T cells or the CD45RO⁺RA⁻ memory CD4 T cells were purified from the peripheral blood, cultured overnight without stimulation, and then treated with R10015 for 1 hour. Resting T cells were infected with HIV-1(NL4-3) for 2 hours, washed, cultured for 5 days in the absence of R10015, and then activated with CD3/CD28 beads to stimulate viral replication. Viral p24 release was measured. As shown in **Figure 5.10**,

we observed that R10015 blocked X4 HIV-1 latent infection of resting CD4 T cells. We also observed a R10015 dosage-dependent inhibition of R5 HIV latent infection of resting memory CD4 T cells (**Figure 5.12**). The inhibition of HIV latent infection of resting T cells did not result from possible drug cytotoxicity, because this short drug treatment did not inhibit T cell function, as judged by the surface expression of CD25 or CD69 following T cell activation (**Figure 5.11** and **Figure 5.13**). (As proved by Caruso et al [114], CD69 is the earliest expressed antigen on stimulated T cells and cellular surface CD25 presentation also marks the activation of T cell, so both CD25 and CD69 were commonly used as T cell activation markers).

Potent LIMK inhibitors including R10015 are tolerable in mice

Our current lead compounds have low molecular weight (< 450) and are amenable to further medicinal chemistry optimization to achieve higher cell potency and appropriate drug metabolism and pharmacokinetics (DMPK) properties. Many of these LIMK inhibitors have demonstrated good antiviral activity in cells, and are generally not toxic in our cell-based assays and in mice (**Figure 5.14**). These results emphasize the feasibility of developing LIMK inhibitors as a new class of anti-HIV drugs in addition to the current AIDS therapy. Noticeably, many of the compounds, including R10015, showed even better weight measurements than results in only DMSO treated mice, suggesting they merely have any negative effects on the mice basic health conditions.

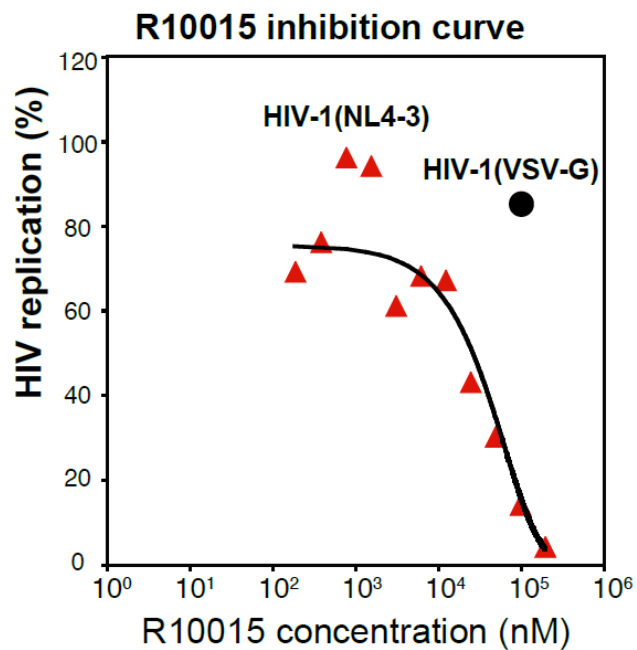


Figure 5.1 Rev-CEM-GFP-Luc cells were pretreated with different dosages of R10015 for 1 hour and then infected with HIV-1(NL4-3) for 3 hours. Cells were washed to remove the virus and the inhibitor, and incubated for 48 hours. HIV-dependent luciferase expression was quantified, and the IC₅₀ of R10015 was calculated (red triangle). For comparison, cells were also treated with 100 μM of R10015 and infected with VSV-G pseudotype HIV for 3 hours (black dot).

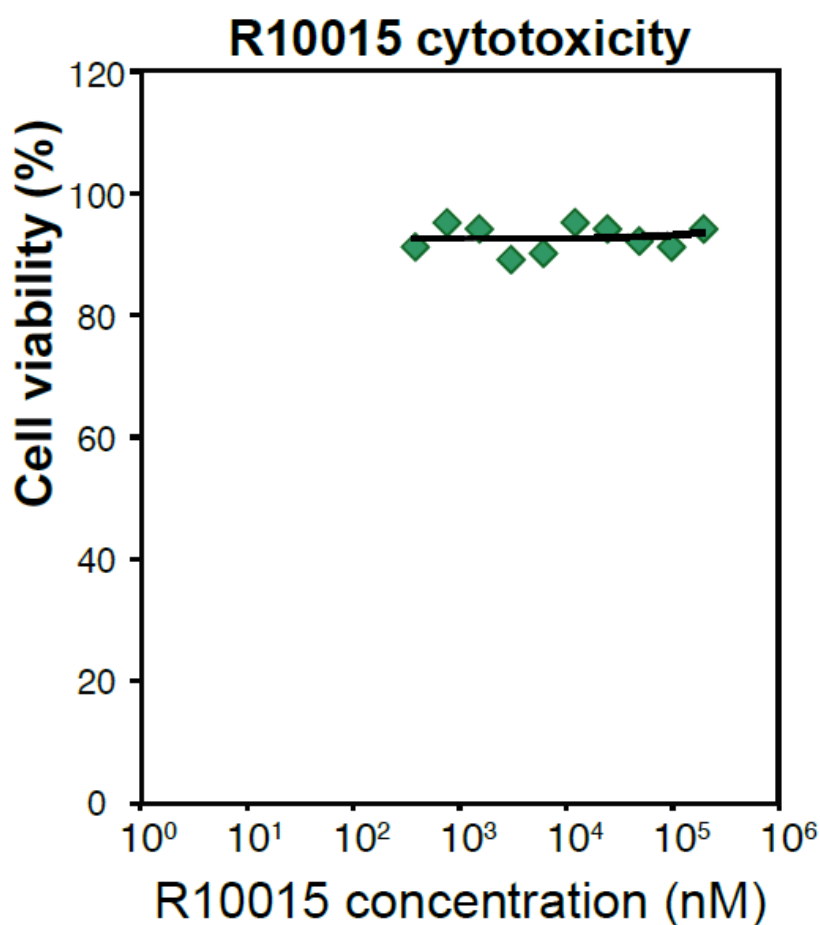


Figure 5.2 Using cells from the same samples as indicated in **Figure 5.1**, the cytotoxicity of R10015 was simultaneously measured by propidium iodide (PI) staining and flow cytometry. No sign of significant cytotoxicity was observed under the concentration as high as 200 μ M which is twice as much as the highest dosage we applied to all other experiments.

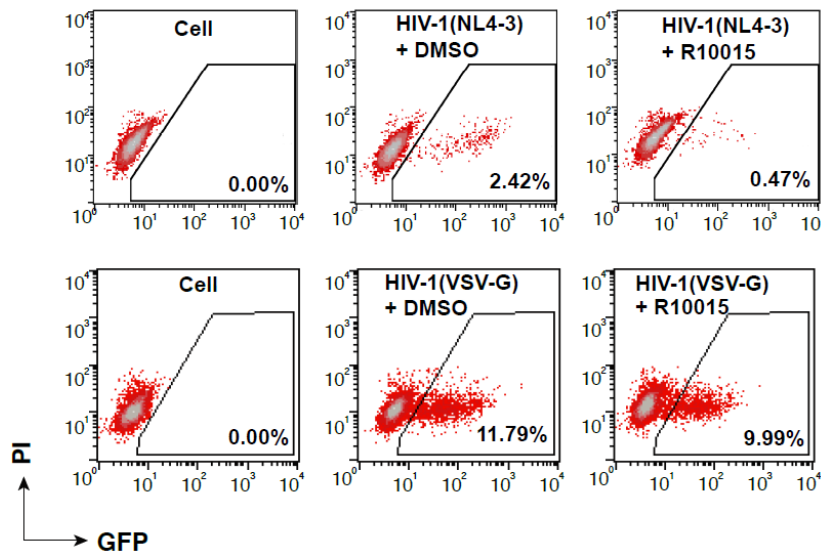


Figure 5.3 Flow cytometry results demonstrating that R10015 inhibited HIV-1(NL4-3), but minimally inhibited HIV-1(VSV-G), when cells were treated with R10015 at early stage during viral infection.

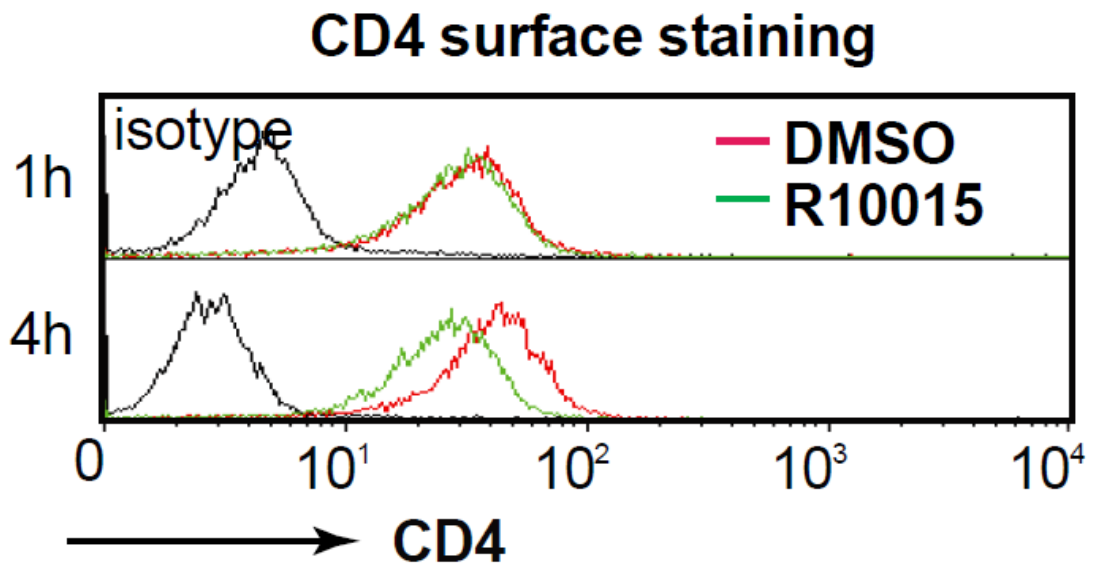


Figure 5.4 Effects of R10015 on surface CD4 expression. CEM-SS T cells were treated with R10015 (100 μ M) and then stained for surface CD4. CD4 was slightly down regulated in cells treated by R10015 for 4 hours.

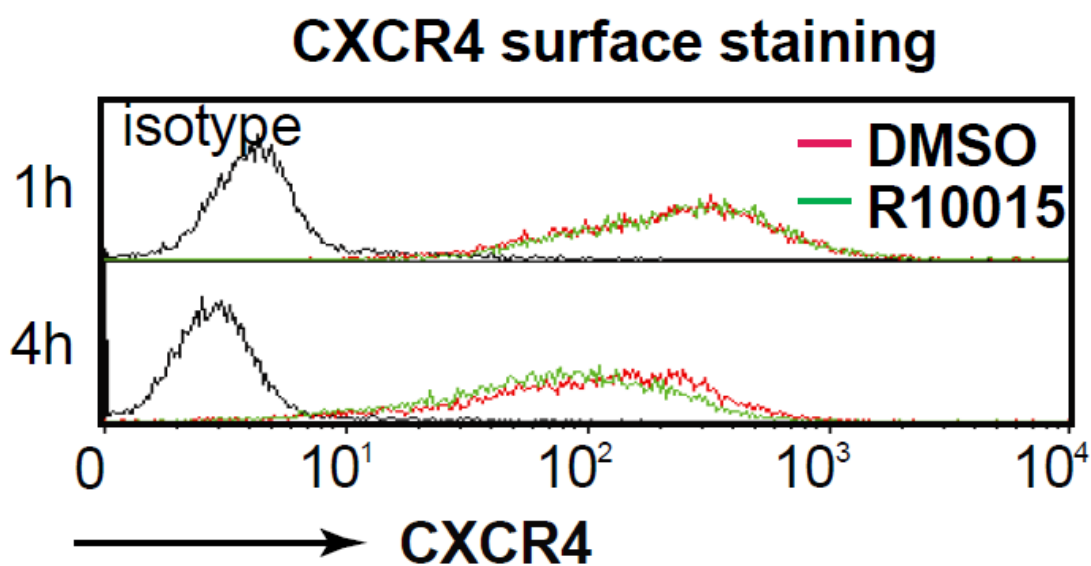


Figure 5.5 Effects of R10015 on surface CXCR4 expression. CEM-SS T cells were treated with R10015 (100 μ M) and then stained for surface CXCR4. CXCR4 was minimally down regulated in cells treated by R10015 for 4 hours.

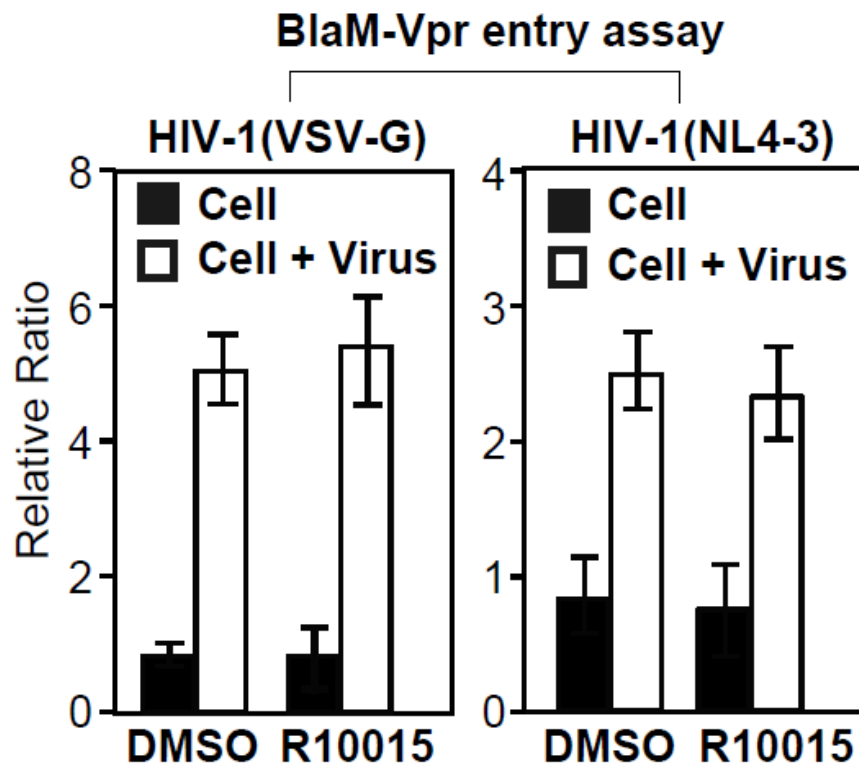


Figure 5.6 R10015 did not inhibit viral entry. CEM-SS T cells were treated with R10015 and then infected with BlaM-Vpr tagged HIV-1(NL4-3) or HIV-1(VSV-G) to measure viral entry. Measurement and analysis were done by flow cytometry and relative activities were calculated. No statistically significant difference was observed from both HIV-1(NL4-3) and HIV-1(VSV-G) infected cells.

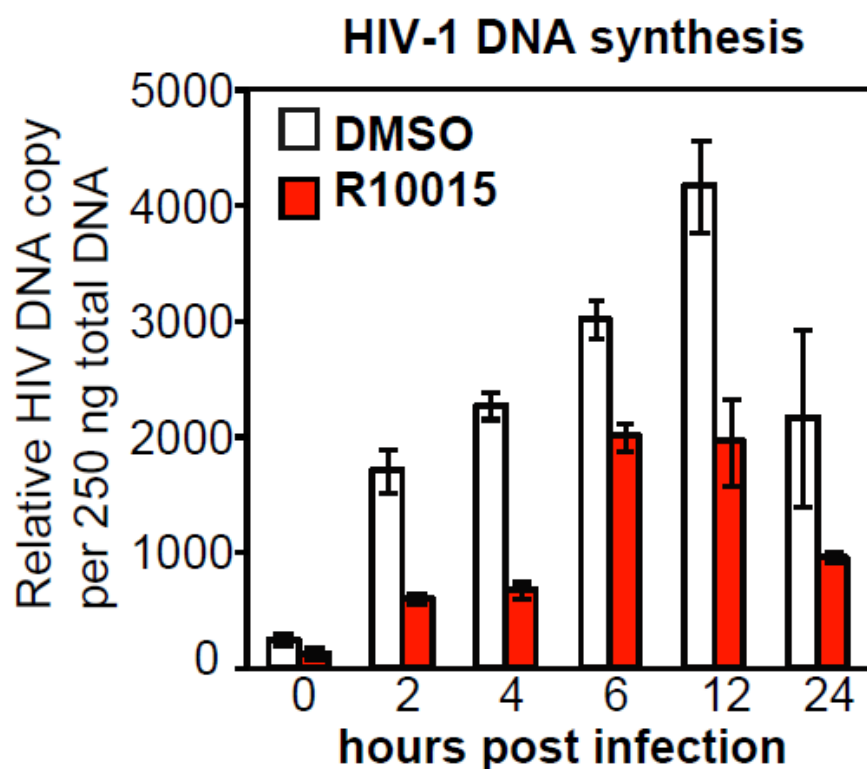


Figure 5.7 R10015 inhibits viral DNA synthesis. CEM-SS T cells were treated with R10015 for 1 hour and then infected with a single-cycle HIV-1(Env) for 2 hours in the presence of R10015. Following infection, cells were washed to remove HIV-1 and R10015. Viral DNA synthesis was measured by real-time PCR. Throughout the whole duration of sample collecting, R10015 treated cells showed lower levels of viral DNA copies than DMSO treated control group.

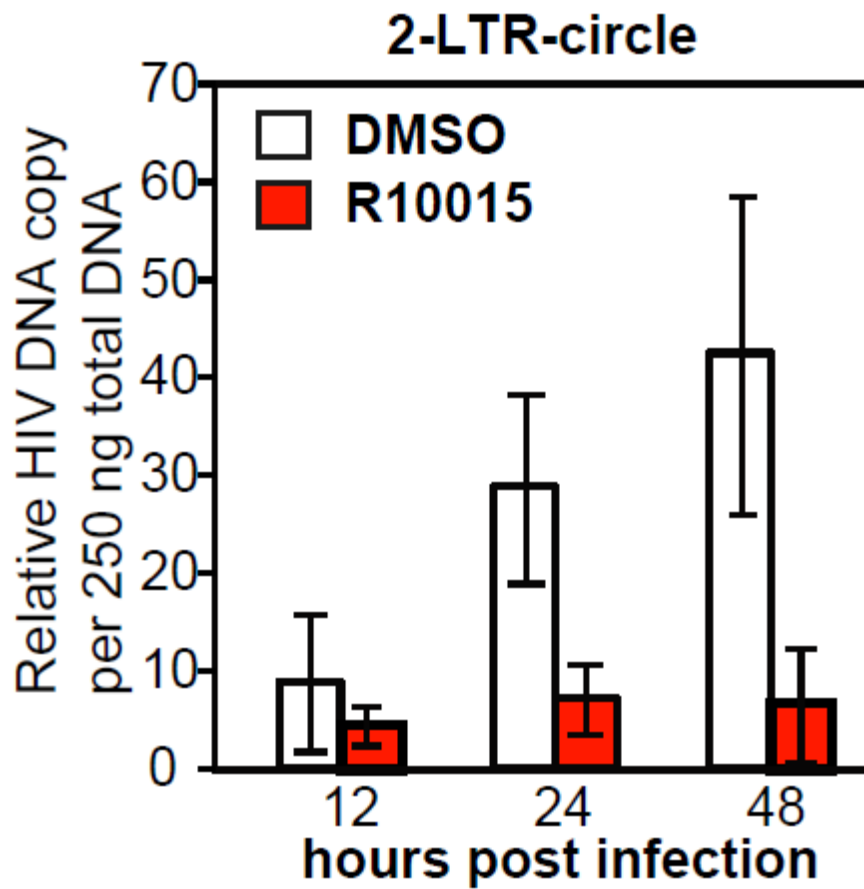


Figure 5.8 R10015 inhibits 2-LTR circle DNA formation. Cells were similarly treated with R10015 and infected. 2-LTR circles were quantified by real-time PCR. R10015 treated cells showed less 2-LTR circle formation than DMSO treated control group from 12 hours to 48 hours post infection.

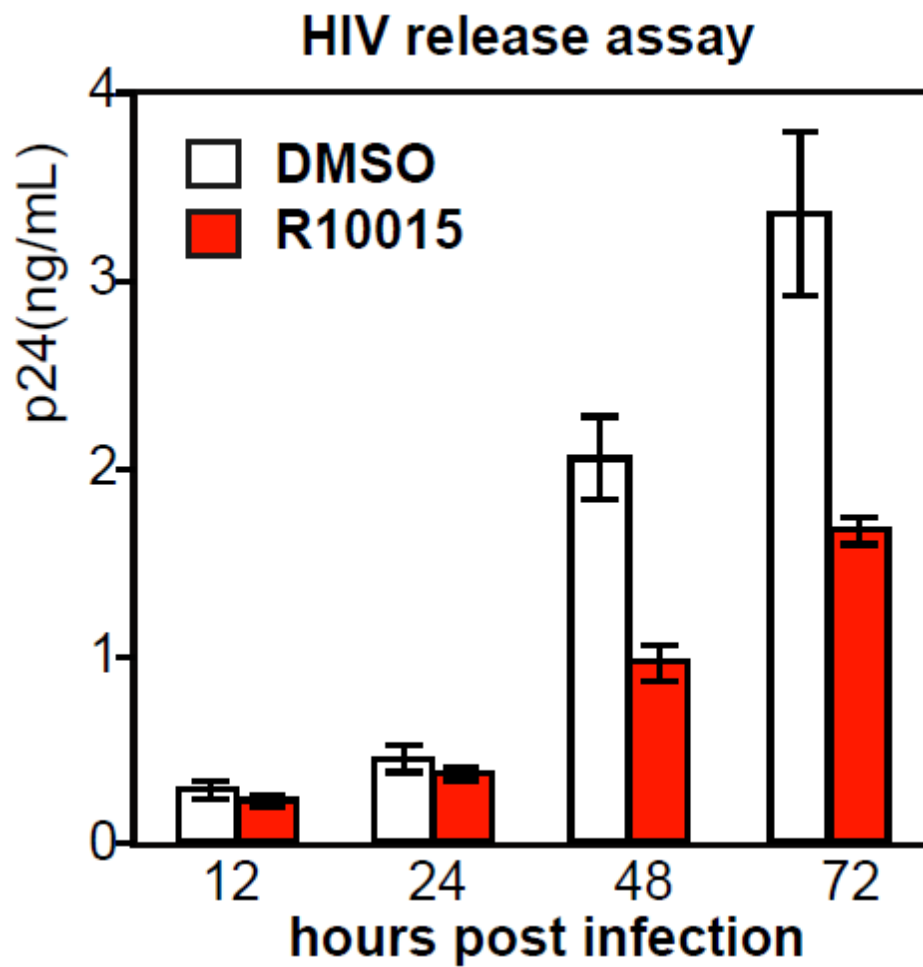


Figure 5.9 R10015 inhibits virion release. CEM-SS T cells were infected with HIV-1(Env) for 2 hours, washed, incubated for 12 hours, and then treated with R10015. Virion release was quantified by measuring p24 in the supernatant. R10015 showed strong inhibition of virion release at 48 hours and 72 hours post infection.

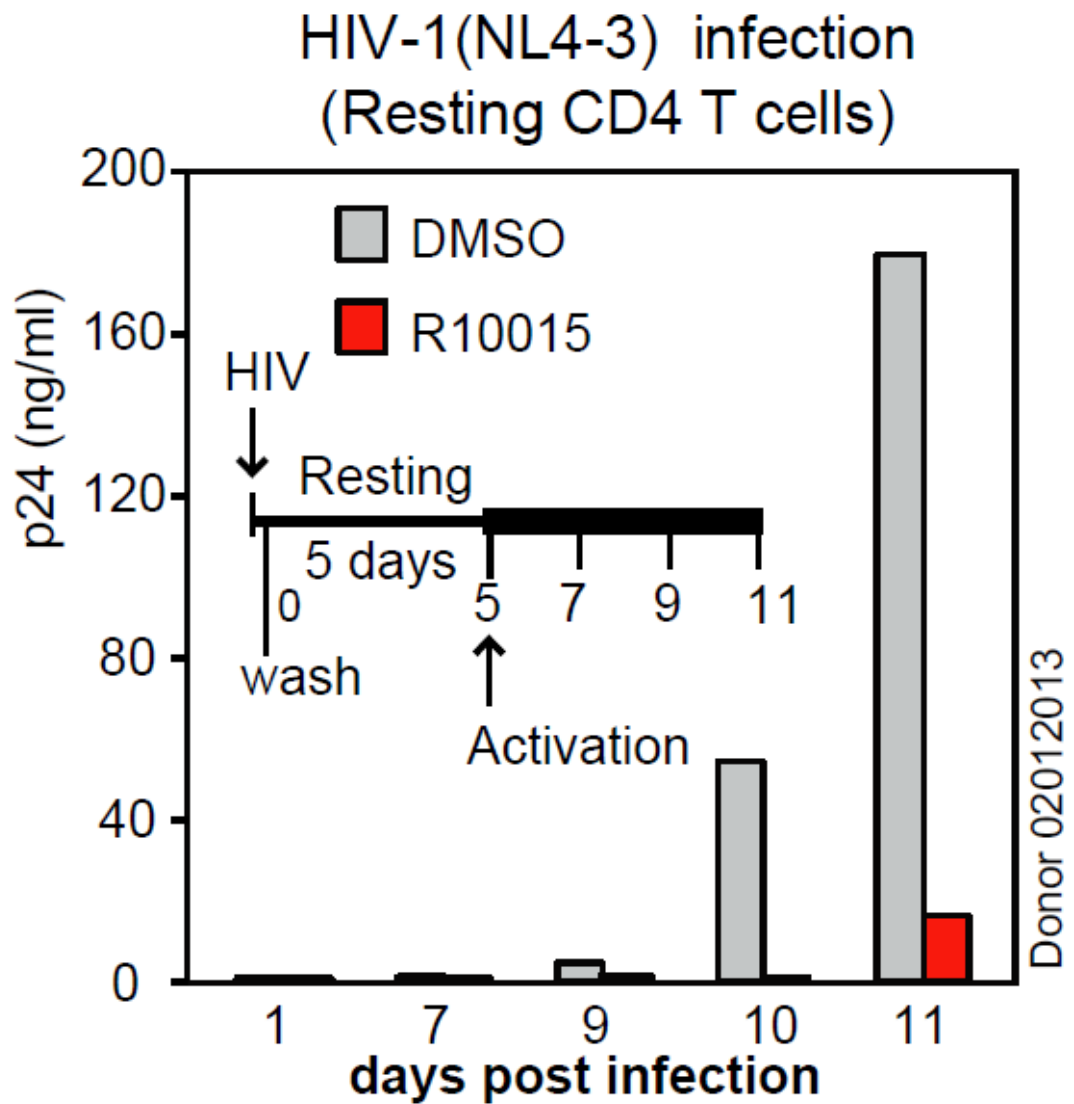


Figure 5.10 R10015 inhibits HIV latent infection of resting CD4⁺ T cells. Cells were treated with R10015 (100 μ M) or DMSO for 1 hour, infected with HIV-1(NL4-3) for 2 hours, washed, cultured for 5 days in the absence of R10015, and then activated with CD3/CD28 beads. Viral p24 release was measured. The p24 levels in R10015 treated cell culture supernatant were prominently lower than DMSO control group.

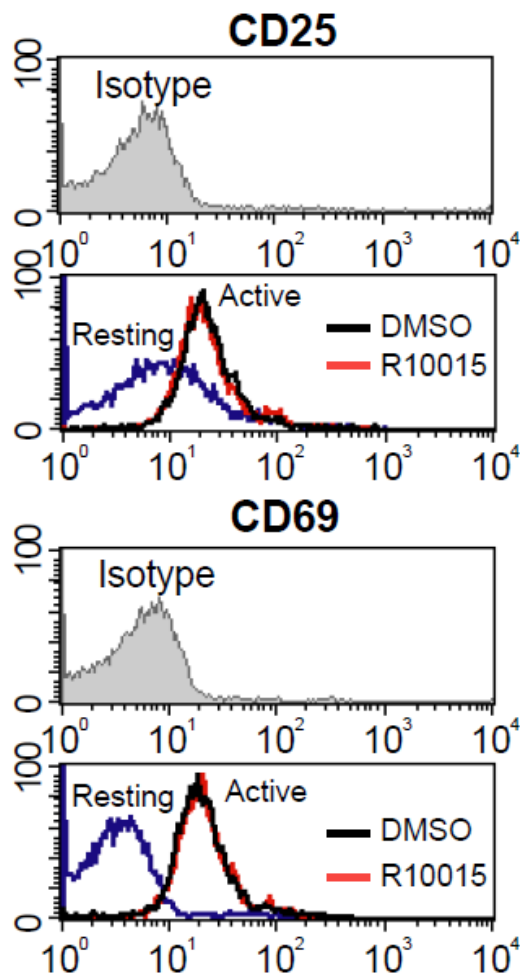


Figure 5.11 R10015 did not inhibit T cell activation in CD4⁺ T cells. CD25 and CD69 surface staining were performed using the same samples as presented **Figure 5.10** and measured by flow cytometry. CD25 and CD69 levels were not decreased in R10015 treated cells, indicating the abated p24 level in R10015 is indeed from inhibition of HIV replication rather than from cytotoxicity.

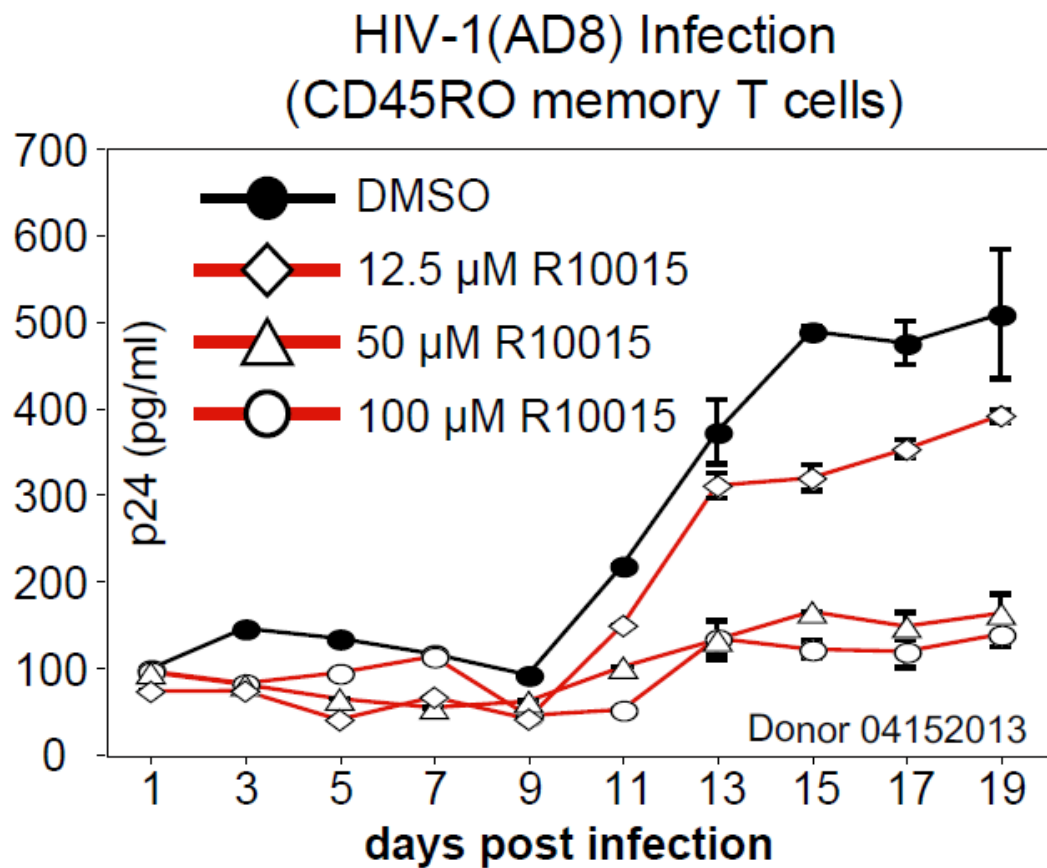


Figure 5.12 R10015 inhibits R5 HIV-1 latent infection of CD45RO⁺ memory CD4 T cells. Cells were treated with R10015 (100 μM) or DMSO for 1 hour, infected with HIV-1(NL4-3) for 2 hours, washed, cultured for 5 days in the absence of R10015, and then activated with CD3/CD28 beads. Viral p24 release was measured. The inhibition of p24 by R10015 follows a dosage dependent pattern.

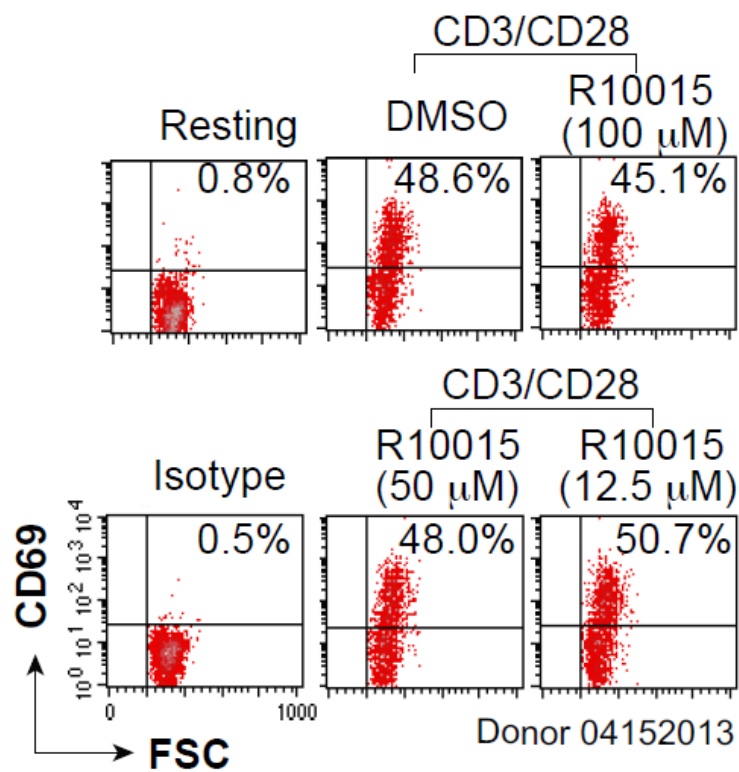


Figure 5.13 R10015 did not inhibit T cell activation in CD45RO memory T cells.

Similar to the resting CD4⁺ T cell infection, CD69 surface staining was performed to indicate R10015 did not inhibit T cell function, as judged by the surface expression of CD69 following T cell activation

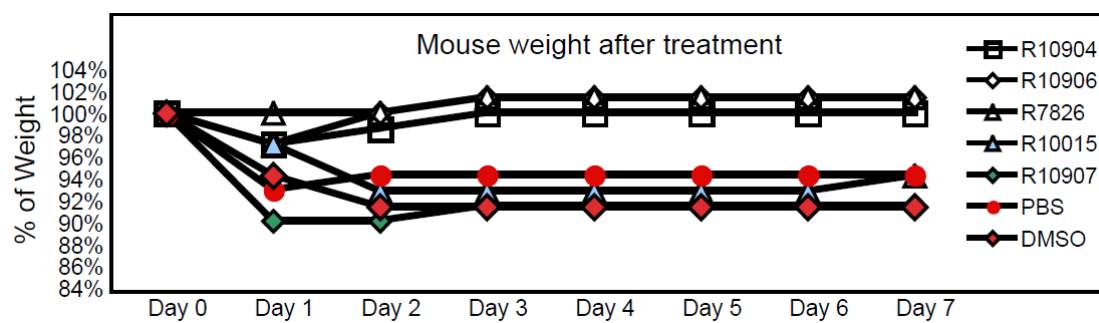


Figure 5.14 C3H/HeN mice were treated daily with LIMK inhibitors for 7 days.

R10904, R10906, R10907, and R7826 were delivered via oral gavage at 20 mg/kg.

R10015 was delivered by intraperitoneal injection at 10 mg/kg. DMSO-treated and

PBS-treated mice were used as controls. Animals were weighed daily and observed

for signs of stress.

Discussion

In this Chapter, the mechanism of R10015 inhibition of HIV-1 viral infection was explored. Surface staining of CD4 and CXCR4 exhibited mild downregulation of both cellular receptors, but this difference seems to be a nuance and merely impact the viral entry as the Blam-Vpr fusion assay indicated that R10015 had no significant inhibition of HIV-1 fusion capability.

VSV-G pseudotyped HIV-1 infection was minimally inhibited by R10015, clearly demonstrating the inhibition on wild type virus with gp120 envelop is due to the dysregulation of actin dynamics and R10015 has no significant impact on microtubule mediated endocytosis.

Reverse transcription was probably inhibited by R10015 since total DNA synthesis measured by PCR showed much lower copies of viral DNA from drug treated samples. As indicated by previous study, actin plays a role in the efficiency of viral reverse transcription [115].

The next step of HIV replication cycles measured in the mechanism study is nuclear migration, as indicated by 2-LTR-circle formation. Using real-time PCR, much less 2-LTR-circle copies were found in the R10015 treated samples, implying that viral PIC nuclear migration was diminished in the drug treated sample.

The viral release assay was done by p24 ELISA. As the drug was added after 12 hours post single-cycle virus infection, by the time R10015 took effect on LIMK, HIV-1 should have passed the time window for viral entry, reverse transcription,

nuclear migration and integration. Therefore, if HIV replication decreased in this case, most likely it was due to the drug interference with viral assembly or budding. Based on all the results regarding HIV replication cycle, we believe that R10015 inhibits HIV replication on multiple stages, including reverse transcription, nuclear migration and viral release.

The drug treatment on resting CD4⁺ T cells and subtype CD45RO memory T cells indicates R10015 can effectively inhibit HIV R5 virus infection of primary T cells. It was also noticed that, comparing with cell lines infection at the same drug dosage, R10015 showed stronger inhibition on primary cells than on cell lines. It's probably due to the difference in the status of their cortical actin. Actin dynamics is stronger in cell lines and assumedly HIV could take advantage of this activity and facilitate its nuclear migration [18].

Lastly, the mice experiments of R10015 treatment showed that multiple LIMK inhibitors, not only R10015 but also another 4 newly designed drugs are tolerable in mice. All drug treated mice showed higher weight measurements than DMSO (drug solvent) treated control group on day 7 day post infection. This result confirmed the feasibility of performing further experiments on animal models.

Chapter 6: Exploration of broad spectrum antiviral activity of R10015

Introduction

HIV infection requires the movement of actin skeleton during multiple stages of infection, including viral entry, nuclear migration, viral release, etc [18, 41, 60]. As a matter of fact, this strategy is not unique for HIV but commonly shared by a large number of viral pathogens. In the Chapter, we are going to discuss the effects of R10015 on EBOV, RVFV, VEEV and HSV replication.

Ebola virus (EBOV) is a member of the Filoviridae family, negative single strand RNA and enveloped virus [116, 117]. It's already known that following attachment of EBOV to host, virions enter the cell by a process of endocytosis, acidification of the endocytic vesicle, and fusion of virus and host membranes resulting in the release of the nucleocapsid (NC) into cytoplasm. EBOV-Z GP mediated entry and fusion are affected by treatment of host cells with agents that disrupt microtubules or inhibit the function of microfilaments [118]. These cytoskeletal components are the key to clathrin-dependent and caveolar-mediated internalization which support the theory that EBOV enters the cell through endocytosis. A more recent study further showed that EBOV virus-like particles (EBOV-VLPs) use macropinnocytosis and clathrin-mediated endocytosis to enter cells which are both actin dynamics related.

The interaction between EBOV-VLPs and host cells induced actin driven ruffling and enhanced the uptake of FITC labeled dextran. Additionally, this step could be inhibited by a toxin, latrunculin A, which inhibits the polymerization of F-actin [119]. This further confirmed that the actin regulated macropinocytosis, rather than clathrin dependent endocytosis is the primary entry route for EBOV [120].

Another virus planned to be tested in this study, Rift Valley Fever Virus (RVFV), is a negative-sense, single-stranded RNA virus of the Bunyavirus family [121]. RVFV is a cytoplasmic virus, and the cellular entry of RVFV is predicted to occur via a class II fusion mechanism that becomes activated by a low pH following endocytosis of the virus [122, 123]. As actin dynamics is involved endocytotic activities, RVFV viral entry may be actin dependent as well. A latest study from our collaborators published in March 2016 indicates that Protein Phosphatase-1 (PP1) is critical for RVFV replication, as deregulation of PP1 by siRNA showed abated viral titers in multiple cell lines [124]. As previously mentioned in the introduction Chapter, it's been reported that PP1 regulates cofilin activity by dephosphorylation and indirectly induces F-actin severing [40, 125], R10015 may also affect RVFV replication. In summary, although not yet completely understood, RVFV's replication cycle is actin-dependent and can possibly be inhibited by drugs interfering actin activity. Similarly, an enveloped, single-stranded, positive-sense RNA virus, VEEV of the Alphaviruses family, is also believed to be dependent on clathrin-mediated endocytosis [126] and was chosen to be tested for R10015's impact.

HSV-1 is the last virus we planned to test on the broad spectrum anti-viral study of R10015. HSV-1 is an enveloped DNA virus belonging to the family Herpesviridae, infecting epithelial cell and neurons with long term latency [127]. Throughout its replication cycle, HSV-1 needs interaction with actin skeleton at multiple stages of infection [128-131]. Recently studies have suggested that LIMK is also involved in HSV-1 infection of neurons [132]. During viral entry, HSV-1 triggers a biphasic remodeling of the actin cytoskeleton through phosphorylation and dephosphorylation of cofilin, which is mediated through the LIMK-cofilin signaling pathway. Therefore, hypothetically, R10015 is also likely to inhibit HSV-1 replication by regulating LIMK-cofilin interaction.

Due to the variety of the virus tested and distinct methodologies required, the broad-spectrum antiviral studies were done by three labs. The EBOV study was done by Sina Bavari's group of US Army Medical Research Institute of Infectious Diseases, the RVFV and VEEV experiments were finished by Dr. Kehn-Hall's lab in National Center for Biodefense and Infectious Diseases, and the HSV-1 plaque assay was performed by me in Dr. Wu's lab.

Materials and Methods

EBOV(Zaire) infection: HFF-1 cells were pre-treated with R10015 for 2 hours and infected with EBOV(Zaire) (MOI, 2.5). Infection was terminated at 48 hours post-infection, and cells were fixed with formalin solution. Infected cells were identified by immunostaining of the EBOV GP protein with a primary mouse

antibody and a secondary Alex488-labeled anti-mouse IgG antibody. The cells were also stained with Hoechst (Invitrogen) for nuclei and Cell Mask cytoplasm stain (Invitrogen) for cytoplasm. The number of nuclei per well was used to determine cell viability. Images were taken with a PE Opera confocal platform with 10× objectives and analyzed using Acapella and GeneData software.

VEEV and RVFV infection: VEEV TC83-Luc virus was kindly provided by Slobodan Paessler of the University of Texas Medical Branch at Galveston. RVFV MP12-luc virus was kindly provided by Shinji Makino of the University of Texas Medical Branch at Galveston. Venezuelan Equine Encephalitis Virus Trinidad Donkey (subtype IA/B), NR-332 was obtained through the NIH Biodefense and Emerging Infections Research Resources Repository, NIAID, NIH. For infections with VEEV-Luc (TC83), VEEV(TC83) (BSL-2 strain), VEEV(TrD) (BSL-3 strain), or RVFV-Luc (MP12), Vero cells were pretreated with R10015 or DMSO, infected with the viruses at an MOI of 0.1 and post-treated with R10015. Viral supernatants were collected 24 hours post-infection and analyzed by plaque assays. Alternatively for luciferase-expressing viruses, luciferase activity was assessed at 24 hours post-expression and DMSO-treated samples were set to 100%.

HSV-1 infection: HSV-1 was kindly provided by Timothy M. Block, Drexel Institute for Biotechnology and Virology Research. Virus was propagated on Vero cells. Briefly, cells were infected with HSV-1 (MOI, 0.001) until 100% of cells

displayed cytopathic effect (CPE). Cell supernatant with HSV-1 was harvested by centrifugation at 2,000 rpm for 5 min at 4°C, filtered through a 0.45 µm filter, and then stored at -80 °C. For HSV-1 infection, Vero cells were seeded in 10 cm Petri dishes and cultured overnight. R10015 or DMSO was added to cells for 2 hours. HSV-1 was serially diluted with 199V medium and added to cells for infection for 2 hours. Cells were washed and cultured in fresh medium (DMEM plus 5% NBCS, Invitrogen, Carlsbad, CA) containing 7.5 µg/ml pooled human immunoglobulin. Viral plaques were stained by rinsing twice in phosphate-buffered saline with potassium (KPBS). Cells were fixed with methanol, and stained with KaryoMax Giemsa Stain solution (Invitrogen, Carlsbad, CA).

Results

R10015 inhibits EBOV infection of HFF-1 cells

To test possible effects of R10015 on EBOV infection, we pre-treated human HFF-1 cells with R10015 for 2 hours, and then infected with EBOV (Zaire) for 48 hours in the continuous presence of R10015. To quantify viral replication, cells were fixed and stained for the EBOV glycoprotein with an Alexa 488-labelled antibody, and then analyzed by confocal imaging. We observed a dosage-dependent inhibition of EBOV (**Figure 6.1** and **Figure 6.2**). This inhibition is likely a combined effect of R10015 on viral early and late processes such as intracellular migration and virion release as drug was not washed away post infection.

R10015 inhibits RVFV-Luc reporter virus replication

We treated cells with R10015 for the entire course of viral replication to block both early and late steps such as viral assembly. We used a luciferase-tagged virus, RVFV-Luc(MP12) to measure viral replication. As shown in **Figure 6.3**, we observed a dosage-dependent inhibition of RVFV with an IC₅₀ at approximately 12.5 μ M.

R10015 inhibits varieties of VEEV strains

To block VEEV replication, we also treated cells with R10015 for the entire course of viral replication. We used a luciferase-tagged virus, VEEV-Luc(TC-83), and the attenuated VEEV(TC-83) (BSL-2), and observed a dosage-dependent inhibition in both luciferase and plaque assays with an IC₅₀ of approximately 5 μ M (Figure 7D). We confirmed these results with the infectious VEEV (TrD) which is a high virulence strain (BSL-3), and observed strikingly two logs of inhibition of VEEV(TrD) with R10015 (**Figure 6.4**).

R10015 showed moderate inhibition of HSV-1 replication

To confirm the involvement of LIMK in the early infection steps of HSV-1 infection, we pretreated Vero cells with R10015 for 2 hours and then infected with HSV-1 for 2 hours. Following infection, both HSV-1 and R10015 were washed away, and cells were cultured in the absence of drug. As shown in **Figure 6.5**, we observed statically significant inhibition of HSV-1 by R10015 for this brief treatment, in agreement with previous report that LIMK is involved in HSV-1 early infection steps. Together, our results demonstrate the broad anti-viral activity of R10015.

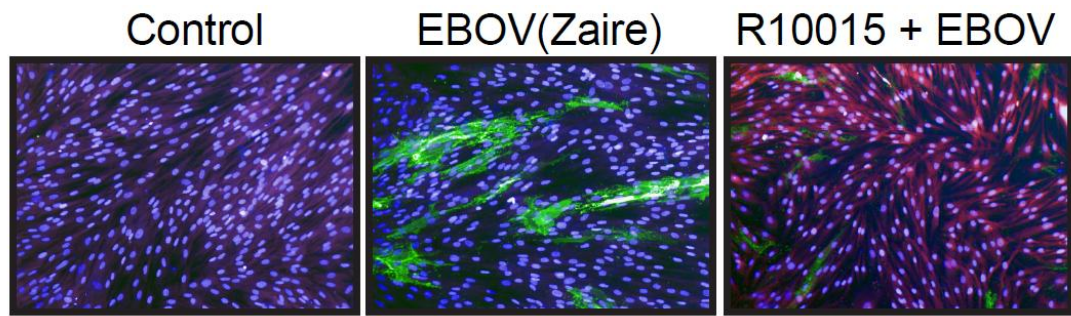


Figure 6.1 Inhibition of EBOV by R10015. HFF-1 cells were treated with R10015 (50 μ M) for 2 hours and infected with EBOV (Zaire) (MOI, 2.5) for 48 hours in the presence of R10015. Cells were fixed and stained for the EBOV GP protein with an Alexa 488-labelled antibody (A, green), or with Hoechst (A, blue nuclei) for confocal imaging.

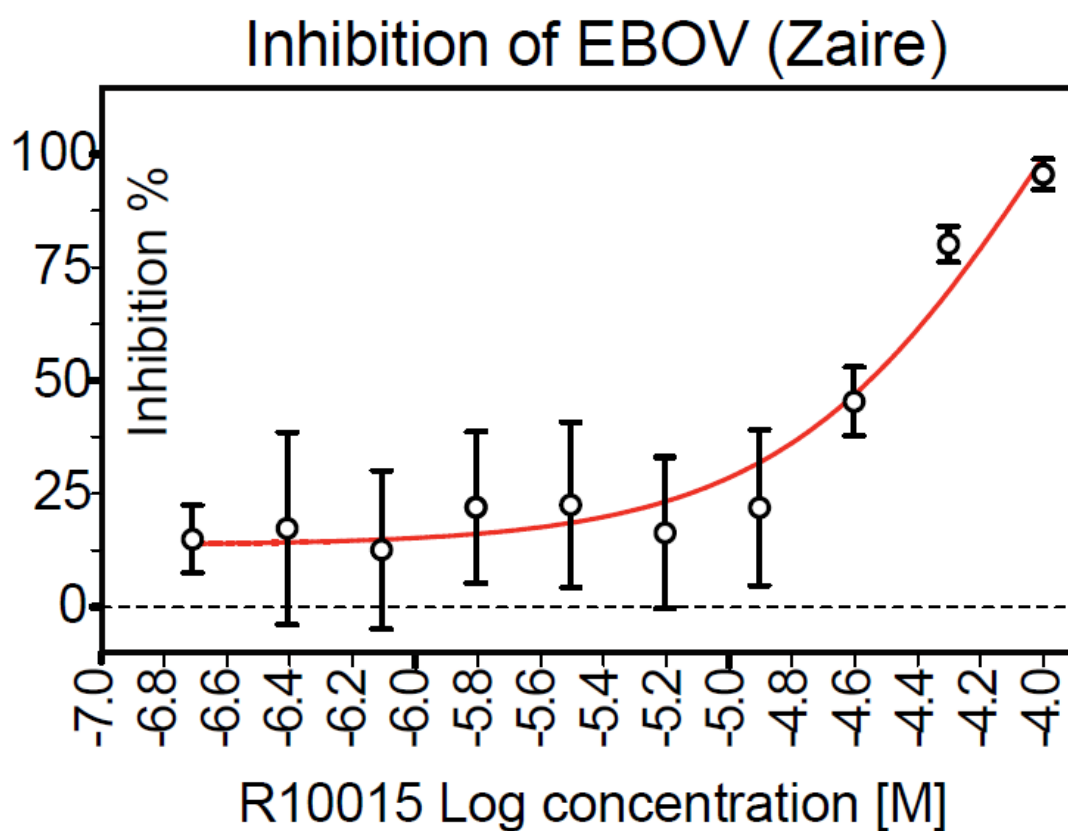


Figure 6.2 Dosage-dependent inhibition of EBOV by R10015. The inhibition of EBOV went up to around 90% at the concentration of 100 μ M. Similarly to the effects on HIV-1 infection, the efficiency of the drug is minimal in nanomolar range.

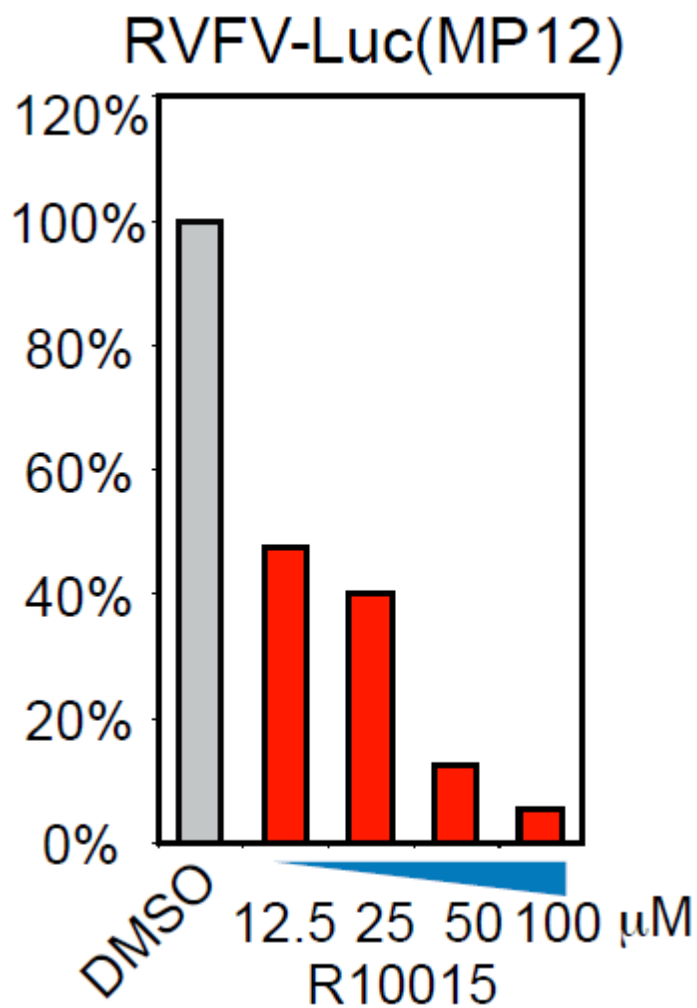


Figure 6.3 Inhibition of RVFV by R10015. Vero cells were treated with R10015 similarly to CEM-SS T cell treatment, infected with a Luciferase reporter strain RVFV-Luc (MP12) (MOI, 0.1), and analyzed with luciferase assay. Inhibition of viral replication maintained higher than 50% in samples with dosages from 12.5μM to 100 μM.

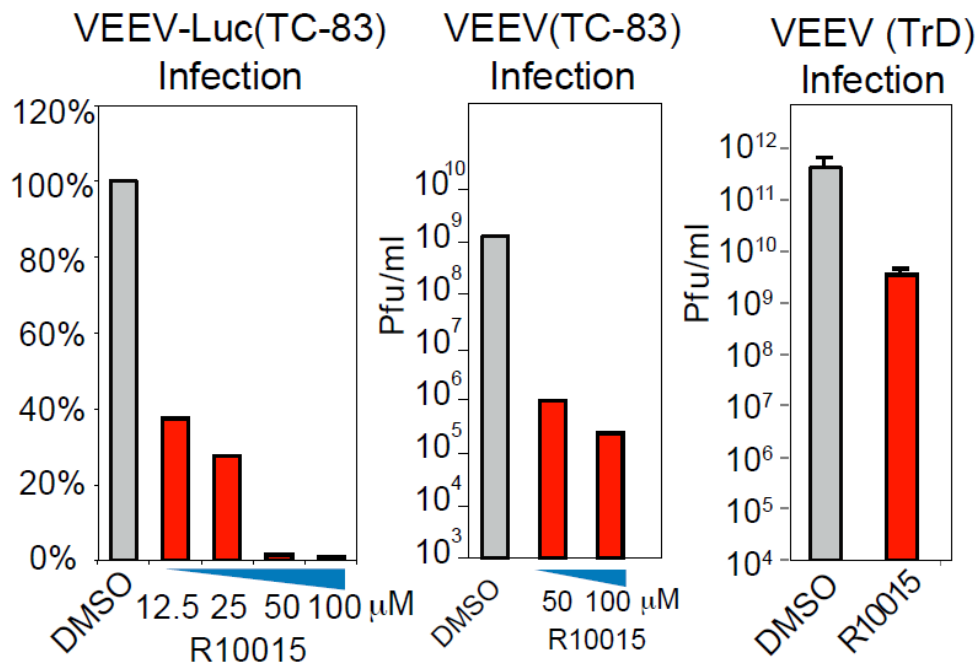


Figure 6.4 Inhibition of VEEV by R10015. Vero cells were similarly treated with R10015 and infected with VEEV-Luc(TC-83), VEEV(TC-83), or VEEV(TrD) (MOI, 0.1). Viral supernatants were collected at 24 hours and analyzed with luciferase or plaque assay.

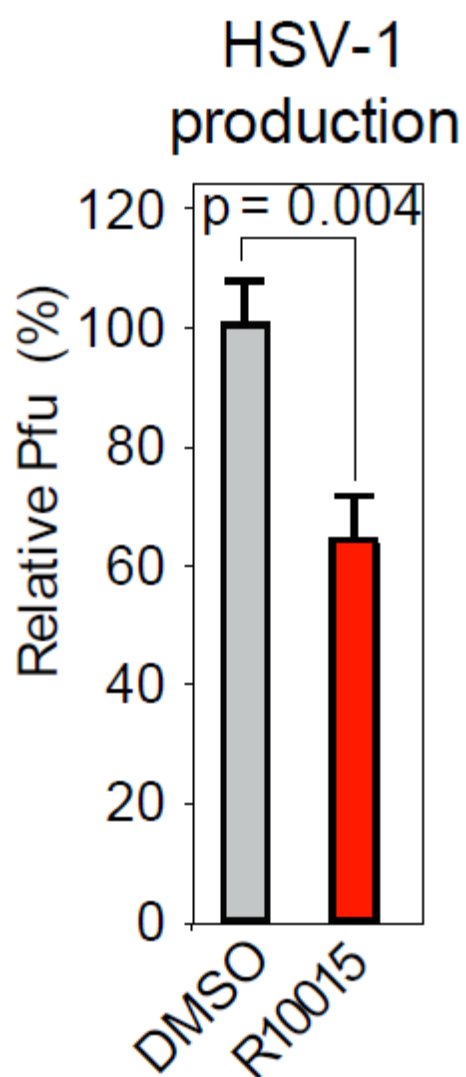


Figure 6.5 Inhibition of HSV-1 by R10015. Vero cells were treated with R10015 (100 μ M) for 2 hours, infected with HSV-1, washed, and cultured in the absence of R10015. Viral plaques were stained and quantified. No significant drug toxicity was observed up to 100 μ M of R10015.

Discussion

Our results showed R10015 inhibits the viral replication on all four viruses, each from a different family of viridae. These data confirmed our theory that R10015 has the potential to act broad-spectrum against viral infection. They also suggested that the inhibition of R10015 differs from virus to virus, even strain to strain. Although valid proofs demonstrated the interaction between HSV-1 and host cells is actin-dependent, the plaque assay showed the mildest viral inhibition among all the viruses we tested, including HIV-1. This result implies that HSV-1 may have other strategies to bypass or counteract the actin dysfunction. Remarkably, we found the inhibition of VEEV is drastic although actin's role in VEEV replication cycle is largely unknown and no report about VEEV and LIMK interaction can be found yet. Similar to EBOV and RVFV, VEEV enters host cell via endocytosis, but it's much more sensitive to R10015 than EBOV and RVFV. This phenomenon hints the bond between VEEV and actin is crucial for this virus; maybe its viral assembly and budding are strictly actin reliant.

Chapter 7: Summary of R10015 project and the future of LIMK inhibitor design

In this article, we described the design, medicinal synthesis, and discovery of highly specific LIMK inhibitors that block HIV-1, EBOV, and other viruses. The rational design and development of LIMK inhibitors, as anti-viral drugs, are largely based on recent studies on the role of LIMK/cofilin in HIV-1 infection [18, 60, 133]. It has been shown that HIV requires LIMK1/cofilin activity for entry, intracellular migration, cell-cell transmission, and budding.

The possibility for developing clinical LIMK inhibitors is also suggested by previous genetic studies based on humans and mice. In the human genome, the LIMK1 gene is located in a region on human chromosome 7 (7q11.23) and is haplodeleted, along with 24 other genes, in adults living with Williams Syndrome (WS), a rare neurodevelopmental genetic disorder associated with mild mental retardation [134-136]. The deletion of elastin (ELN) has been explicitly linked to most of the cardiovascular problems in WS [137]. However, the neurodevelopmental genotype-phenotype correlation is still uncertain, and may be related to the hemizyosity of WBSCR11, CYLN2, GTF2I, NCF1, and perhaps LIMK1 [136]. Specifically, LIMK1 knockout in mice has been linked to alterations in spine morphology and synaptic function. The knockout mice also showed heightened locomotor activities, and altered fear responses and spatial learning [138].

Nevertheless, LIMK1-null mice and human adults with WS do not have the severe multiple developmental disorders normally seen in other developmental genetic diseases, suggesting that blocking LIMK1 is not fatal, and short-term or localized LIMK inhibition is likely tolerable in adults. Therefore, LIMK is considered a valuable target for treating various human diseases such as metastatic cancer, Alzheimer's disease, and drug addiction [58, 139, 140]. Our study suggested the possibility of developing highly specific LIMK inhibitors for inhibiting HIV and other viral infections. Given the lack of an effective HIV vaccine, these novel inhibitors may prove to be valuable alternatives for preventing HIV sexual transmission. These LIMK inhibitors inhibit viral reverse transcription, nuclear migration, and release, and are expected to be broad-spectrum for HIV strains because of the highly conserved nature of viral dependence on actin dynamics for infection. In addition, these LIMK inhibitors have anti-inflammatory properties, and can inhibit the migration of infected immune cells for HIV cell-cell transmission (**Figure 4.4**) [133]. Thus, these LIMK inhibitors are ideal candidates, as potential topical microbicides, for pre-exposure prophylaxis that may complement the current anti-retroviral drugs.

Our current lead compounds have low molecular weight (< 450) and are amenable to further medicinal chemistry optimization to achieve higher cell potency and appropriate drug metabolism and pharmacokinetics (DMPK) properties. Many of these LIMK inhibitors have demonstrated good anti-viral activity in cells, and are generally not toxic in our cell-based assays and in mice (**Figure 5.14**). These results

emphasize the feasibility of developing LIMK inhibitors as a new class of broad-spectrum antiviral drugs for urgent treatment of viral infection or exposure to viral agents.

For the future design of novel LIMK inhibitors, there are two major concerns. One is to lower the HIV replication IC₅₀. The data from in vitro and in vivo experiments showed great difference in R10015's effectiveness. This could be caused by the low efficiency of drug delivery into cells or could be due to the fast metabolic changes of the drug in target cells. We could address this problem by measuring the amount of isotope labeled drug in cells following a time course. Another concern is the specificity of the inhibitor. As mentioned in **Table 3.1**, R10015 inhibits 93.6% of LIMK kinase activity but also inhibits 70.5% of ROCK2's activity. Due to the fact that ROCK 1/2 proteins are the direct upstream kinase of LIMK, inactivating ROCK2 could alter LIMK enzyme activity. Fortunately, we did not observe significant p-LIMK abatement from Western blot data, indicating the side-effect on ROCK is not critical for LIMK functions. At least there could be two possible explanations for this result: LIMK can be activated by another kinase PAK protein; LIMK is also an autophosphorylated kinase that can be activated by itself [141]. Therefore, ROCK kinase activity seems to be unnecessary for LIMK's activation. Nevertheless, to make LIMK inhibitors applied to clinical therapeutics, designing the next generation of LIMK inhibitors with lower effective dosage and higher specificity is an inevitable task.

Supplementary Figures

Drug screening of 25 compounds for anti-HIV activity on day 2 post infection

Drug treatment: 3 dosages of each compound (100 μ M, 10 μ M and 1 μ M), 1 hour pretreatment and 3 hours with viral infection

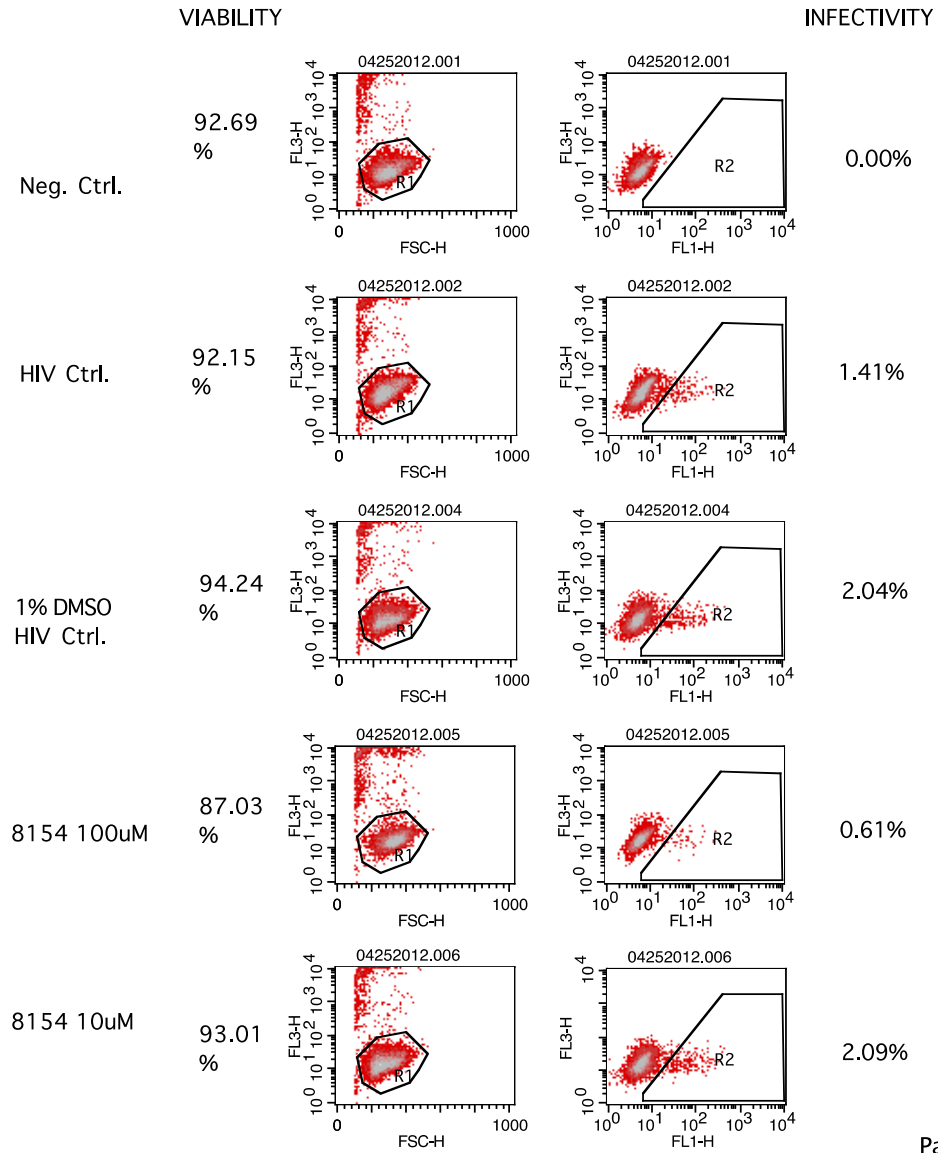
Cell line: Rev-CEM-GFP-Luc

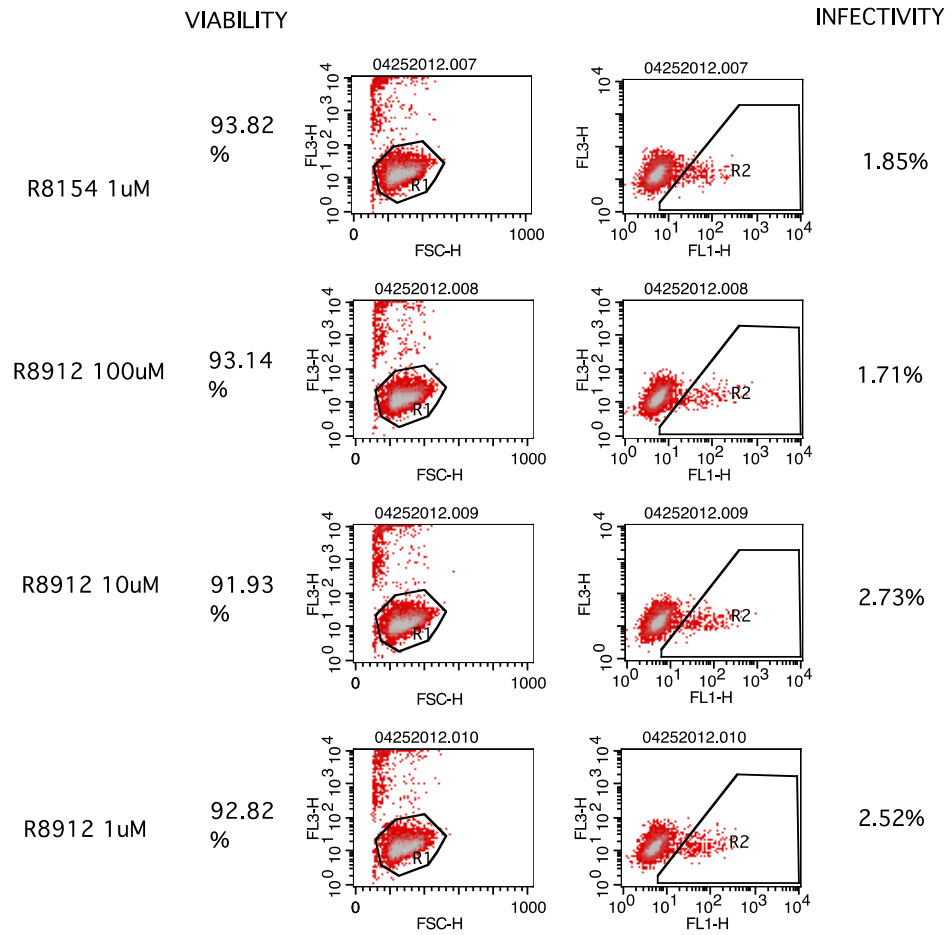
Virus: Wild type HIV-1(NL4-3), 3 hours treatment

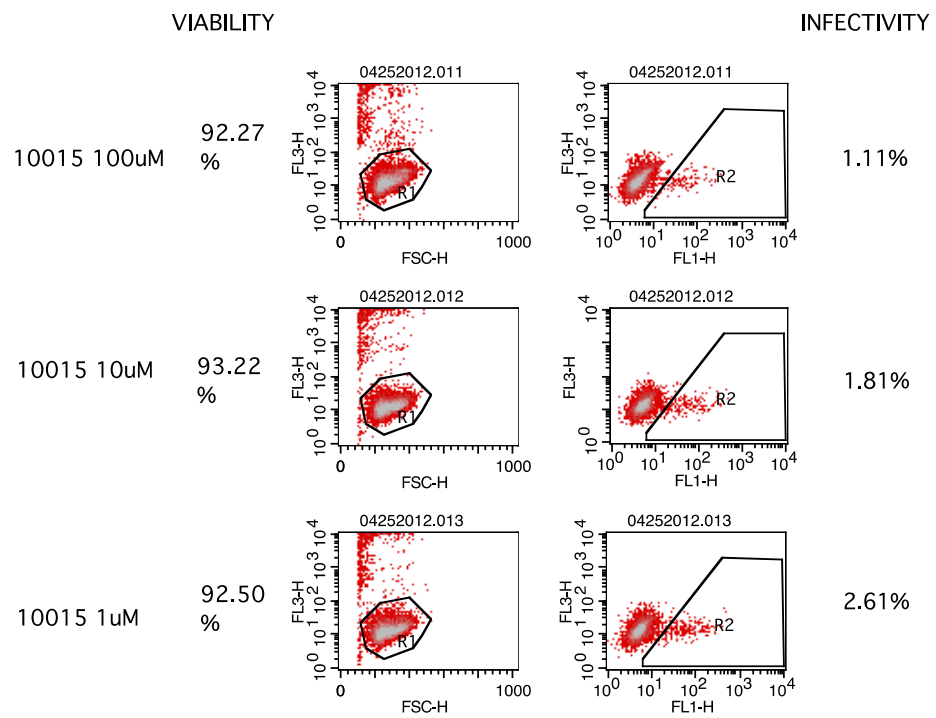
FL1-H: GFP (HIV infectivity)

FL3-H: PI (cell viability)

SCREEN OF R8154, R8912, R10015



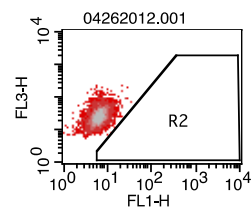
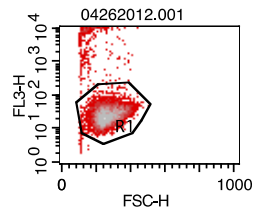




SCREEN OF R7793, R8176, R8212

Neg. Ctrl.

94.58 %

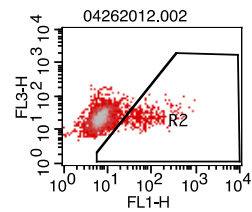
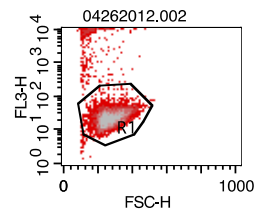


INFECTIVITY

0.00%

1% DMSO
HIV Ctrl.

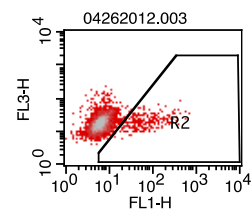
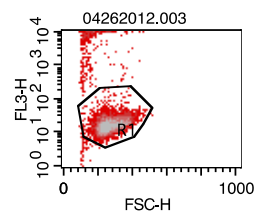
94.82 %



3.43%

R7793 100uM

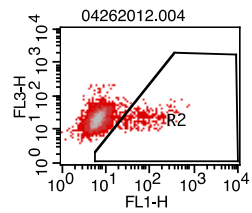
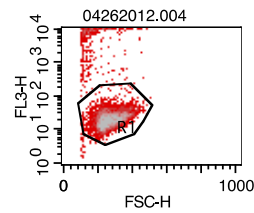
94.31 %



2.74%

R7793 10uM

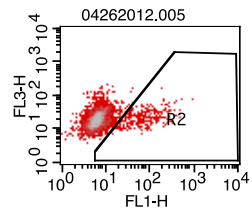
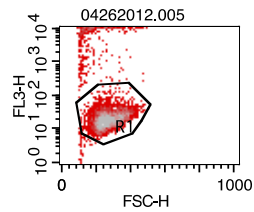
93.30 %



3.16%

R7793 1uM

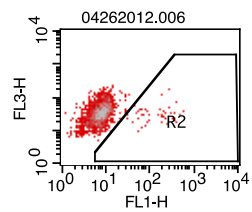
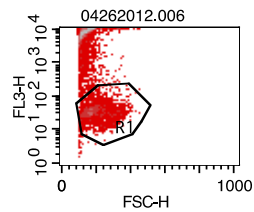
92.28 %



2.07%

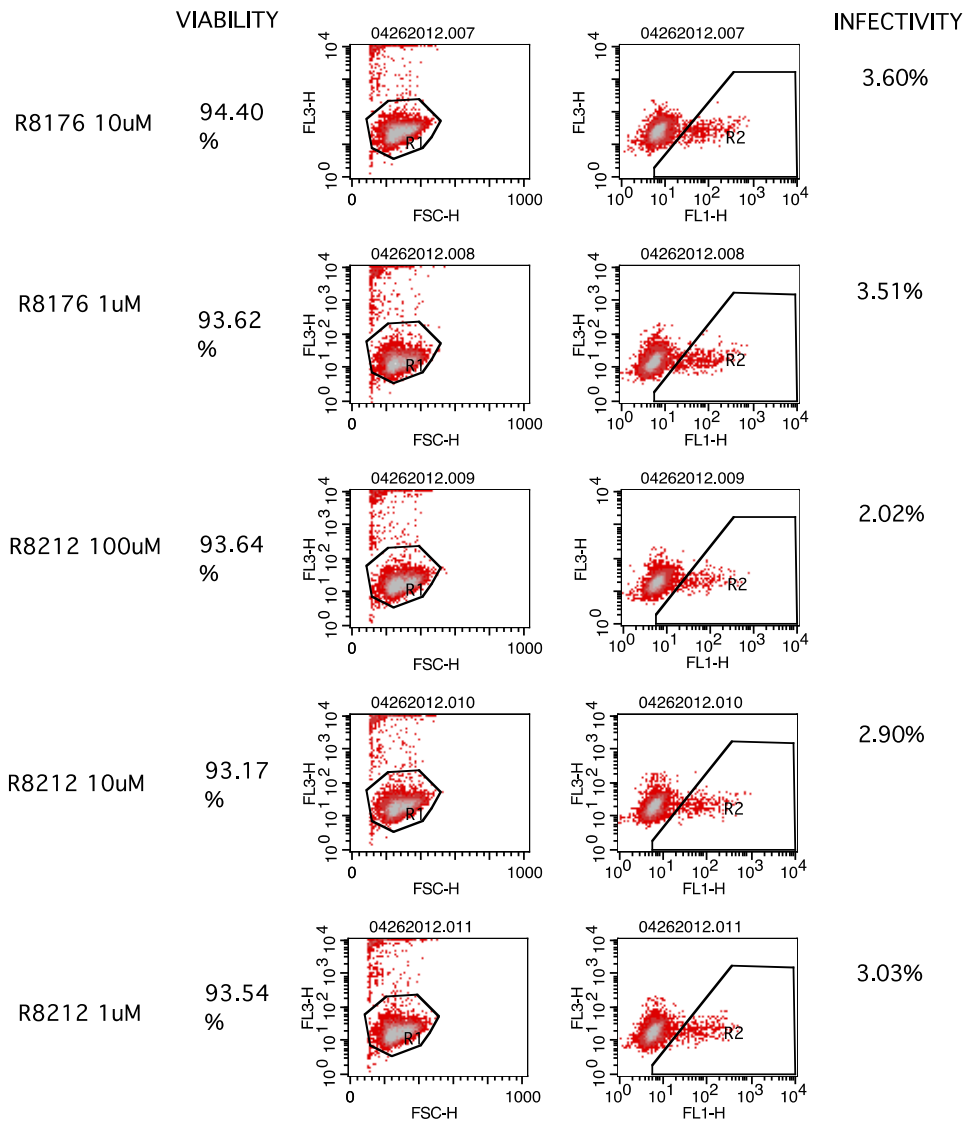
R8176 100uM

33.12 %



1.33%

page 1

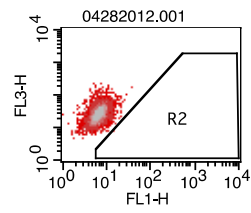
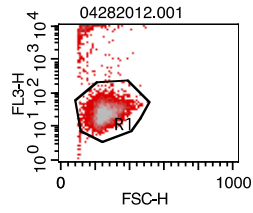


SCREEN OF R7799,
R8208, R8213

VIABILITY

94.21
%

Neg. Ctrl.

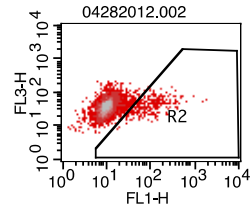
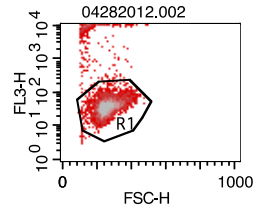


INFECTIVITY

0.00%

1% DMSO
HIV Ctrl.

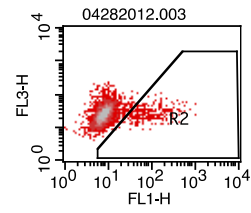
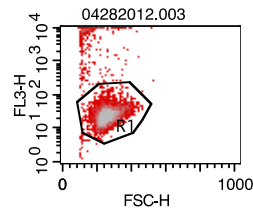
92.90
%



3.25%

R7799 100uM

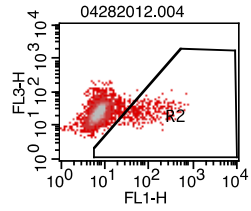
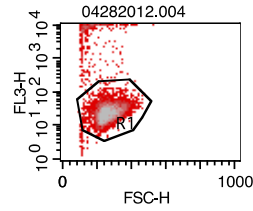
94.12
%



2.94%

R7799 10uM

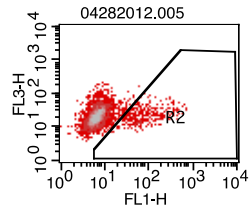
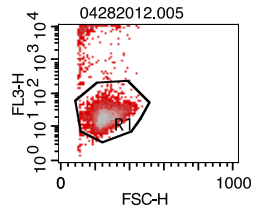
92.33
%



3.63%

R7799 1uM

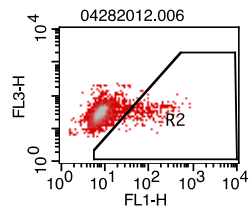
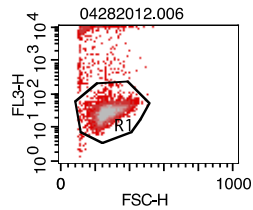
93.56
%



3.86%

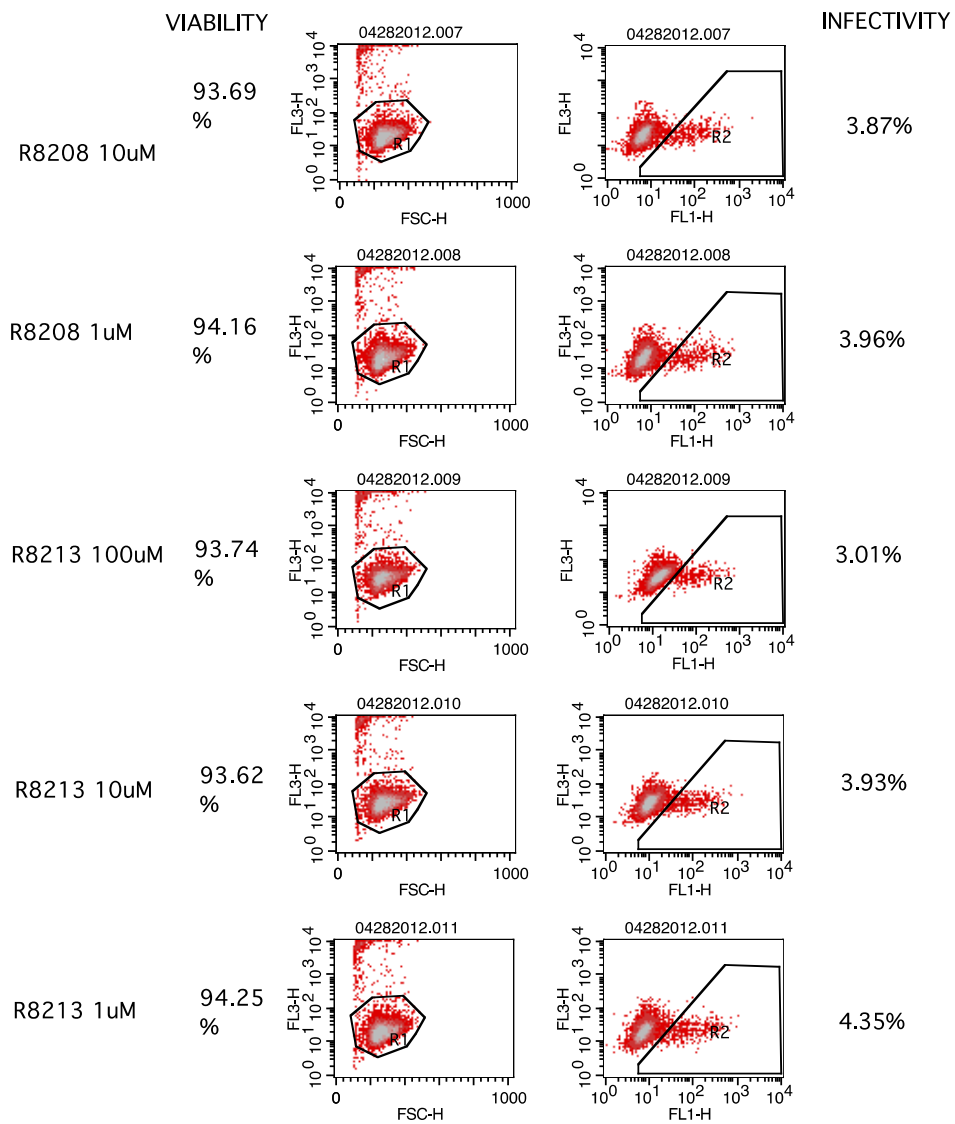
R8208 100uM

94.09
%

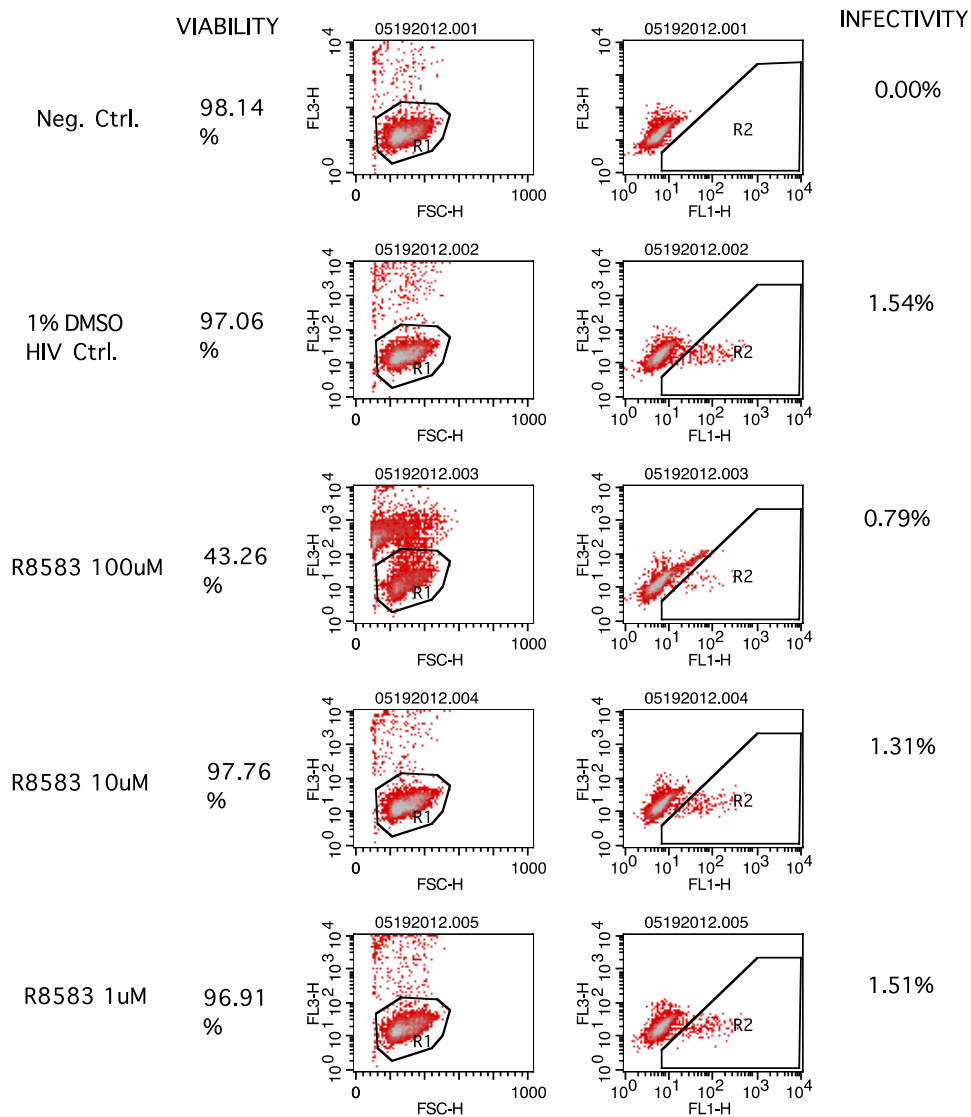


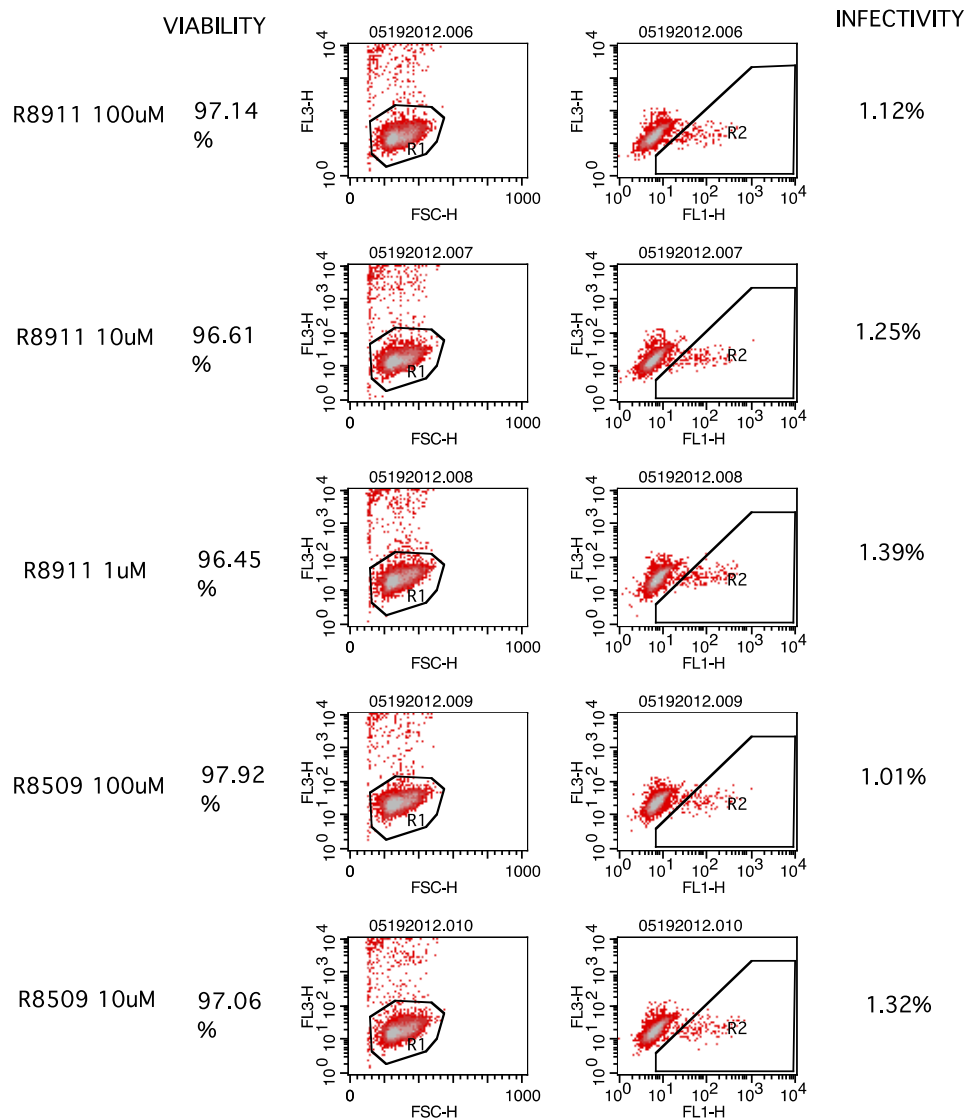
2.84%

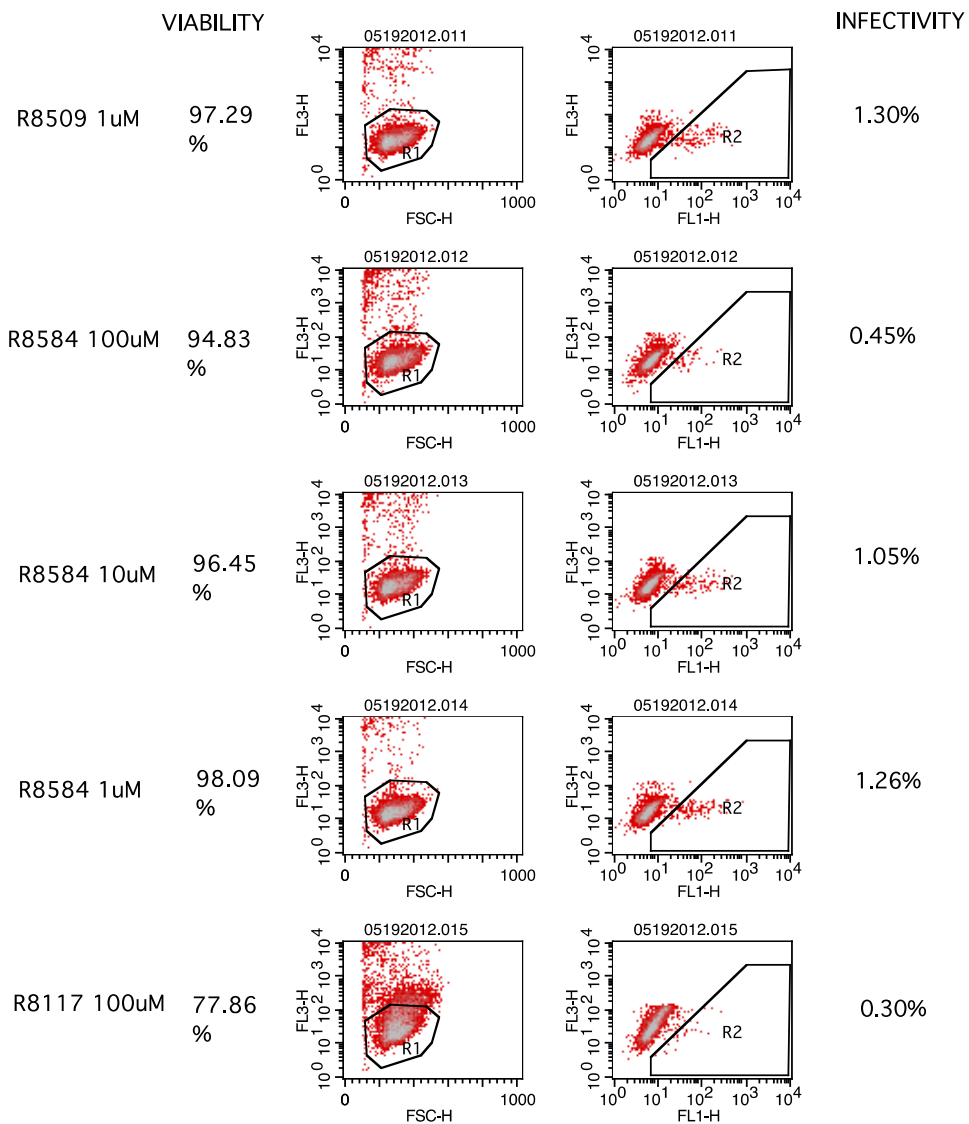
page 1

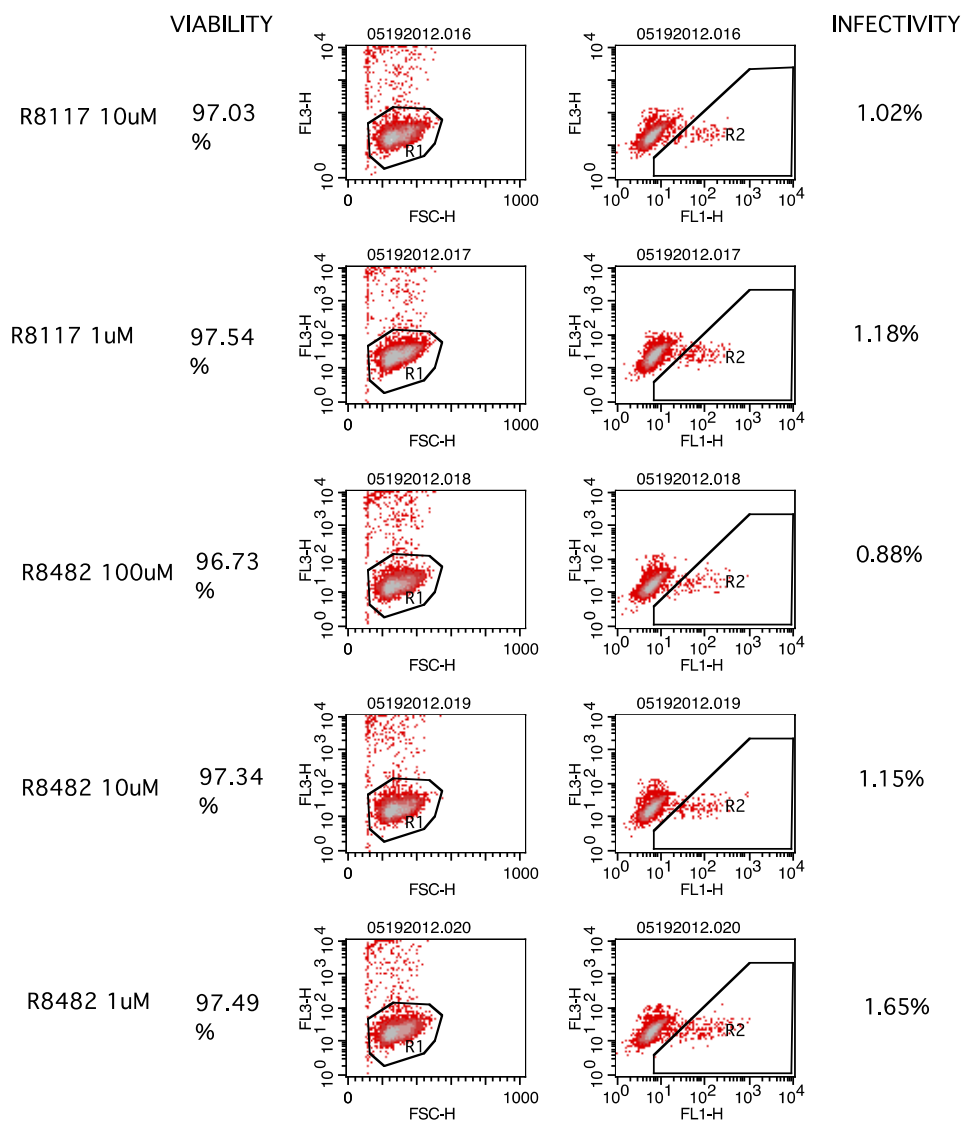


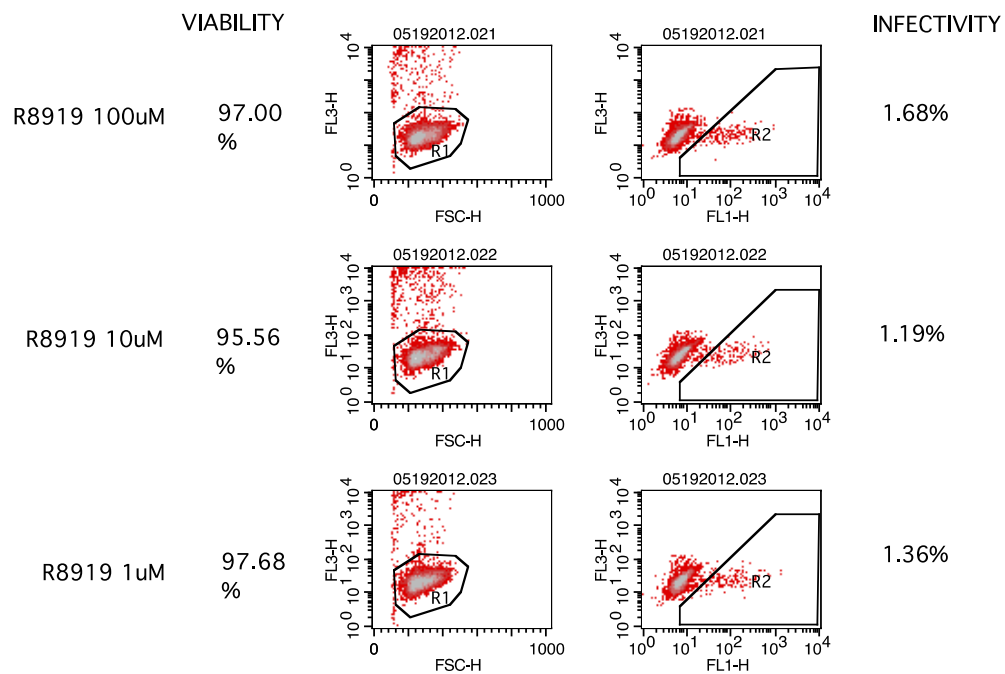
SCREEN OF R8583, R8911, R8509, R8584, R8117, R8482, R8919



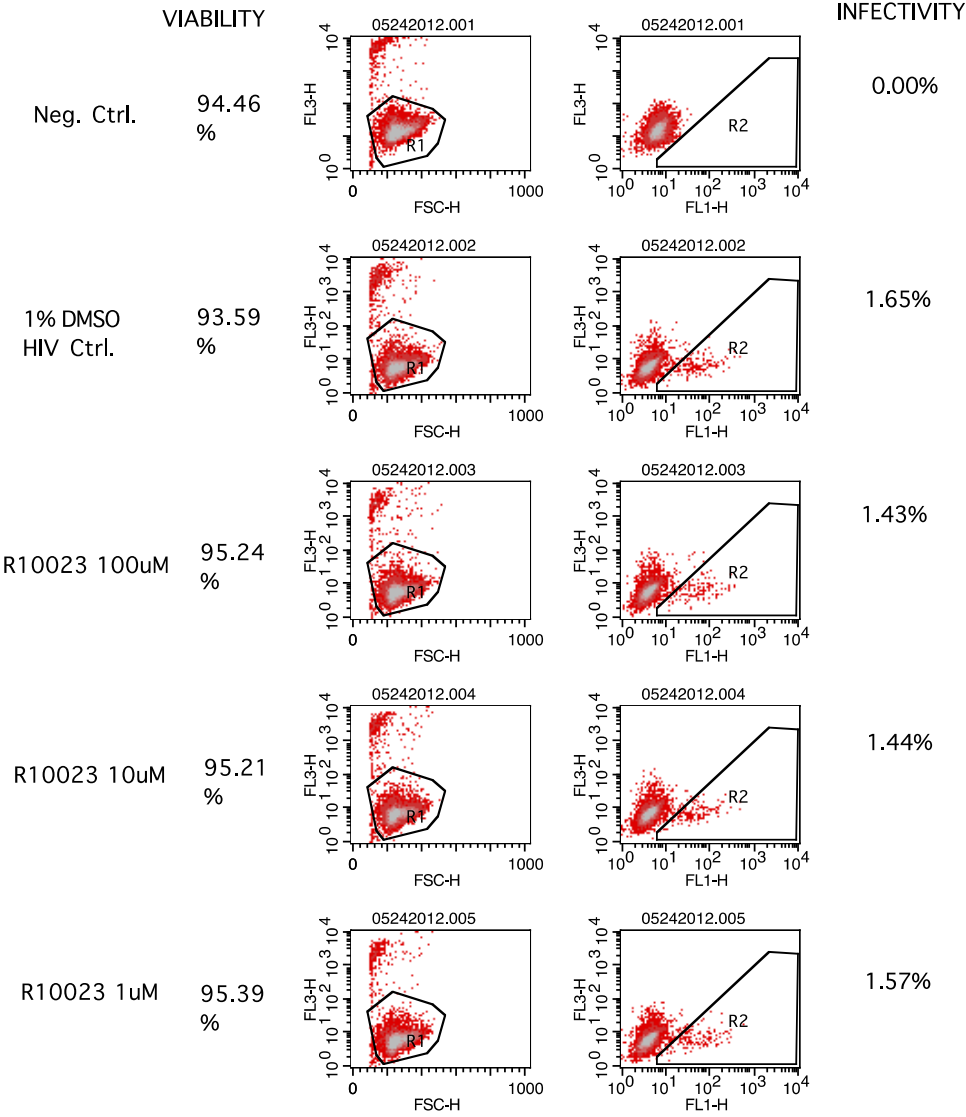


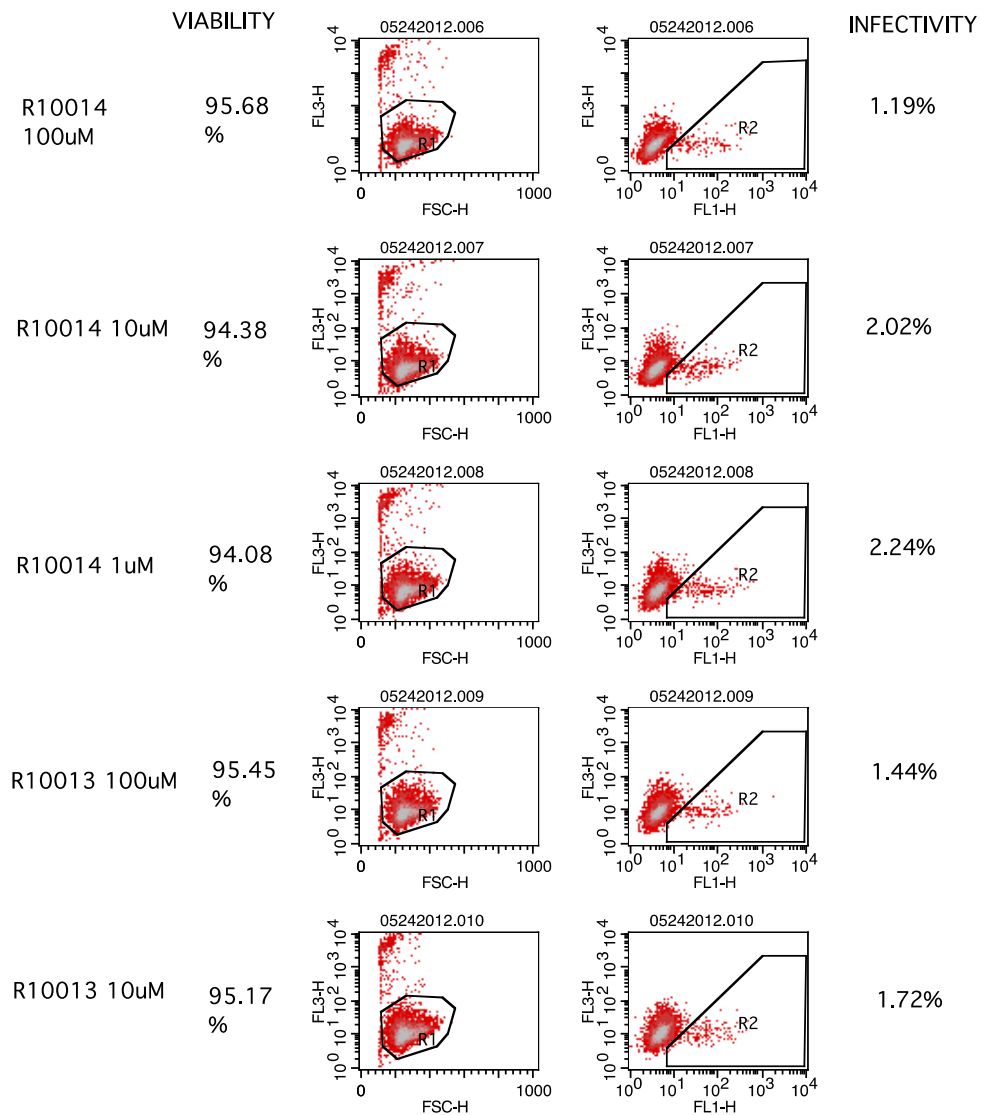


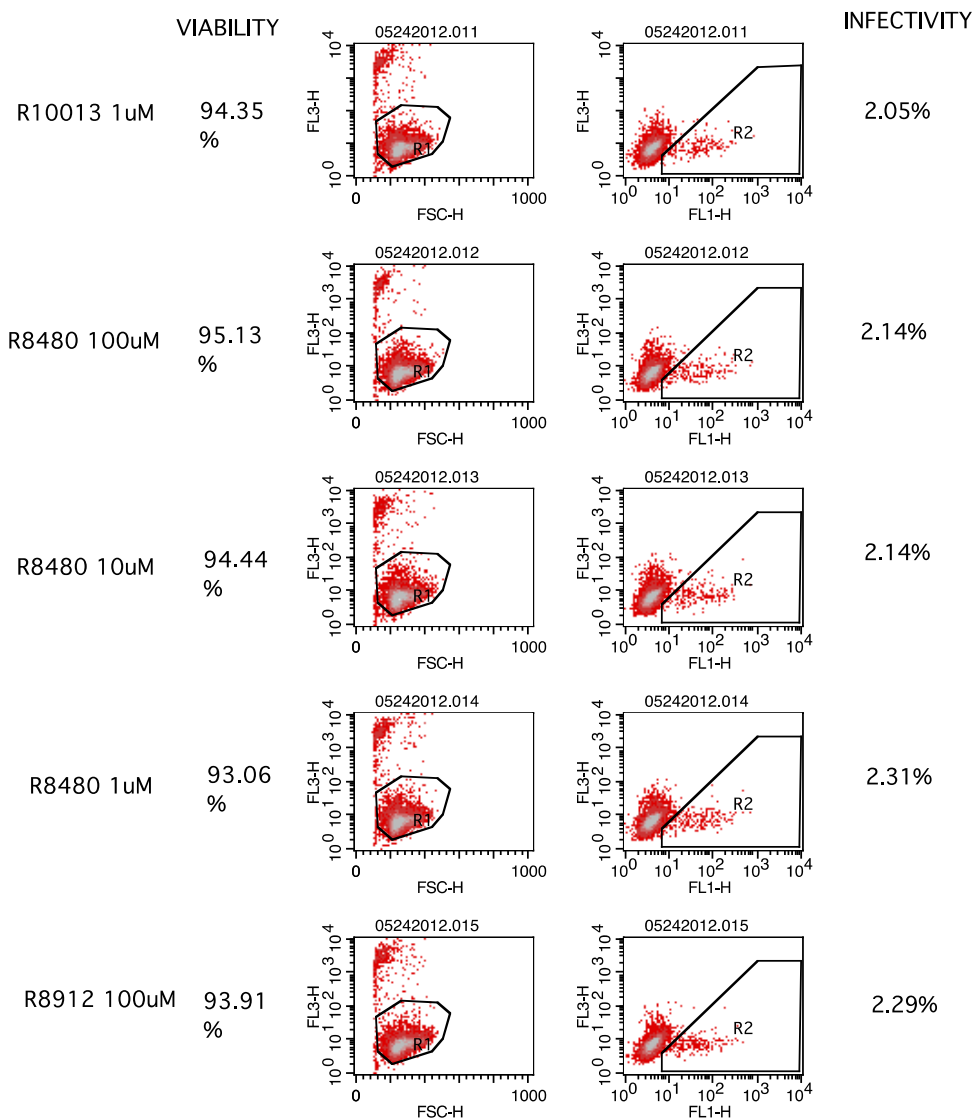


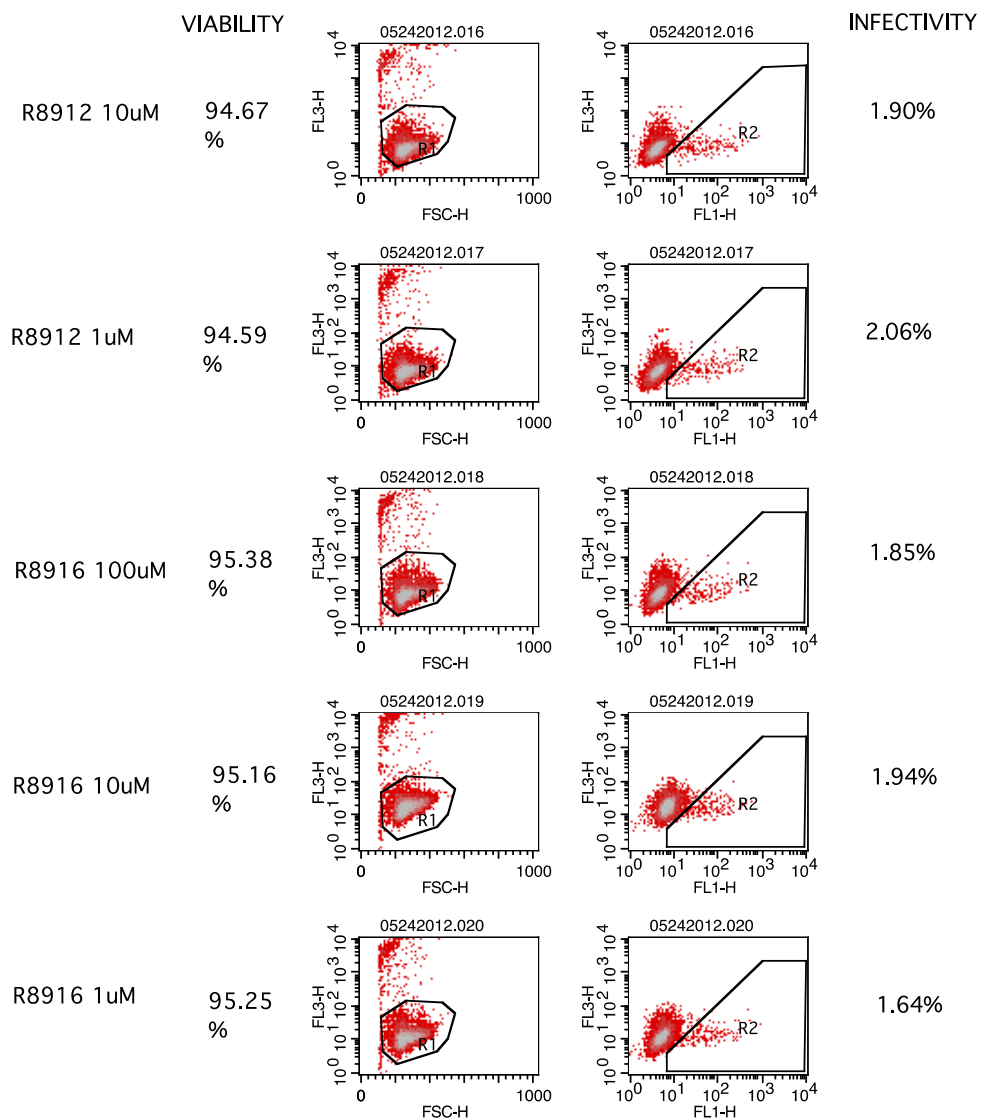


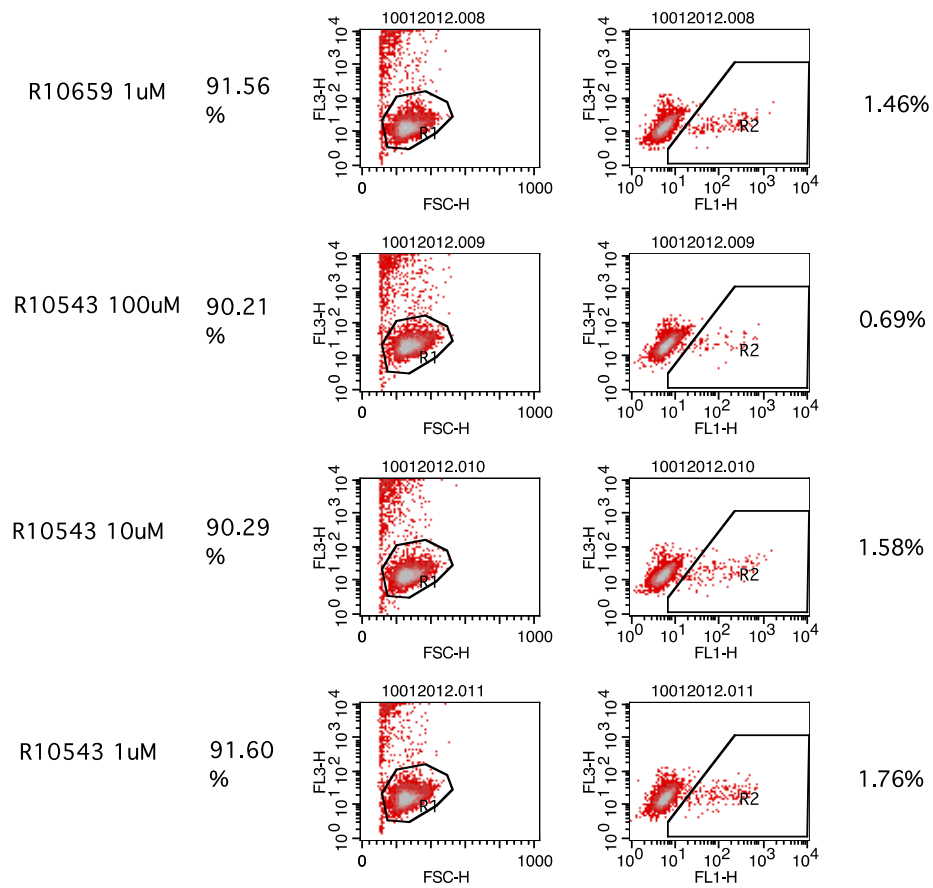
SCREEN OF R10023, R10014, R10013, R8408, R8912











References

- [1]. Gottlieb, M.S., et al., *Pneumocystis carinii* pneumonia and mucosal candidiasis in previously healthy homosexual men: evidence of a new acquired cellular immunodeficiency. *N Engl J Med*, 1981. 305(24): p. 1425-31.
- [2]. McCauley, D.I., et al., Radiographic patterns of opportunistic lung infections and Kaposi sarcoma in homosexual men. *AJR Am J Roentgenol*, 1982. 139(4): p. 653-8.
- [3]. Godwin, J.D., C.E. Ravin and V.L. Roggli, Fatal pneumocystis pneumonia, cryptococcosis, and Kaposi sarcoma in a homosexual man. *AJR Am J Roentgenol*, 1982. 138(3): p. 580-1.
- [4]. Goudsmit, J., et al., IgG antibodies to HTLV-III associated antigens in patients with AIDS and at risk for AIDS in The Netherlands. *AIDS Res*, 1983. 1(4): p. 231-6.
- [5]. Gallo, R.C., et al., Isolation of human T-cell leukemia virus in acquired immune deficiency syndrome (AIDS). *Science*, 1983. 220(4599): p. 865-7.
- [6]. Barre-Sinoussi, F., et al., Isolation of a T-lymphotropic retrovirus from a patient at risk for acquired immune deficiency syndrome (AIDS). *Science*, 1983. 220(4599): p. 868-71.
- [7]. Keele, B.F., et al., Chimpanzee reservoirs of pandemic and nonpandemic HIV-1. *Science*, 2006. 313(5786): p. 523-6.
- [8]. Baier, M., et al., Development of vivo of genetic variability of simian immunodeficiency virus. *Proc Natl Acad Sci U S A*, 1991. 88(18): p. 8126-30.
- [9]. Daniel, M.D., et al., A new type D retrovirus isolated from macaques with an immunodeficiency syndrome. *Science*, 1984. 223(4636): p. 602-5.
- [10]. Wain-Hobson, S., et al., Nucleotide sequence of the AIDS virus, LAV. *Cell*, 1985. 40(1): p. 9-17.

- [11]. Klatzmann, D., et al., T-lymphocyte T4 molecule behaves as the receptor for human retrovirus LAV. *Nature*, 1984. 312(5996): p. 767-8.
- [12]. McDougal, J.S., et al., Binding of HTLV-III/LAV to T4+ T cells by a complex of the 110K viral protein and the T4 molecule. *Science*, 1986. 231(4736): p. 382-5.
- [13]. Dalgleish, A.G., et al., The CD4 (T4) antigen is an essential component of the receptor for the AIDS retrovirus. *Nature*, 1984. 312(5996): p. 763-7.
- [14]. Feng, Y., et al., HIV-1 entry cofactor: functional cDNA cloning of a seven-transmembrane, G protein-coupled receptor. *Science*, 1996. 272(5263): p. 872-7.
- [15]. Alkhatib, G., et al., CC CKR5: a RANTES, MIP-1alpha, MIP-1beta receptor as a fusion cofactor for macrophage-tropic HIV-1. *Science*, 1996. 272(5270): p. 1955-8.
- [16]. Doranz, B.J., et al., A dual-tropic primary HIV-1 isolate that uses fusin and the beta-chemokine receptors CKR-5, CKR-3, and CKR-2b as fusion cofactors. *Cell*, 1996. 85(7): p. 1149-58.
- [17]. Buzon, V., et al., Crystal structure of HIV-1 gp41 including both fusion peptide and membrane proximal external regions. *PLoS Pathog*, 2010. 6(5): p. e1000880.
- [18]. Yoder, A., et al., HIV envelope-CXCR4 signaling activates cofilin to overcome cortical actin restriction in resting CD4 T cells. *Cell*, 2008. 134(5): p. 782-92.
- [19]. Miller, M.D., C.M. Farnet and F.D. Bushman, Human immunodeficiency virus type 1 preintegration complexes: studies of organization and composition. *J Virol*, 1997. 71(7): p. 5382-90.
- [20]. Miller, M.D., B. Wang and F.D. Bushman, Human immunodeficiency virus type 1 preintegration complexes containing discontinuous plus strands are competent to integrate in vitro. *J Virol*, 1995. 69(6): p. 3938-44.
- [21]. Piller, S.C., L. Caly and D.A. Jans, Nuclear import of the pre-integration complex (PIC): the Achilles heel of HIV? *Curr Drug Targets*, 2003. 4(5): p. 409-29.

- [22]. Shine, J., et al., Nucleotide sequence at the 5' terminus of the avian sarcoma virus genome. *Proc Natl Acad Sci U S A*, 1977. 74(4): p. 1473-7.
- [23]. Shine, J., et al., Nucleotide sequence at the 5' terminus of the avian sarcoma virus genome. *Proc Natl Acad Sci U S A*, 1977. 74(4): p. 1473-7.
- [24]. Sodroski, J., et al., Location of the trans-activating region on the genome of human T-cell lymphotropic virus type III. *Science*, 1985. 229(4708): p. 74-7.
- [25]. Wei, P., et al., A novel CDK9-associated C-type cyclin interacts directly with HIV-1 Tat and mediates its high-affinity, loop-specific binding to TAR RNA. *Cell*, 1998. 92(4): p. 451-62.
- [26]. Malim, M.H., et al., The HIV-1 rev trans-activator acts through a structured target sequence to activate nuclear export of unspliced viral mRNA. *Nature*, 1989. 338(6212): p. 254-7.
- [27]. D'Agostino, D.M., et al., The Rev protein of human immunodeficiency virus type 1 promotes polysomal association and translation of gag/pol and vpu/env mRNAs. *Mol Cell Biol*, 1992. 12(3): p. 1375-86.
- [28]. Felber, B.K., C.M. Drysdale and G.N. Pavlakis, Feedback regulation of human immunodeficiency virus type 1 expression by the Rev protein. *J Virol*, 1990. 64(8): p. 3734-41.
- [29]. Ganser, B.K., et al., Assembly and analysis of conical models for the HIV-1 core. *Science*, 1999. 283(5398): p. 80-3.
- [30]. Cooper, D.A., et al., Characterization of T lymphocyte responses during primary infection with human immunodeficiency virus. *J Infect Dis*, 1988. 157(5): p. 889-96.
- [31]. Lee, L.M., et al., Survival after AIDS diagnosis in adolescents and adults during the treatment era, United States, 1984-1997. *JAMA*, 2001. 285(10): p. 1308-15.
- [32]. Ho, D.D. and P.D. Bieniasz, HIV-1 at 25. *Cell*, 2008. 133(4): p. 561-5.
- [33]. Gu, W.G., et al., Discovery of a novel HIV-1 integrase inhibitor from natural compounds through structure based virtual screening and cell imaging. *FEBS Lett*, 2014. 588(18): p. 3461-8.

- [34]. Haqqani, A.A. and J.C. Tilton, Entry inhibitors and their use in the treatment of HIV-1 infection. *Antiviral Res*, 2013. 98(2): p. 158-70.
- [35]. Bamburg, J.R. and O.P. Wiggan, ADF/cofilin and actin dynamics in disease. *Trends Cell Biol*, 2002. 12(12): p. 598-605.
- [36]. Bukrinskaya, A., et al., Establishment of a functional human immunodeficiency virus type 1 (HIV-1) reverse transcription complex involves the cytoskeleton. *J Exp Med*, 1998. 188(11): p. 2113-25.
- [37]. Lappalainen, P. and D.G. Drubin, Cofilin promotes rapid actin filament turnover in vivo. *Nature*, 1997. 388(6637): p. 78-82.
- [38]. Arber, S., et al., Regulation of actin dynamics through phosphorylation of cofilin by LIM-kinase. *Nature*, 1998. 393(6687): p. 805-9.
- [39]. Jimenez-Baranda, S., et al., Filamin-A regulates actin-dependent clustering of HIV receptors. *Nat Cell Biol*, 2007. 9(7): p. 838-46.
- [40]. Ambach, A., et al., The serine phosphatases PP1 and PP2A associate with and activate the actin-binding protein cofilin in human T lymphocytes. *Eur J Immunol*, 2000. 30(12): p. 3422-31.
- [41]. Spear, M., et al., HIV-1 triggers WAVE2 phosphorylation in primary CD4 T cells and macrophages, mediating Arp2/3-dependent nuclear migration. *J Biol Chem*, 2014. 289(10): p. 6949-59.
- [42]. Mendoza, M.C., Phosphoregulation of the WAVE regulatory complex and signal integration. *Semin Cell Dev Biol*, 2013. 24(4): p. 272-9.
- [43]. Higgs, H.N. and T.D. Pollard, Regulation of actin filament network formation through ARP2/3 complex: activation by a diverse array of proteins. *Annu Rev Biochem*, 2001. 70: p. 649-76.
- [44]. Kovar, D.R., Arp2/3 ATP hydrolysis: to branch or to debranch? *Nat Cell Biol*, 2006. 8(8): p. 783-5.
- [45]. Bernard, O., et al., Kiz-1, a protein with LIM zinc finger and kinase domains, is expressed mainly in neurons. *Cell Growth Differ*, 1994. 5(11): p. 1159-71.
- [46]. Stanyon, C.A. and O. Bernard, LIM-kinase1. *Int J Biochem Cell Biol*, 1999. 31(3-4): p. 389-94.

- [47]. Mizuno, K., et al., Identification of a human cDNA encoding a novel protein kinase with two repeats of the LIM/double zinc finger motif. *Oncogene*, 1994. 9(6): p. 1605-12.
- [48]. Osada, H., et al., Subcellular localization and protein interaction of the human LIMK2 gene expressing alternative transcripts with tissue-specific regulation. *Biochem Biophys Res Commun*, 1996. 229(2): p. 582-9.
- [49]. Bernard, O., Lim kinases, regulators of actin dynamics. *Int J Biochem Cell Biol*, 2007. 39(6): p. 1071-6.
- [50]. Acevedo, K., et al., LIM kinase 2 is widely expressed in all tissues. *J Histochem Cytochem*, 2006. 54(5): p. 487-501.
- [51]. Hoogenraad, C.C., et al., LIMK1 and CLIP-115: linking cytoskeletal defects to Williams syndrome. *Bioessays*, 2004. 26(2): p. 141-50.
- [52]. Piccioli, Z.D. and J.T. Littleton, Retrograde BMP signaling modulates rapid activity-dependent synaptic growth via presynaptic LIM kinase regulation of cofilin. *J Neurosci*, 2014. 34(12): p. 4371-81.
- [53]. Heredia, L., et al., Phosphorylation of actin-depolymerizing factor/cofilin by LIM-kinase mediates amyloid beta-induced degeneration: a potential mechanism of neuronal dystrophy in Alzheimer's disease. *J Neurosci*, 2006. 26(24): p. 6533-42.
- [54]. Bongalon, S., et al., PDGF and IL-1beta upregulate cofilin and LIMK2 in canine cultured pulmonary artery smooth muscle cells. *J Vasc Res*, 2004. 41(5): p. 412-21.
- [55]. Dai, Y.P., et al., Upregulation of profilin, cofilin-2 and LIMK2 in cultured pulmonary artery smooth muscle cells and in pulmonary arteries of monocrotaline-treated rats. *Vascul Pharmacol*, 2006. 44(5): p. 275-82.
- [56]. Harrison, B.A., et al., Novel class of LIM-kinase 2 inhibitors for the treatment of ocular hypertension and associated glaucoma. *J Med Chem*, 2009. 52(21): p. 6515-8.
- [57]. Xu, X., et al., Involvement of LIM kinase 1 in actin polarization in human CD4 T cells. *Commun Integr Biol*, 2012. 5(4): p. 381-3.
- [58]. Manetti, F., HIV-1 proteins join the family of LIM kinase partners. *New*

roads open up for HIV-1 treatment. *Drug Discov Today*, 2012. 17(1-2): p. 81-8.

[59]. Manetti, F., LIM kinases are attractive targets with many macromolecular partners and only a few small molecule regulators. *Med Res Rev*, 2012. 32(5): p. 968-98.

[60]. Vorster, P.J., et al., LIM kinase 1 modulates cortical actin and CXCR4 cycling and is activated by HIV-1 to initiate viral infection. *J Biol Chem*, 2011. 286(14): p. 12554-64.

[61]. Rak, R., et al., Novel LIMK2 Inhibitor Blocks Panc-1 Tumor Growth in a mouse xenograft model. *Oncoscience*, 2014. 1(1): p. 39-48.

[62]. Ohashi, K., et al., Damnacanthal, an effective inhibitor of LIM-kinase, inhibits cell migration and invasion. *Mol Biol Cell*, 2014. 25(6): p. 828-40.

[63]. Yin, Y., et al., Bis-aryl urea derivatives as potent and selective LIM kinase (Limk) inhibitors. *J Med Chem*, 2015. 58(4): p. 1846-61.

[64]. Tybulewicz, V.L. and R.B. Henderson, Rho family GTPases and their regulators in lymphocytes. *Nat Rev Immunol*, 2009. 9(9): p. 630-44.

[65]. Wu, Y., M.H. Beddall and J.W. Marsh, Rev-dependent lentiviral expression vector. *Retrovirology*, 2007. 4: p. 12.

[66]. Wu, Y., M.H. Beddall and J.W. Marsh, Rev-dependent indicator T cell line. *Curr HIV Res*, 2007. 5(4): p. 394-402.

[67]. Sloan, R.D., et al., Transcription of preintegrated HIV-1 cDNA modulates cell surface expression of major histocompatibility complex class I via Nef. *J Virol*, 2011. 85(6): p. 2828-36.

[68]. Sloan, R.D., et al., Expression of Nef from unintegrated HIV-1 DNA downregulates cell surface CXCR4 and CCR5 on T-lymphocytes. *Retrovirology*, 2010. 7: p. 44.

[69]. Shuck-Lee, D., et al., Single-nucleotide changes in the HIV Rev-response element mediate resistance to compounds that inhibit Rev function. *J Virol*, 2011. 85(8): p. 3940-9.

[70]. Sigal, A., et al., Cell-to-cell spread of HIV permits ongoing replication despite antiretroviral therapy. *Nature*, 2011. 477(7362): p. 95-8.

- [71]. Yoder, A., et al., Effects of microtubule modulators on HIV-1 infection of transformed and resting CD4 T cells. *J Virol*, 2011. 85(6): p. 3020-4.
- [72]. Guo, J., et al., Spinoculation triggers dynamic actin and cofilin activity that facilitates HIV-1 infection of transformed and resting CD4 T cells. *J Virol*, 2011. 85(19): p. 9824-33.
- [73]. Iyer, S.R., et al., Measurement of human immunodeficiency virus type 1 preintegration transcription by using Rev-dependent Rev-CEM cells reveals a sizable transcribing DNA population comparable to that from proviral templates. *J Virol*, 2009. 83(17): p. 8662-73.
- [74]. Aguilar-Cordova, E., et al., A sensitive reporter cell line for HIV-1 tat activity, HIV-1 inhibitors, and T cell activation effects. *AIDS Res Hum Retroviruses*, 1994. 10(3): p. 295-301.
- [75]. Gervaix, A., et al., A new reporter cell line to monitor HIV infection and drug susceptibility in vitro. *Proc Natl Acad Sci U S A*, 1997. 94(9): p. 4653-8.
- [76]. Kimpton, J. and M. Emerman, Detection of replication-competent and pseudotyped human immunodeficiency virus with a sensitive cell line on the basis of activation of an integrated beta-galactosidase gene. *J Virol*, 1992. 66(4): p. 2232-9.
- [77]. Siekevitz, M., et al., Activation of the HIV-1 LTR by T cell mitogens and the trans-activator protein of HTLV-I. *Science*, 1987. 238(4833): p. 1575-8.
- [78]. Swingler, S., A. Morris and A. Easton, Tumour necrosis factor alpha and interleukin-1 beta induce specific subunits of NFkB to bind the HIV-1 enhancer: characterisation of transcription factors controlling human immunodeficiency virus type 1 gene expression in neural cells. *Biochem Biophys Res Commun*, 1994. 203(1): p. 623-30.
- [79]. Merzouki, A., et al., HIV-1 gp120/160 expressing cells upregulate HIV-1 LTR directed gene expression in a cell line transfected with HIV-1 LTR-reporter gene constructs. *Cell Mol Biol (Noisy-le-grand)*, 1995. 41(3): p. 445-52.
- [80]. Akan, E., et al., The effects of vinblastine on the expression of human immunodeficiency virus type 1 long terminal repeat. *Leuk Res*, 1997. 21(5): p. 459-64.
- [81]. Sweet, M.J. and D.A. Hume, RAW264 macrophages stably transfected with

an HIV-1 LTR reporter gene provide a sensitive bioassay for analysis of signalling pathways in macrophages stimulated with lipopolysaccharide, TNF-alpha or taxol. *J Inflamm*, 1995. 45(2): p. 126-35.

[82]. Das, K., et al., Roles of conformational and positional adaptability in structure-based design of TMC125-R165335 (etravirine) and related non-nucleoside reverse transcriptase inhibitors that are highly potent and effective against wild-type and drug-resistant HIV-1 variants. *J Med Chem*, 2004. 47(10): p. 2550-60.

[83]. Wu, Y. and J.W. Marsh, Selective transcription and modulation of resting T cell activity by preintegrated HIV DNA. *Science*, 2001. 293(5534): p. 1503-6.

[84]. Paisan-Ruiz, C., et al., Cloning of the gene containing mutations that cause PARK8-linked Parkinson's disease. *Neuron*, 2004. 44(4): p. 595-600.

[85]. Zimprich, A., et al., Mutations in LRRK2 cause autosomal-dominant parkinsonism with pleomorphic pathology. *Neuron*, 2004. 44(4): p. 601-7.

[86]. Lin, Y.L., et al., Syndecan-2 induces filopodia and dendritic spine formation via the neurofibromin-PKA-Ena/VASP pathway. *J Cell Biol*, 2007. 177(5): p. 829-41.

[87]. Watanabe, N., et al., Cooperation between mDia1 and ROCK in Rho-induced actin reorganization. *Nat Cell Biol*, 1999. 1(3): p. 136-43.

[88]. Maekawa, M., et al., Signaling from Rho to the actin cytoskeleton through protein kinases ROCK and LIM-kinase. *Science*, 1999. 285(5429): p. 895-8.

[89]. Gorovoy, M., et al., LIM kinase 1 coordinates microtubule stability and actin polymerization in human endothelial cells. *J Biol Chem*, 2005. 280(28): p. 26533-42.

[90]. Manetti, F., LIM kinases are attractive targets with many macromolecular partners and only a few small molecule regulators. *Med Res Rev*, 2012. 32(5): p. 968-98.

[91]. Acevedo, K., et al., The phosphorylation of p25/TPPP by LIM kinase 1 inhibits its ability to assemble microtubules. *Exp Cell Res*, 2007. 313(20): p. 4091-106.

[92]. Heng, Y.W., et al., TPPP acts downstream of RhoA-ROCK-LIMK2 to regulate astral microtubule organization and spindle orientation. *J Cell Sci*, 2012. 125(Pt 6): p. 1579-90.

- [93]. Ovadi, J. and F. Orosz, An unstructured protein with destructive potential: TPPP/p25 in neurodegeneration. *Bioessays*, 2009. 31(6): p. 676-86.
- [94]. Edwards, D.C., et al., Activation of LIM-kinase by Pak1 couples Rac/Cdc42 GTPase signalling to actin cytoskeletal dynamics. *Nat Cell Biol*, 1999. 1(5): p. 253-9.
- [95]. Nishita, M., H. Aizawa and K. Mizuno, Stromal cell-derived factor 1alpha activates LIM kinase 1 and induces cofilin phosphorylation for T-cell chemotaxis. *Mol Cell Biol*, 2002. 22(3): p. 774-83.
- [96]. Sampath, P. and T.D. Pollard, Effects of cytochalasin, phalloidin, and pH on the elongation of actin filaments. *Biochemistry*, 1991. 30(7): p. 1973-80.
- [97]. Cooper, J.A., Effects of cytochalasin and phalloidin on actin. *J Cell Biol*, 1987. 105(4): p. 1473-8.
- [98]. Spear, M., et al., HIV-1 triggers WAVE2 phosphorylation in primary CD4 T cells and macrophages, mediating Arp2/3-dependent nuclear migration. *J Biol Chem*, 2014. 289(10): p. 6949-59.
- [99]. Audoly, G., M.R. Popoff and P. Gluschankof, Involvement of a small GTP binding protein in HIV-1 release. *Retrovirology*, 2005. 2: p. 48.
- [100]. Martin-Serrano, J. and S.J. Neil, Host factors involved in retroviral budding and release. *Nat Rev Microbiol*, 2011. 9(7): p. 519-31.
- [101]. Cavrois, M., C. De Noronha and W.C. Greene, A sensitive and specific enzyme-based assay detecting HIV-1 virion fusion in primary T lymphocytes. *Nat Biotechnol*, 2002. 20(11): p. 1151-4.
- [102]. Wild, C.T., et al., Peptides corresponding to a predictive alpha-helical domain of human immunodeficiency virus type 1 gp41 are potent inhibitors of virus infection. *Proc Natl Acad Sci U S A*, 1994. 91(21): p. 9770-4.
- [103]. Wu, Y. and J.W. Marsh, Early transcription from nonintegrated DNA in human immunodeficiency virus infection. *J Virol*, 2003. 77(19): p. 10376-82.
- [104]. Burns, J.C., et al., Vesicular stomatitis virus G glycoprotein pseudotyped retroviral vectors: concentration to very high titer and efficient gene transfer into mammalian and nonmammalian cells. *Proc Natl Acad Sci U S A*, 1993. 90(17): p. 8033-7.

- [105]. Yu, D., et al., The HIV envelope but not VSV glycoprotein is capable of mediating HIV latent infection of resting CD4 T cells. *PLoS Pathog*, 2009. 5(10): p. e1000633.
- [106]. Stein, B.S., et al., pH-independent HIV entry into CD4-positive T cells via virus envelope fusion to the plasma membrane. *Cell*, 1987. 49(5): p. 659-68.
- [107]. Spear, M., J. Guo and Y. Wu, The trinity of the cortical actin in the initiation of HIV-1 infection. *Retrovirology*, 2012. 9: p. 45.
- [108]. Butler, S.L., E.P. Johnson and F.D. Bushman, Human immunodeficiency virus cDNA metabolism: notable stability of two-long terminal repeat circles. *J Virol*, 2002. 76(8): p. 3739-47.
- [109]. Friedrich, B., et al., Quantitative PCR used to assess HIV-1 integration and 2-LTR circle formation in human macrophages, peripheral blood lymphocytes and a CD4+ cell line. *Virol J*, 2010. 7: p. 354.
- [110]. Mandal, D. and V.R. Prasad, Analysis of 2-LTR circle junctions of viral DNA in infected cells. *Methods Mol Biol*, 2009. 485: p. 73-85.
- [111]. Veazey, R.S., et al., Gastrointestinal tract as a major site of CD4+ T cell depletion and viral replication in SIV infection. *Science*, 1998. 280(5362): p. 427-31.
- [112]. Brenchley, J.M., et al., CD4+ T cell depletion during all stages of HIV disease occurs predominantly in the gastrointestinal tract. *J Exp Med*, 2004. 200(6): p. 749-59.
- [113]. Zhang, Z., et al., Sexual transmission and propagation of SIV and HIV in resting and activated CD4+ T cells. *Science*, 1999. 286(5443): p. 1353-7.
- [114]. Caruso, A., et al., Flow cytometric analysis of activation markers on stimulated T cells and their correlation with cell proliferation. *Cytometry*, 1997. 27(1): p. 71-6.
- [115]. Hottiger, M., et al., The large subunit of HIV-1 reverse transcriptase interacts with beta-actin. *Nucleic Acids Res*, 1995. 23(5): p. 736-41.
- [116]. Chan, S.Y., M.C. Ma and M.A. Goldsmith, Differential induction of cellular detachment by envelope glycoproteins of Marburg and Ebola (Zaire) viruses. *J Gen Virol*, 2000. 81(Pt 9): p. 2155-9.

- [117]. Chan, S.Y., et al., Distinct mechanisms of entry by envelope glycoproteins of Marburg and Ebola (Zaire) viruses. *J Virol*, 2000. 74(10): p. 4933-7.
- [118]. Yonezawa, A., M. Cavrois and W.C. Greene, Studies of ebola virus glycoprotein-mediated entry and fusion by using pseudotyped human immunodeficiency virus type 1 virions: involvement of cytoskeletal proteins and enhancement by tumor necrosis factor alpha. *J Virol*, 2005. 79(2): p. 918-26.
- [119]. Yarmola, E.G., et al., Actin-latrunculin A structure and function. Differential modulation of actin-binding protein function by latrunculin A. *J Biol Chem*, 2000. 275(36): p. 28120-7.
- [120]. Aleksandrowicz, P., et al., Ebola virus enters host cells by macropinocytosis and clathrin-mediated endocytosis. *J Infect Dis*, 2011. 204 Suppl 3: p. S957-67.
- [121]. Hewlett, M.J., R.F. Pettersson and D. Baltimore, Circular forms of Uukuniemi virion RNA: an electron microscopic study. *J Virol*, 1977. 21(3): p. 1085-93.
- [122]. Filone, C.M., et al., Development and characterization of a Rift Valley fever virus cell-cell fusion assay using alphavirus replicon vectors. *Virology*, 2006. 356(1-2): p. 155-64.
- [123]. Dessau, M. and Y. Modis, Crystal structure of glycoprotein C from Rift Valley fever virus. *Proc Natl Acad Sci U S A*, 2013. 110(5): p. 1696-701.
- [124]. Baer, A., et al., Protein Phosphatase-1 regulates Rift Valley fever virus replication. *Antiviral Res*, 2016. 127: p. 79-89.
- [125]. Huet, G., et al., Actin-regulated feedback loop based on Phactr4, PP1 and cofilin maintains the actin monomer pool. *J Cell Sci*, 2013. 126(Pt 2): p. 497-507.
- [126]. Leung, J.Y., M.M. Ng and J.J. Chu, Replication of alphaviruses: a review on the entry process of alphaviruses into cells. *Adv Virol*, 2011. 2011: p. 249640.
- [127]. Baringer, J.R. and P. Swoveland, Recovery of herpes-simplex virus from human trigeminal ganglions. *N Engl J Med*, 1973. 288(13): p. 648-50.
- [128]. Favoreel, H.W., L.W. Enquist and B. Feuerbach, Actin and Rho GTPases in herpesvirus biology. *Trends Microbiol*, 2007. 15(9): p. 426-33.
- [129]. Lyman, M.G. and L.W. Enquist, Herpesvirus interactions with the host

cytoskeleton. *J Virol*, 2009. 83(5): p. 2058-66.

[130]. Radtke, K., K. Dohner and B. Sodeik, Viral interactions with the cytoskeleton: a hitchhiker's guide to the cell. *Cell Microbiol*, 2006. 8(3): p. 387-400.

[131]. Taylor, M.P., O.O. Koyuncu and L.W. Enquist, Subversion of the actin cytoskeleton during viral infection. *Nat Rev Microbiol*, 2011. 9(6): p. 427-39.

[132]. Xiang, Y., et al., Cofilin 1-mediated biphasic F-actin dynamics of neuronal cells affect herpes simplex virus 1 infection and replication. *J Virol*, 2012. 86(16): p. 8440-51.

[133]. Wen, X., et al., ROCK1 and LIM kinase modulate retrovirus particle release and cell-cell transmission events. *J Virol*, 2014. 88(12): p. 6906-21.

[134]. WILLIAMS, J.C., B.G. BARRATT-BOYES and J.B. LOWE, Supravalvular aortic stenosis. *Circulation*, 1961. 24: p. 1311-8.

[135]. Peoples, R., et al., A physical map, including a BAC/PAC clone contig, of the Williams-Beuren syndrome--deletion region at 7q11.23. *Am J Hum Genet*, 2000. 66(1): p. 47-68.

[136]. Hoogenraad, C.C., et al., LIMK1 and CLIP-115: linking cytoskeletal defects to Williams syndrome. *Bioessays*, 2004. 26(2): p. 141-50.

[137]. Li, D.Y., et al., Elastin point mutations cause an obstructive vascular disease, supravalvular aortic stenosis. *Hum Mol Genet*, 1997. 6(7): p. 1021-8.

[138]. Meng, Y., et al., Abnormal spine morphology and enhanced LTP in LIMK-1 knockout mice. *Neuron*, 2002. 35(1): p. 121-33.

[139]. Yoshioka, K., et al., A role for LIM kinase in cancer invasion. *Proc Natl Acad Sci U S A*, 2003. 100(12): p. 7247-52.

[140]. Ma, Q.L., et al., PAK in Alzheimer disease, Huntington disease and X-linked mental retardation. *Cell Logist*, 2012. 2(2): p. 117-125.

[141]. Proschel, C., et al., Limk1 is predominantly expressed in neural tissues and phosphorylates serine, threonine and tyrosine residues in vitro. *Oncogene*, 1995. 11(7): p. 1271-81.

Curriculum Vitae

Fei Yi was born in Nanchang, China. He received his Doctoral degree of Medicine from Tongji Medical College, Huazhong University of Science and Technology in 2010.